



MAX-PLANCK-INSTITUT
FÜR METEOROLOGIE

A transforming Arctic: Unraveling Climate Change Impacts on Sea-Ice Evolution and Oceanic pCO₂



Markus Ritschel
Hamburg 2024

Berichte zur Erdsystemforschung
Reports on Earth System Science

281
2024

Hinweis

Die Berichte zur Erdsystemforschung werden vom Max-Planck-Institut für Meteorologie in Hamburg in unregelmäßiger Abfolge herausgegeben.

Sie enthalten wissenschaftliche und technische Beiträge, inklusive Dissertationen.

Die Beiträge geben nicht notwendigerweise die Auffassung des Instituts wieder.

Die "Berichte zur Erdsystemforschung" führen die vorherigen Reihen "Reports" und "Examensarbeiten" weiter.

Anschrift / Address

Max-Planck-Institut für Meteorologie
Bundesstrasse 53
20146 Hamburg
Deutschland

Tel./Phone: +49 (0)40 4 11 73 - 0
Fax: +49 (0)40 4 11 73 - 298

name.surname@mpimet.mpg.de
www.mpimet.mpg.de

Notice

The Reports on Earth System Science are published by the Max Planck Institute for Meteorology in Hamburg. They appear in irregular intervals.

They contain scientific and technical contributions, including PhD theses.

The Reports do not necessarily reflect the opinion of the Institute.

The "Reports on Earth System Science" continue the former "Reports" and "Examensarbeiten" of the Max Planck Institute.

Layout

Bettina Diallo and Norbert P. Noreiks
Communication

Copyright

Photos below: ©MPI-M
Photos on the back from left to right:
Christian Klepp, Jochem Marotzke,
Christian Klepp, Clotilde Dubois,
Christian Klepp, Katsumasa Tanaka



A transforming Arctic: Unraveling Climate Change Impacts on Sea-Ice Evolution and Oceanic pCO₂



Markus Ritschel

Hamburg 2024

Markus Ritschel

aus Rosenheim, Deutschland

Max-Planck-Institut für Meteorologie

The International Max Planck Research School on Earth System Modelling
(IMPRS-ESM)

Bundesstrasse 53
20146 Hamburg

Universität Hamburg
Fachbereich Erdsystemwissenschaften
Institut für Meereskunde
Bundesstraße 53
20146 Hamburg

Tag der Disputation: 29. Februar 2024

Folgende Gutachter empfehlen die Annahme der Dissertation:

Prof. Dr. Dirk Notz
Dr. Peter Landschützer

Vorsitzender des Promotionsausschusses:

Prof. Dr. Hermann Held

Dekan der MIN-Fakultät:

Prof. Dr.-Ing. Norbert Ritter

Titelbild: Typische Küstenregionen der Arktis mit schwindendem Meereis, erstellt mit Adobe Firefly

ABSTRACT

The Arctic undergoes profound transformations due to global warming, with climate change impacts varying at regional levels. While many changes, such as declining sea ice and alterations in ocean biochemistry, are often discussed based on the pan-Arctic average, their local implications and intensity variations across regions have been largely overlooked, despite their importance for stakeholders. This thesis aims to help shift the perspective towards understanding regional changes in the Arctic by investigating two crucial indicators affected by a warming climate: Arctic sea-ice coverage and surface ocean partial pressure of carbon dioxide ($p\text{CO}_2$). The first is of interest to a variety of stakeholders, particularly to those interested in changes along the coast–ice transition zone, such as the shipping industry and indigenous people. The latter is a key factor in the exchange of CO_2 between ocean and atmosphere and is, therefore, decisive for the acidification of the oceans.

The sensitivity of sea-ice area to near-surface air temperature changes, i. e. how strongly sea-ice area diminishes for a given rise in temperature, exhibits a high seasonal dependence, characterized by significant variability in summer and low variability in winter. This study reveals that the transition between summer and winter, along with the observed low variability in winter, can be attributed to the geographic blocking of the sea-ice edge by surrounding land masses. By quantifying the timing of the blocking, the analysis links the timing changes to rising global temperatures. The findings indicate that as the timing shifts and the season during which the ice edge is blocked shortens (by around 7 days per tenth degree of global warming on average), adjacent seasons will experience heightened sensitivity in sea-ice area. Particularly, sensitivities in areas along the coasts of the high Arctic Ocean will undergo a sudden change in the future.

Expanding the sensitivity analysis to a regional scale, the study provides new perspectives on how the sea ice in individual Arctic regions responds to global warming, anticipating future changes. The East Siberian Sea, the Chukchi Sea, and the Laptev Sea are identified as regions likely to lose their summer sea ice first. The Barents Sea is projected to become the first region to lose its remaining winter sea ice, ultimately becoming ice-free year-round.

Shifting focus to surface ocean $p\text{CO}_2$, two data products estimating surface ocean $p\text{CO}_2$ to fill the sparse observations in the Arctic are used to investigate the evolution of surface ocean $p\text{CO}_2$ in the Arctic domain. Both products reveal consistent increases in most regions over the last two decades. However, substantial differences in the magnitudes of inter- and intra-annual changes are observed between the two

datasets. Separating the spatial and temporal variability in the pCO₂ via EOF analysis reveals the dominant drivers of changes in the pCO₂ in different domains of the Arctic. The study identifies sub-Arctic domain changes primarily related to the seasonal solar irradiance cycle, while high Arctic pCO₂ changes are dominated by changes in sea-ice cover. Examining seasonality, shifts and changes in intra-annual amplitude are noted already in the historical record, particularly north of Canada, indicating potential impact on ecosystems.

This thesis underscores the necessity of taking a regional perspective on Arctic climate change. By systematically analyzing and quantifying the blocking effect for the first time, it provides a foundation for understanding sea-ice area changes in the high Arctic, benefiting stakeholders interested in Arctic Ocean transformations, particularly in coastal regions. Additionally, the pCO₂ analysis offers insights into the drivers of pCO₂ in the Arctic Ocean, serving as a benchmark to enhance future data products, crucial for investigating regional changes in the Arctic surface ocean carbon cycle. These findings contribute to the groundwork for future research in the Arctic.

ZUSAMMENFASSUNG

Die Arktis ist aufgrund der globalen Erwärmung tiefgreifenden Veränderungen unterworfen, wobei sich die Auswirkungen des Klimawandels je nach Region stark unterscheiden. Während viele Veränderungen, wie der Rückgang des Meereises und Veränderungen in der Meeres-Biochemie, oft auf pan-arktischer Ebene diskutiert werden, blieben ihre lokalen Auswirkungen und Unterschiede in deren Intensität zwischen den Regionen lange Zeit weitgehend unbeachtet, obwohl sie für verschiedene Interessensgruppen von großer Bedeutung sind. Diese Dissertation soll dazu beitragen, den Fokus auf das Verständnis regionaler Änderungen in der Arktis zu verlagern, indem sie zwei wesentliche Indikatoren untersucht, die von einem wärmeren Klima betroffen sind: die Meereisbedeckung der Arktis und der Partialdruck von Kohlendioxid ($p\text{CO}_2$) an der Meeresoberfläche. Erstere ist von Interesse für eine Vielzahl von Interessensgruppen, insbesondere für diejenigen, die an Veränderungen entlang der Küsten-Eis-Übergangszone interessiert sind, wie z. B. die Schifffahrtsindustrie und indigene Bevölkerungsgruppen. Letztere ist ein Schlüsselfaktor für den Austausch von CO_2 zwischen Ozean und Atmosphäre und entsprechend maßgeblich entscheidend für die Versauerung der Ozeane.

Die Sensitivität der Meereisfläche gegenüber Veränderungen in der oberflächennahen Lufttemperatur, d. h. wie stark sich die Meereisfläche bei gegebenem Temperaturanstieg verringert, zeigt eine hohe saisonale Abhängigkeit, die durch starke Variabilität im Sommer und geringe Variabilität im Winter gekennzeichnet ist. Diese Studie zeigt, dass der Übergang zwischen Sommer und Winter sowie die geringe Variabilität im Winter auf das Blockieren des Meereises durch umliegende Landmassen zurückzuführen ist. Dies wird in der Arbeit als "geographic muting" oder auch "geographic blocking" bezeichnet. Durch die Quantifizierung des Zeitpunkts dieses Blocking-Effekts wird eine klare Relation zwischen dem Timing dem globalen Temperaturanstieg festgestellt. Die Ergebnisse deuten darauf hin, dass mit der Verschiebung des Timings und der Verkürzung der Saison, über welche das Meereis blockiert ist, (im Durchschnitt etwa 7 Tage pro Zehntelgrad globaler Erwärmung) benachbarte Jahreszeiten eine erhöhte Sensitivität der Meereisfläche zeigen werden. Insbesondere Sensitivitäten in küstennahen Regionen werden zukünftig einer plötzlichen Veränderung unterliegen.

Durch Ausweiten der Sensitivitätsanalyse auf regionale Ebene zeigt die Studie neue Perspektiven auf, wie das Meereis in einzelnen Regionen der Arktis auf die globale Erwärmung reagiert, und antizipiert zukünftige Änderungen. Die Ost-Sibirische See, die Tschuktschensee

und die Laptewsee werden als Regionen identifiziert, die mit großer Wahrscheinlichkeit zuerst ihr Sommer-Meereis verlieren werden. Die Barentssee wird dagegen voraussichtlich die erste Region sein, die ihr verbleibendes Winter-Meereis verliert und letztendlich das ganze Jahr über eisfrei sein wird.

Bei der anschließenden Betrachtung des oberflächennahen Partialdrucks von Kohlendioxid ($p\text{CO}_2$) werden zwei Datensätze verwendet, welche $p\text{CO}_2$ aus lückenhaften Beobachtungen schätzen, um die Entwicklung des $p\text{CO}_2$ in der Arktis zu untersuchen. Beide Datensätze zeigen über die letzten zwei Jahrzehnte eine konsistente Zunahme des $p\text{CO}_2$ für die meisten Regionen. Dabei werden jedoch erhebliche Unterschiede im Ausmaß der zwischenjährlichen und innerjährlichen Veränderungen zwischen den beiden Datensätzen beobachtet. Indem räumliche und zeitliche Variabilität im $p\text{CO}_2$ mittels EOF-Analyse separiert werden, lassen sich die dominierenden Treiber jener Veränderungen identifizieren. Die Studie zeigt, dass Veränderungen im subarktischen Bereich hauptsächlich dem saisonalen Zyklus der Sonneneinstrahlung zugeordnet werden können, während in der hohen Arktis Prozesse dominieren, die mit Änderungen in der Meereisbedeckung in Verbindung stehen. Bei der Untersuchung der Saisonalität, lassen sich Hinweise auf Verschiebungen und Änderungen in der saisonalen Amplitude bereits in den historischen Daten feststellen (insbesondere nördlich von Kanada), was potenzielle Auswirkungen auf die dortigen Ökosysteme vermuten lässt.

Diese Dissertation unterstreicht die Notwendigkeit, eine regionale Perspektive auf den arktischen Klimawandel einzunehmen. Indem der Blocking-Effekt erstmals systematisch analysiert und quantifiziert wird, legt diese Arbeit die Grundlage für das Verständnis von Veränderungen in der Meereisfläche in der hohen Arktis und dürfte somit von Nutzen für Interessengruppen sein, für welche die Transformationen des Arktischen Ozeans, insbesondere in Küstenregionen, von Bedeutung sind. Darüber hinaus bietet die $p\text{CO}_2$ -Analyse Einblicke in die Treiber des $p\text{CO}_2$ im Arktischen Ozean und dient somit auch der Verbesserung zukünftiger Datensätze, die für die Untersuchung regionaler Veränderungen im Kohlenstoffkreislauf der arktischen Meeresoberfläche entscheidend sind. Diese Erkenntnisse tragen zur Grundlagenforschung für zukünftige Studien in der Arktis bei.

ACKNOWLEDGMENTS

So many people have played an important role for me in the last few years that it is hard to mention everyone. I am very grateful for all the professional support I received throughout my PhD. But probably as important as the professional support was the personal support I got from so many during that time.

Dirk! Thanks for giving me the opportunity to work in such a human-friendly environment. Thanks for all the inspiring discussions we had and for the great support I could always count on. Thanks for the freedom you gave me (including the opportunity to teach and supervise) and for always trusting in me. You had much more confidence in me than I had most of the time. Thanks for keeping pushing me ;-).

Peter! Thank you so much for your support and for being a great mentor. I've learned a lot from you and am very grateful for the opportunity to work with you. I am also very thankful for the great discussions we had and for all the input you gave me.

Eleanor! Thanks so much for jumping in when things got difficult due to unforeseen circumstances! Honestly, I don't know what I would have done without you. I am so grateful for all the time and energy you've dedicated over the last year. I enjoyed our fruitful discussions a lot and am glad to have joined yet another wonderful working group.

Victor, thanks for your support and for being an excellent panel chair. You gave the panel meetings a relaxed yet professional character, and you were there with an open ear when external circumstances made it challenging to proceed with the project.

Being part of three different working groups has been a terrific experience, and I am grateful for the company of so many interesting people over the last few years.

Niels, thanks for being a great colleague and friend. I am glad we had the opportunity to create and teach our own course together. Developing the concept and teaching together was a fantastic experience, a nice switch from the daily duties, and a lot of fun.

Antje, Michaela, Connie, Xisca, Maite. Thank you for all your support! You made all the bureaucratic stuff a breeze.

Lea, Dana, Julia. You guys were the first students I supervised, and you made it a truly great experience. I had a lot of fun working with you and learned surely a lot in this process. Thanks for trusting in me and for becoming friends.

Tommy. Thanks for convincing me to pursue a PhD. Even though the timing was not the best considering the COVID outbreak right before I started ;-).

Jonathan and the β-2 cohort. Thanks for the nice and enriching meetings we had over the last year. I benefitted a lot from your input, the discussions, and the exchange.

Working in such an enriching environment as the MPI and the Uni Hamburg has been a privilege. I am very grateful for all the encounters I made on my way. The PhD retreats, although stressful, have been a wonderful time and opportunity to exchange and connect with peers. I am hopeful that many of these connections will last beyond this PhD phase. Also, thanks to all the other people I have met at conferences or during my stay in Canada and who have enriched my last few years. Thank you to all my friends in Hamburg and elsewhere in the world. I wouldn't be where I am now without all of you.

Last but not least: I don't think I would have made my way to this point without my loving family. Thank you so much for going all the way with me and for always being there for me and backing me up when I needed it! Hannes, I think you don't know how much your friendship supported me over the last few years. I am deeply grateful for your support and the long and interesting discussions in our kitchen. Nayeli, thanks for being there during my final spurt. I am so thankful that you always found the time and energy to support and cheer me up, despite the many tasks you had to deal with.

This contribution was funded by the Deutsche Forschungsgemeinschaft (DFG, German Research Foundation) under Germany's Excellence Strategy – EXC 2037 'CLICCS - Climate, Climatic Change, and Society' – Project Number: 390683824, contribution to the Center for Earth System Research and Sustainability (CEN) of Universität Hamburg (Hamburg, Germany). Financial support was also provided by the doctoral school *International Max Planck Research School on Earth System Modeling* (Max Planck Institute for Meteorology, Hamburg, Germany).

CONTENTS

Unifying Essay

1	Introduction	3
1.1	A transforming Arctic	3
1.2	Why we need a regional perspective	4
1.3	The implications of climate change on Arctic sea-ice retreat	7
1.4	The oceanic carbon cycle in the Arctic	9
1.5	Structure of this thesis	12
2	The response of Arctic sea-ice area to global warming	13
2.1	Sea-ice sensitivity	13
2.2	Geographic muting as a driver of sensitivity changes .	16
2.3	The sensitivities of individual regions	19
3	An assessment of Arctic surface ocean pCO ₂	23
3.1	The mean state of pCO ₂ at different scales	24
3.2	Dominating patterns in the high and the sub-Arctic .	26
3.3	Changes in timing and amplitude of seasonality	28
4	Summary and Conclusions	31
4.1	My findings on seasonal and regional changes of SIA and pCO ₂	31
4.2	Implications of this dissertation	34
4.3	Concluding remarks	35

Appendix

A	Regional and seasonal sea-ice sensitivities	39
A.1	Introduction	42
A.2	Data and Methods	44
A.2.1	Arctic sea ice and temperature data	44
A.2.2	Sensitivity analyses	46
A.2.3	Geographic muting	49
A.3	Seasonal cycle of NH SIA sensitivities to local tempera- ture changes	50
A.4	Understanding the regional processes and the separa- tion of the seasonal cycle of NH sensitivities	52
A.5	Conclusions	60
	Additional tables	62
B	Unlocking the Arctic Ocean's carbon cycle	71
B.1	Introduction	74
B.2	Data and Methods	75
B.3	Results & Discussion	78
B.3.1	The mean sea surface pCO ₂	78
B.3.2	A spatio-temporal decomposition hints at dom- inating drivers	80

B.3.3	Changes in timing and amplitude of the seasonal cycle	84
B.4	Conclusions	86
	Additional Figures	88
	 Bibliography	
		89

LIST OF FIGURES

Figure 1.1	Time series of global/Arctic surface temperature & Arctic Amplification	4
Figure 1.2	Bathymetric map of the Arctic with an overview of the different regions used in this study	5
Figure 1.3	Time series of September SIA and its sensitivity to changes in anthropogenic CO ₂ emissions	8
Figure 2.1	Seasonal cycle of NH SIA and Arctic mean surface temperature	14
Figure 2.2	Blocking of the sea-ice edge along the Arctic perimeter (monthly time series)	17
Figure 2.3	Day of the year at which the sea-ice edge attaches to and detaches from the coast, plotted against global mean temperature anomalies	18
Figure 2.4	Observed sensitivities of individual regions of the Arctic	20
Figure 3.1	Mean states of Arctic ocean surface pCO ₂ and its evolution over time	25
Figure 3.2	EOF and PC of the first two modes	26
Figure A.1	Regions of the Arctic	47
Figure A.2	Figure to demonstrate the data-selection prior to linear regression	48
Figure A.3	Seasonal cycles of SIA, TAS, and sensitivities	51
Figure A.4	Regional sensitivities and historical sea-ice loss	53
Figure A.5	Observed sensitivities for the entire Northern Hemisphere	55
Figure A.6	Blocking of the sea-ice edge along the Arctic perimeter (monthly time series)	57
Figure A.7	Timing (day-of-year) of the geographic blocking of the sea-ice edge	59
Figure B.1	Overview of the different Arctic regions alongside the total number of pCO ₂ measurements in the SOCAT database between 1982 and 2021	77

Figure B.2	Mean states of ocean pCO ₂ for different pentads	79
Figure B.3	Time series of atmospheric and oceanic pCO ₂	80
Figure B.4	Varimax-rotated empirical orthogonal functions (EOFs) and principal components (time series and seasonality) of the first two modes	81
Figure B.5	Timing of the ocean surface pCO ₂ minimum and maximum and the amplitude for different periods	85
Figure B.6	SOCAT coverage for selected regions	88

LIST OF TABLES

Table 1.1	A non-comprehensive overview of various studies trying to estimate the annual carbon flux of the Arctic Ocean	11
Table A.1	Sensitivity values and error for all regions and seasons with respect to Arctic temperature	63
Table A.2	Sensitivity values and error for all regions and seasons with respect to global temperature	64
Table A.3	Sensitivity values and error for all regions and seasons with respect to anthropogenic CO ₂ emissions	65
Table A.4	r^2 for temperature-related sensitivities for every region and season	66
Table A.5	r^2 for CO ₂ -related sensitivities every region and season	67
Table A.6	Amount of data points available for the temperature-related regression analysis.	68
Table A.7	Amount of data points available for the CO ₂ -related regression analysis.	68
Table A.8	Sizes of the different Arctic regions including the total ocean area of the Arctic and the Northern Hemisphere	69

ACRONYMS

DIC	dissolved inorganic carbon
EOF	empirical orthogonal function
Jena-MLS	Jena-Carboscope mixed layer scheme
MPIM-SOM-FFN	Max Planck Institute for Meteorology Self-Organizing Map Feed-Forward Network
NASA	National Aeronautics and Space Administration
NH	northern-hemispheric
NOAA	National Oceanic and Atmospheric Administration
NSIDC	National Snow and Ice Data Center
OISST	Optimum Interpolation Sea Surface Temperature
PC	principal component
SIA	sea-ice area
SIC	sea-ice concentration
SIE	sea-ice extent
SOCAT	Surface Ocean CO ₂ Atlas
SST	sea-surface temperature
TA	total alkalinity
TAS	atmospheric near-surface temperature

UNIFYING ESSAY



INTRODUCTION

1.1. A TRANSFORMING ARCTIC

Since the first scientific expeditions to the high Arctic in the early 19th century, much has changed in this remote, unique region of the Earth. Reports of early explorers of this hostile environment describe a massive pack-ice in the Arctic Ocean, making it challenging to navigate (e.g. Ross, 1835). While such conditions can still be encountered in some seasons and areas, most of the Arctic nowadays bears witness to a very different picture.

As satellite records since 1979 show, the Arctic sea-ice cover has been undergoing a substantial retreat since the late 20th century. According to satellite estimates by NASA, September sea-ice extent has declined by about 50 % since 1979 (Fetterer et al., 2017). While the areal estimates from early ship-based observations are often restricted to what seamen had logged while moving along the ice edge, modern observations from space allow us to get estimates that include the sea-ice cover's interior. This way, also areas of open water within the sea ice-covered area can be detected and taken into account when the total sea-ice area (SIA) is determined. These regionally resolved images from a birds-eye perspective empower us to better track how sea ice changes on these finer scales. Not only does this allow for a more precise estimate of the sea-ice cover, but one also finds that changes in this white lid on top of the ocean do not proceed at the same rate everywhere and in every season.

This ongoing retreat of the once so solid "eternal ice" has vast implications on the environment, fauna, society, and industry; the firm ice cover, which used to reach all the way to the coast, no longer protects the land masses, promoting erosion of entire coastlines (Overeem et al., 2011; Barnhart et al., 2014). Whole species are moving due to increasing water temperatures and changing feeding conditions (Moore and Huntington, 2008; Davidson et al., 2020). Indigenous people from different regions in the Arctic report on aggravated hunting conditions, facing difficulties in driving across the sea ice to get to their hunting territories because the ice is either gone or too thin (Meier et al., 2014; Rolph et al., 2018; Huntington et al., 2022). The same applies to animal predators that rely on the sea ice as their hunting ground.

In addition to the sea ice decline caused by warming temperatures, feedback mechanisms in the system, such as ice-albedo feedback, lead to self-amplifying processes that can even accelerate these developments (Serreze and Barry, 2011; Pithan and Mauritsen, 2014; Hankel



and Tziperman, 2021). Due to the intricate interplay of physical processes, such feedback mechanisms lead to the Arctic warming at a rate of up to four times faster than the global average, as was recently laid out in a study from Rantanen et al. (2022, Figure 1.1 a). However, even this amplification of the increase in Arctic temperatures has a seasonal dependency, leading to rates of changes that are differently pronounced throughout the year (Figure 1.1 b).

Furthermore, increasingly present open-water areas promote the uptake of atmospheric CO₂ (e.g. Anderson and Kaltin, 2001; Bates and Mathis, 2009; Qi et al., 2022) by seawater that has long been undersaturated compared to the atmospheric CO₂ concentration levels due to the isolation of the ocean from the atmosphere by the solid ice cover. This increased uptake of CO₂ enhances what is known as ocean acidification with severe consequences for the oceanic ecosystems and the food chain (e.g. Orr et al., 2005; Søreide et al., 2010; Hunt et al., 2014).

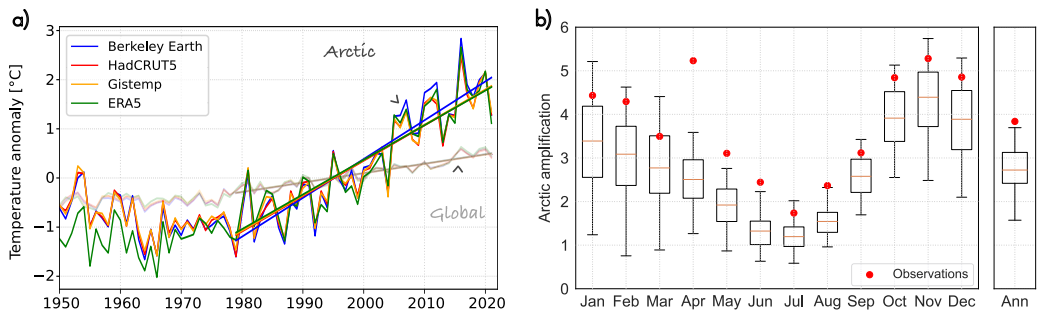


Figure 1.1: (a) Time series of global average (faint colors) and Arctic average (dark colors) near-surface temperature anomalies (relative to 1981–2010) for various observational data sets (adapted Fig. 1a from Rantanen et al., 2022). Straight lines mark the linear temperature trends for the period 1979–2021. (b) Seasonality of the Arctic Amplification calculated for 1979–2021. Red circles indicate the observed average from the four observational data sets listed in (a). The box plots represent the Arctic Amplification estimates from CMIP6 model simulations (adapted Fig. 5 from Rantanen et al., 2022).

1.2. WHY WE NEED A REGIONAL PERSPECTIVE

In this thesis, I focus on regional studies of two key components of the Arctic system: sea ice and the oceanic carbon cycle. The question of why a large-scale average view of the Arctic is not sufficient to understand the system's behavior can be answered by looking at the regional characteristics of the Arctic domain: The Arctic is a complex area with multiple oceanic basins, shelves along the coast, archipelagoes and islands, and straits that connect the high-latitude Arctic Ocean with the lower-latitude Atlantic and Pacific (see Figure 1.2). These ge-

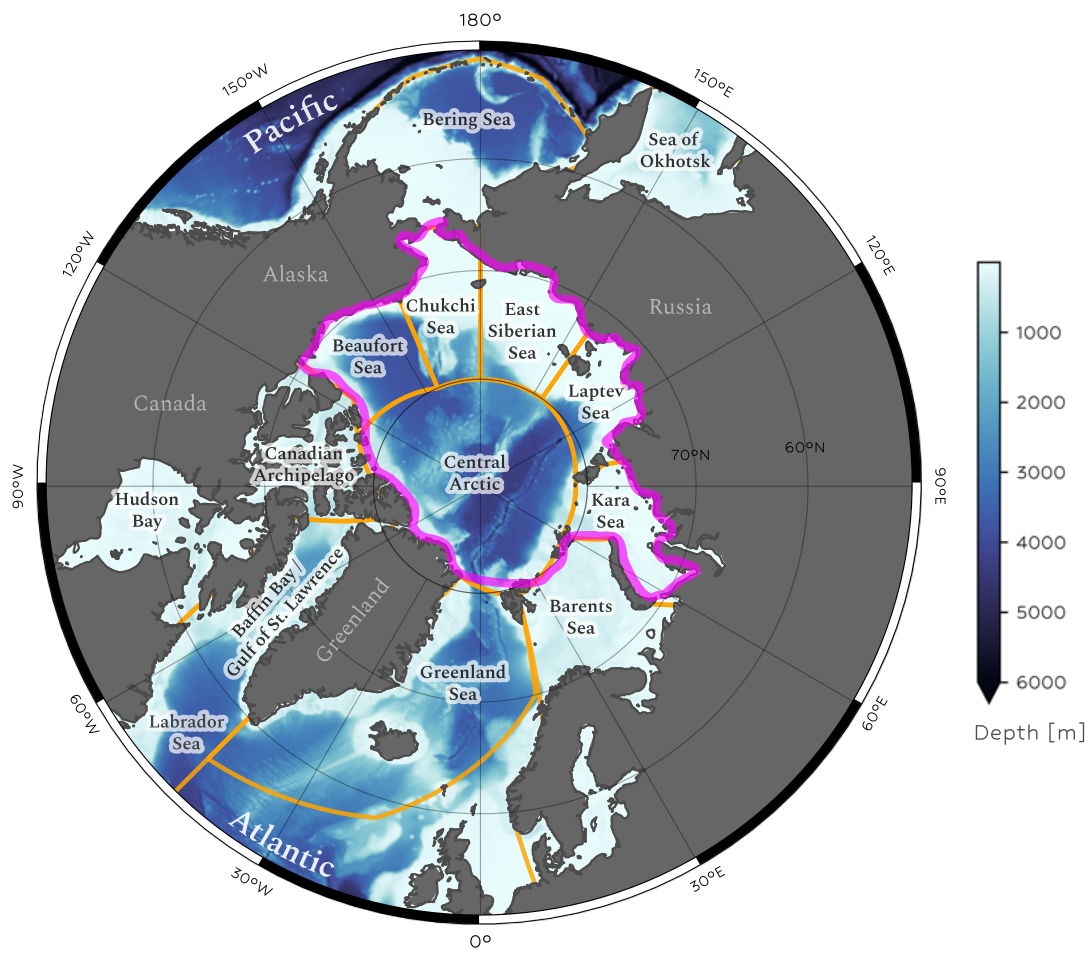


Figure 1.2: Bathymetric map of the Arctic with an overview of the different Arctic regions used in this study. The magenta line separates the high Arctic from the sub-Arctic. The orange boundaries indicate the individual regions based on ocean basin segments.

Regions of the high Arctic: Central Arctic, Beaufort Sea, Chukchi Sea, East Siberian Sea, Laptev Sea, and Kara Sea.

Regions of the sub-Arctic: Bering Sea and Sea of Okhotsk on the Pacific Side. Barents Sea, Greenland Sea, and Labrador Sea on the Atlantic side, alongside Baffin Bay / Gulf of St. Lawrence, Hudson Bay, and the Canadian Archipelago.

Bathymetric data used from GEBCO Compilation Group (2022).

ographic features have significant implications for the distribution of water masses and heat, but also for winds, the formation of clouds, precipitation, and lateral exchange processes (Serreze and Barry, 2014).

The rapid cooling of warm, low-latitude water masses entering the Arctic Ocean via the Atlantic and Pacific openings, combined with the formation of sea ice, leads to cold, dense water masses sinking to the ocean floor and spreading out along the Arctic shelves (Aagaard and Carmack, 1989). In addition, wind and ocean currents drag the sea ice around, leading to a heterogeneous distribution of sea ice across the Arctic Ocean. The Fram Strait, for example, which connects the Arctic



Ocean with the North Atlantic, is a key region for wind-driven sea-ice export in the East Greenland Sea (e.g. Martin and Wadhams, 1999; Tsukernik et al., 2010).

The ongoing accumulation of anthropogenic carbon emissions and the resulting increase in atmospheric temperatures lead to a progressing retreat of the Arctic sea ice cover, giving rise to different environmental impacts. Coastal regions that used to be protected by the sea-ice cover are now exposed to the open ocean, resulting in coastal erosion and, hence, loss of landmasses and carbon input into the sea (Nielsen et al., 2020, 2022). However, the retreat of the sea ice from the coasts also has manyfold industrial and societal impacts; coastlines and harbors become more easily accessible, promoting the shipping industry and tourism (Smith and Stephenson, 2013; Lasserre, 2019; Lasserre and Faury, 2019; Wei et al., 2020). At the same time, indigenous people and their hunting traditions become endangered as the sea ice gets thinner or disappears entirely (Sellheim, 2019; Huntington et al., 2022).

But also regions off the shore are experiencing enormous changes. Oceanic regions that used to be covered by sea ice are now exposed to the atmosphere, leading to enhanced heat and gas exchange (Steiner et al., 2013; Parmentier et al., 2013). This has severe consequences on whole ecosystems as the distribution of marine species changes (e.g. Moore and Huntington, 2008) but also because the enhanced acidification of the ocean leads to stark alterations of the carbonate system, thereby affecting ecosystems and the food web. Not least, these changes in the carbonate system may have a significant impact on the Arctic's role in the global carbon cycle (e.g. Bates and Mathis, 2009; Friedlingstein et al., 2022).

Despite global warming being a global phenomenon, its impacts and consequences are primarily apparent on a regional scale, thereby being highly diverse and hard to quantify. Hence, it is crucial that we find metrics and tools to describe these changes on a regional scale in order to better understand the processes at play and to be able to make predictions about future developments. Many studies have been published describing the Arctic's state from a large-scale average perspective. However, with high-resolution satellite imagery and the fast-progressing development of high-resolution climate models, it is time to move beyond and put regional studies more into focus.

With this work, I want to contribute to a better understanding of the Arctic's system by investigating the regional evolution of sea ice and how it responds to global warming alongside oceanic surface CO₂ as a critical indicator for changes in the oceanic carbon system. The work focuses on regional and seasonal changes in sea-ice coverage and oceanic surface partial pressure of CO₂ (pCO₂), which is a crucial quantity driving the exchange of CO₂ between ocean and atmosphere. However,

instead of looking only at specific regions from an isolated view, I keep the Arctic domain as a whole in mind and investigate regional changes in the context of the larger scale.

1.3. THE IMPLICATIONS OF CLIMATE CHANGE ON ARCTIC SEA-ICE RETREAT

The continuing retreat of Arctic sea ice has become a key indicator of human-induced climate change. While most studies have long focused on the pan-Arctic average sea-ice cover and mainly on September sea ice, regional studies have gained increasing attention over the past few years.

Of these regional studies, most concentrate on changes in the sea-ice extent over time or use spatio-temporal signal processing techniques, such as EOF analysis, to investigate the spatial patterns of sea-ice variability. While the first approach mainly describes the temporal changes and often entirely neglects the physical processes at play, the latter approach has a few limitations for investigating long-term changes in sea ice cover. This is because techniques such as EOF analysis rely on the assumption of having a static pattern that varies in its amplitude over time, whereas sea ice extent, on the other hand, not only exhibits a strong seasonal cycle with a spatially heterogeneous distribution but also changes its spatial pattern over time. However, EOF analysis can be a powerful tool for getting a first impression of the variability patterns in spatio-temporal data.

While there is no problem with time series analysis *per se*, such investigations exhibit one major shortcoming: They point out the temporal evolution of the subject of interest, thereby relating it to human-induced global warming. However, anthropogenic climate change is not simply a function of time but most of all a question of how much carbon we emit in a given period of time.

Notz and Stroeve (2016) were the first who put the decline of Arctic sea-ice area into context with anthropogenic CO₂ emissions. Following their line of arguments, anthropogenic CO₂ emissions lead to an increase in downwelling atmospheric longwave radiation, which, in turn, results in a northward retreat of the sea-ice edge. In their study from 2016, they found that changes in Arctic sea-ice area are linearly related to cumulative anthropogenic CO₂ emissions—a relation that is commonly referred to as *sea-ice sensitivity*. This relationship has been found to be robust and consistent across different observational records and state-of-the-art climate models (compare Figure 1.3 as well as Notz and Stroeve, 2016; SIMIP Community, 2020). While models consistently underestimate the observed sea-ice sensitivity, the estimates cover a wide range across the different models. This wide intermodel spread seems to correspond to the models' ability to reproduce the observed Arctic Amplification (Stolla, 2023).



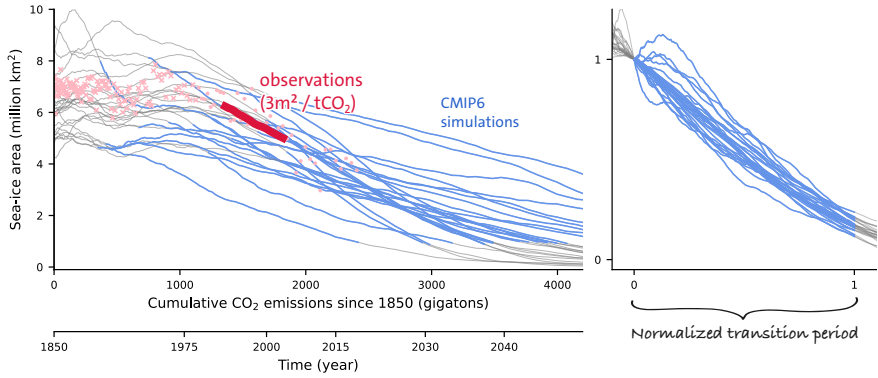


Figure 1.3: Time series of September SIA and its sensitivity to changes in anthropogenic CO₂ emissions (with permission from Stolla, 2023; labels modified). The left panel shows the data from both observations and model simulations. The thick red line marks the 30-year running average of the observations (light red markers), and the thin lines mark the 30-year running averages of the model simulations. The blue segments of the model data highlight the period in which the running average is between the 90th percent threshold and the 1 million km² minimum, defined as the *transition period* in Notz and Stroeve (2016). The right panel shows the normalized values of the model simulations, starting the transition period at $x = 0$ and ending at $x = 1$. The SIA on the y -axis was normalized such that their value at the start of the transition period is at $y = 1$.

Follow-up studies have built up on this relationship, for example, to estimate the remaining carbon budget that we have left to a certain level of global warming at which the Arctic Ocean will be practically ice-free in summer. For this purpose, the sensitivity of a specific record is calculated and then extrapolated until the sea-ice area falls below a given threshold of commonly 1 million km². Niederdrenk and Notz (2018) performed a seasonal analysis based on the findings of Notz and Stroeve (2016) and extrapolated the sensitivities of each month of the year in order to determine the respective level of global warming at which the Arctic Ocean will become ice-free.

While their results, based on the historical record, were statistically significant throughout the entire seasonal cycle, long-term model studies often predict a change in the sensitivity pattern for high CO₂ concentrations. Li et al. (2013) simulated a gradual increase of the atmospheric CO₂ concentration up to 1112 ppm, keeping the concentration constant for a couple of thousand years, and then gradually decreased it again. In the response of March sea-ice area, they found a rapid transition from an ice-covered state to an ice-free state once the northern-hemispheric annual-mean surface temperature has increased by around 8 K. Although there has been discussion about this phenomenon, it is still under debate whether or not this “kink” in these model runs indicates a breakdown of the linearity at high CO₂ concentrations.

To get a better understanding of how and why the sensitivity of the sea-ice cover to global warming changes on a seasonal and regional level, I performed sensitivity analyses on different satellite products of sea-ice area (SIA) estimates alongside re-analysis of atmospheric near-surface temperature (TAS). Starting from investigating the seasonal cycle of pan-Arctic SIA sensitivities to changes in the global mean TAS, I pursue a series of research questions that have arisen in the study process.

From the pan-Arctic perspective, I find that there is a distinct separation between a high-variable summer and a low-variable winter season. Therefore, the first question I pursue is about the processes causing this separation of the seasons. I find that geographic blocking of the sea-ice edge is mainly responsible for both the separation of the seasons and the low variability in winter.

To better understand the geographic blocking, I then focus on the region where the blocking occurs, namely the coastline of the high Arctic Ocean. This land–ice transition zone is of high importance for various stakeholders, such as indigenous people and the shipping industry, but also for animals living in these areas and depending on the seasonal presence of sea ice. Additional impacts on the coasts, such as coastal erosion, are also of high interest. Therefore, a better understanding of the blocking effect is key for a regional research perspective on coastal and offshore sea-ice dynamics and for better future predictions.

As a next step, I investigate the timing of when these blocking and detaching events happen. By determining the day of the year when these events occur, I find that the blocking and the detaching change linearly with increasing global temperatures, decreasing the length of the season during which the sea ice is blocked by the coast.

These blocking and detaching events occur on a highly regional scale and also affect the sea-ice sensitivities in different regions of the Arctic Ocean. Therefore, as a final step, I examine the characteristics of sea-ice sensitivities for different regions. I find that the linear relationship between changes in sea-ice area and global mean atmospheric near-surface temperature holds also on this regional scale, and I identify regions that are most likely subject to near-future sensitivity changes.

1.4. THE OCEANIC CARBON CYCLE IN THE ARCTIC

Human-induced climate change also affects the oceanic carbon cycle. Ocean acidification, which results from changes in ion concentrations in seawater due to changes in the carbonate system, has dire impacts on oceanic ecosystems and the entire food chain. Therefore, getting a clearer picture of the dynamics and changes in the Arctic's oceanic carbon cycle is of utmost interest to various stakeholders.

The oceanic carbonate system can be altered by various processes. These include the direct exchange of carbon dioxide (CO_2) between



ocean and atmosphere, the uptake of CO₂ by phytoplankton during photosynthesis and its release due to respiration, and the dissolution of CO₂ in seawater. One distinguishes commonly between physical, biological, and chemical processes. Whereas physical gas transfer of CO₂ directly changes the concentration of the aqueous carbonate species, other drivers rather shift the balance between the different species, leading to a new equilibrium state (Sarmiento and Gruber, 2006; Millero, 2013).

For CO₂ to be able to exchange between ocean and atmosphere, different drivers are at play. Generally, the flux of CO₂ across the air-sea interface is described as a function of the so-called transfer velocity and the partial pressure gradient of CO₂ ($\Delta p\text{CO}_2$) between ocean and atmosphere (Sarmiento and Gruber, 2006; Millero, 2013):

$$F_{\text{CO}_2}^{\text{ocean-atm}} = k \cdot (p\text{CO}_2^{\text{ocean}} - p\text{CO}_2^{\text{atm}}) = k \cdot \Delta p\text{CO}_2 \quad (1.1)$$

While the transfer velocity k depends on various factors and is generally a function of the wind velocity, the partial pressure gradient is the key indicator determining the direction and magnitude of the CO₂ flux.

Although many studies focus on the flux itself, quantifying it accurately is very difficult as the equation needs precise estimates of wind and ocean current velocities, which are commonly hard to obtain on a larger scale. Since large parts of the Arctic are also covered by sea ice, which effectively impedes the CO₂ gas exchange between ocean and atmosphere, I focus instead on the partial pressure of oceanic CO₂ ($p\text{CO}_2$) as a key indicator for the oceanic carbonate system. Knowledge of the $p\text{CO}_2$ also allows for estimates of the exchange potential should the ice disappear at some point.

However, sea ice does not only directly affect the CO₂ exchange by modulating the flux. During its growth and decay, brine drainage and meltwater flushing lead to a redistribution of carbonate species and alter certain seawater properties, affecting the oceanic carbonate system and hence the oceanic $p\text{CO}_2$ (Grimm et al., 2016; Moreau et al., 2016; Thomas, 2017).

When sea ice forms, various components of the carbonate system, in particular, dissolved inorganic carbon (DIC) and total alkalinity (TA), are first incorporated into the ice and then rejected along with the brine during the freezing process (Shcherbina et al., 2003; Rysgaard et al., 2007; Notz and Worster, 2009; Rysgaard et al., 2009). Biological activity in and under the ice leads to consumption of CO₂, even more so when the ice is absent and sunlight is abundant, stimulating photosynthetically active organisms. The presence and absence of sea ice naturally also affect the seawater temperature and the salinity, both inducing chemical changes in the $p\text{CO}_2$ (Millero et al., 2006; Millero, 2013).

However, we still lack detailed knowledge of the magnitude and direction of these processes in the Arctic despite having a fairly good

Table 1.1: A non-comprehensive overview of various studies trying to estimate the annual carbon flux of the Arctic Ocean. Uncertainties are given as absolute deviations (same units).

Study	Flux estimate [Tg C/yr]
Bates and Mathis (2009)	66 to 199
Manizza et al. (2013)	58 ± 6
MacGilchrist et al. (2014)	166 ± 60
Yasunaka et al. (2018)	180 ± 130
Manizza et al. (2019)	153 ± 14

qualitative understanding of the mechanisms involved. Determining the dynamics of these processes quantitatively, especially on a larger regional scale, is highly challenging, particularly in these high-latitude regions where sea ice inhibits long-term observations, both in situ and remote. Consequently, the estimates of these processes and the resulting CO₂ fluxes are often highly uncertain (Friedlingstein et al., 2022). This is apparent in a multitude of studies that appeared over the last decade and gave estimates for the carbon flux over the Arctic Ocean ranging from around 50 Tg C/yr to 300 Tg C/yr (compare Table 1.1). Even more so, most of the available estimates stem either from pointwise observation studies or from regional model studies. To date, it remains challenging to find reliable estimates of the as-is state of the Arctic Ocean's carbon cycle.

However, there is light on the horizon. Recent advances in techniques to fill sparse data sets allow now for more detailed regional investigations. Over the past years, multiple such products have been published, providing large-scale continuous fields of sea surface pCO₂. These products have been proven successful on a global scale and in low-latitude areas. So far, however, there has been no comprehensive study on the Arctic Ocean's domain.

Yasunaka et al. (2023) published a synthesis report considering a wide selection of both models and observation-based data products in which they lay out the present state of the Arctic Ocean's pCO₂ field. Taking the average of each sub-group of the data sets, they demonstrate how the observation-based data products compare against assimilation models and hindcasts. While one of their concluding remarks is that uncertainties across the estimates remain large, they do not discuss nor quantify how large the uncertainties across the individual estimates are, where the estimates are based on different techniques and proxies to fill missing values in the pCO₂ field.

To my knowledge, no study to date has been evaluating the quality of these estimates in the Arctic, making it hard to build confidence in these data products. Hence, in the second part of my thesis, I want to in-



vestigate regional and seasonal characteristics of the carbonate system in the surface ocean of the Arctic. I focus on the partial pressure of CO₂ (pCO₂) as a key variable of the oceanic carbonate system and explore two observation-based data products that rely on different techniques to fill the gaps in the observations. More details on the data products can be found in the Infobox 3.1 in chapter 3 (page 24).

From a first analysis, I find a general increase of the surface ocean pCO₂ in most regions of the Arctic Ocean, consistently captured by both data products. However, regional differences are large between the two data products. Therefore, as a next step, I separate the spatial and the temporal information by performing an EOF analysis.

Here, I found that I can distinguish the variability in the surface ocean pCO₂ by two larger domains, namely the sub-Arctic and the high-Arctic domain. From the temporal evolution of the variability patterns in these two domains, I identify the drivers that are most dominant and responsible for the pCO₂ variability in either of the two domains.

The results from my EOF analysis and a long-term model study by Orr et al. (2022) let me look deeper into the seasonality of the pCO₂. Hence, as a final step, I analyze the timing of seasonal maxima and minima to explore shifts in the seasonality pattern. I also study how the intra-annual amplitude of the seasonal cycle changes over time and whether or not there is a trend that can let us make conclusions about future changes.

1.5. STRUCTURE OF THIS THESIS

After this introduction, I continue with two chapters dedicated to the above-outlined research subjects: Chapter 2 focuses on seasonal and regional changes in Arctic sea-ice cover and how they relate to global warming, and chapter 3 investigates regional characteristics of oceanic surface pCO₂ in the Arctic Ocean. In each chapter, I present and discuss the results of the studies I have conducted on this matter. The study blocks resulted in two manuscripts, both planned for submission and included in the appendix of this thesis (page 39 ff.). After the two following chapters, I conclude with a summary of my findings and a statement about the implications of my studies for future Arctic Ocean research.

2

THE RESPONSE OF ARCTIC SEA-ICE AREA TO GLOBAL WARMING

2.1. SEA-ICE SENSITIVITY

In 2016, Notz and Stroeve published a study in which they linked the long-term loss of Arctic sea ice to the increase in cumulative anthropogenic CO₂ emissions. They stated that, in order to keep the surface energy balance closed, the ice edge needs to move northwards as the incoming non-shortwave radiation increases as a consequence of increasing anthropogenic CO₂ emissions. Notz and Stroeve (2016) found that the observed decline of September sea-ice area (SIA) correlates linearly with cumulative anthropogenic CO₂ emissions. Via linear regression analysis, they determined the sensitivity to be around 3 m² per metric ton of emitted CO₂ in the observational record. The linear nature of this relationship has been found to be a consistent feature of both different observational data sets and state-of-the-art climate models, although the latter have a strong tendency to underestimate the observed sensitivity (e.g. Winton, 2011; SIMIP Community, 2020).

Subsequently, several studies have used this relationship to extrapolate the future evolution of Arctic SIA in order to predict the year in which the Arctic will eventually become ice-free. Niederdrenk and Notz (2018) eventually conducted a follow-up study based on observational and model data, covering the period until 2100, and investigated the relationship between SIA and global atmospheric near-surface temperature (TAS) also for months other than September. Despite their finding that the linear relationship is a robust feature throughout the entire seasonal cycle, with a general tendency of the simulations to underestimate the observations, a more thorough investigation of the changes in sensitivities over the year is still lacking.

In addition, different model studies have investigated the long-term response of Arctic SIA to rising CO₂ levels on a millennial scale. Some of these studies also focused on the difference between summer and winter sea ice (commonly September and March), thereby finding that the sensitivity of winter SIA rapidly increases at a certain level of atmospheric CO₂ concentration (e.g. Armour et al., 2011; Li et al., 2013; Bathiany et al., 2016). Although the event of this “rapid ice loss” is a common feature of these studies, there is still disagreement about its triggers, requiring further investigations.

To better understand the seasonal dependency of Arctic SIA sensitivities, I started my investigation by examining the seasonal cycle in more detail. For this first step, and before trying to link any changes to



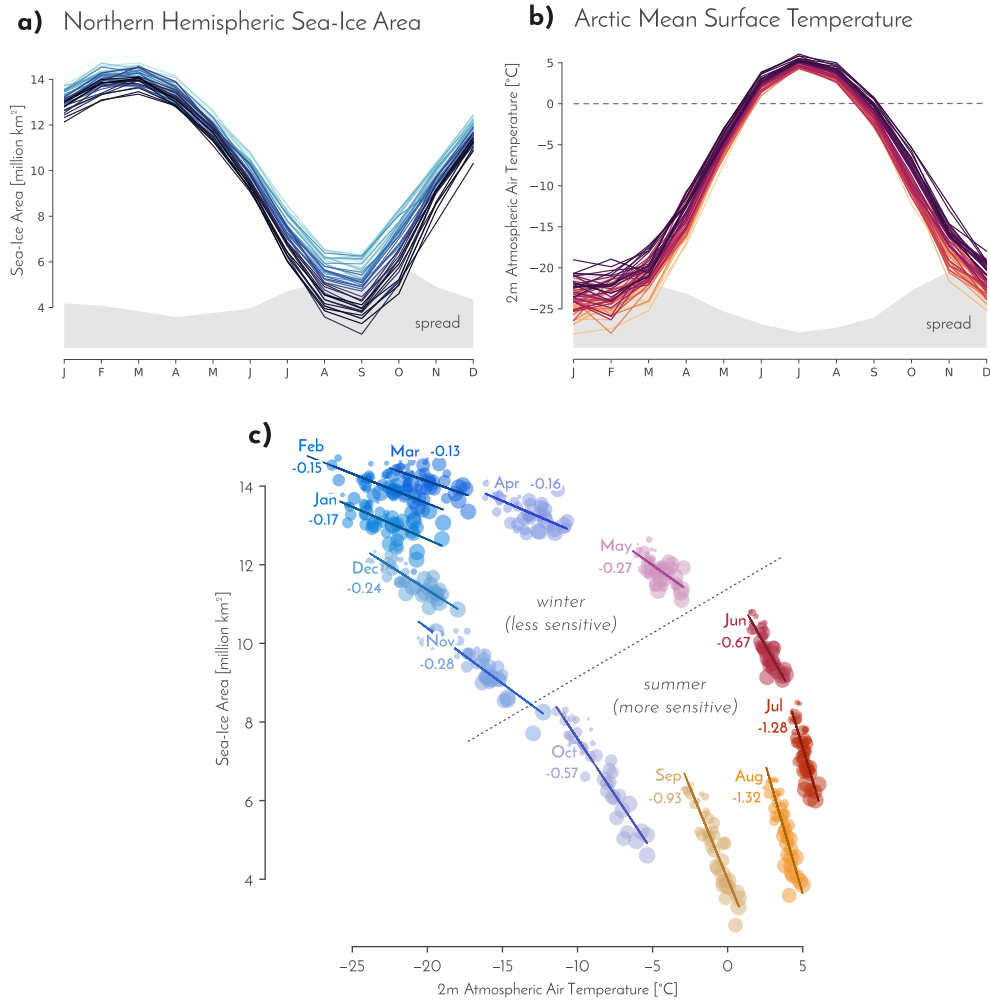


Figure 2.1: (a) and (b) show the seasonal cycle of NH SIA and Arctic mean TAS and its change over time. Darker line shadings represent more recent time steps. The grey-shaded area represents the spread in the respective month across the entire time series from 1979 to 2022. (c) shows monthly sensitivities of NH SIA to Arctic mean TAS. Values denote the respective seasonal sensitivity in million km²/°C. Markers of one month share the same color, increasing their size over time. The transitions around May/June and October/November mark the breakpoints, separating the seasonal cycle into a winter and a summer season.

global warming, I first computed sensitivities with respect to changes in the Arctic average TAS, as this is the temperature the ice ultimately responds to (Figure 2.1). The infobox 2.1 provides more details about the SIA and TAS data sets I used for this study. Combining the time series of both quantities, northern-hemispheric (NH) sea-ice area (Figure 2.1 a) and Arctic atmospheric near-surface temperature (Figure 2.1 b), I derived sensitivities for each month of the year (Figure 2.1 c).

Assuming a perfect linear relationship between SIA and TAS, one would expect all the points in Figure 2.1 (c) to be scattered around

Infobox 2.1: Data sets used for this study

Sea-ice area (SIA)

In this study, I used three different observational estimates of sea-ice concentration (SIC): NASA Team (Cavalieri et al., 1984, 1997), NASA Bootstrap (Comiso, 1986, 1995), and OSI-SAF (Lavergne et al., 2019; OSI SAF, 2017). Sea-ice area is computed by multiplying the respective sea-ice concentration with the area of the grid cell. This is a common approach.

NASA Bootstrap is known to maximize sea-ice concentration wherever possible, whereas NASA Team tends to underestimate the true sea-ice coverage. OSI-SAF often lies somewhere in between the other two products. In the text, if not declared otherwise, I will typically refer to the ensemble mean of the three SIC data sets as observations of SIA.

Atmospheric near-surface temperature (TAS)

For the temperature-related sensitivity analyses, I use the near-surface temperature data from the ERA5 reanalysis project (Muñoz Sabater, 2019; Hersbach et al., 2020), and the anomalies estimates from GISTEMP dataset (GISTEMP Team, 2023) and from HadCRUT (version 4, Morice et al., 2012).

ERA5 has a meridional resolution of 31 km and is retrieved from the *Copernicus Climate Data Store*. The GISTEMP anomalies are on a $2^\circ \times 2^\circ$ regular latitude-longitude grid. The HadCRUT data set combines land (CRUTEM4) and ocean sea-surface temperature (SST) anomalies (HadSST3) provided on a $5^\circ \times 5^\circ$ regular grid.

a straight line. However, what stands out at first glance is the quasi-circular shape of the seasonal cycle, followed by the fact that winter-month sensitivities are all relatively close to each other and rather weak compared to summer-month sensitivities. Another striking feature is the substantial increase in sensitivities toward summer and the also substantial but more gradual decrease toward winter.

These two seasonal transitions can be assigned to two breakpoints in the seasonal cycle: the transition between May and June and the transition between October and November. I found that these breakpoints are also apparent if I consider other domains for the independent variable (temperature), such as northern-hemispheric or global temperature, although changes are not as pronounced as with Arctic temperature due to Arctic Amplification.

A note on the computation of sensitivities: To obtain sensitivities, I used the monthly mean values of the respective SIA data sets and performed linear regression statistics against TAS. Sensitivities are hence expressed in million $\text{km}^2/\text{ }^\circ\text{C}$. The linear regression is usually computed first for each individual data product combination (sea-ice area and temperatures) and then averaged over the resulting values. Also, I use the terms “high” or “large” sensitivities in the rest of this work for large absolute values even if the actual values of the regression slopes are negative (declining SIA with increasing TAS). The analog holds for low absolute values.



2.2. GEOGRAPHIC MUTING AS A DRIVER OF SENSITIVITY CHANGES

To understand the mechanisms behind these transitions between winter and summer sensitivities, I studied the breakpoints in May/June and October/November in more detail. By looking at satellite records of the time steps at which the transition between winter and summer occurs, I found that the timing of these transitions coincides with the blocking of the sea ice by surrounding land masses.

When sea ice is expanding in winter, coastlines of the land masses surrounding the Arctic Ocean block the southward expansion of the sea-ice edge, thereby dampening changes in the winter sea-ice extent—an effect Eisenman (2010) introduced as “geographic muting”. In summer, on the other hand, this effect is minimal as the sea-ice edge barely reaches the land masses. This effect also seems to cause the observed changes in sensitivities over the year.

In this study, I systematically investigated for the first time what time of the year the blocking effect takes place and how its occurrence changes over time. This can give us confirmation of Eisenman’s blocking hypothesis and, more importantly, an understanding of how the event of blocking and detaching of the sea-ice edge from the coast affects the seasonal changes in SIA sensitivities.

To identify the timing of the blocking and detaching of the sea-ice edge, I proceeded as follows: First, I created a mask of the coastline that surrounds the Arctic Ocean (compare Figure 2.2 b). I refer to this as the *Arctic perimeter* in the following. Then, I considered grid cells along this coastline as “blocked” if they show a value of at least 95 % of sea-ice concentration (SIC). Counting grid cells that exceed this threshold and dividing this number by the total number of grid cells in the Arctic-perimeter mask results in a time series of fractional values, representing how much of the Arctic-perimeter coastline “blocks” the body of Arctic sea ice at any given time step.

Plotting these time series for each month of the year, I find my assumption confirmed (Figure 2.2 a); the changes I observed in the seasonal cycle of sensitivities coincide indeed with the transition between the Arctic perimeter being largely covered and the Arctic perimeter being largely ice-free. Performing the above with monthly data reveals a pronounced transition in the coverage of the Arctic perimeter between May and June (detaching of the ice edge from the coast) and between October and November (attaching of the ice edge to the coast and subsequent blocking of the ice).

However, when we look at Figure 2.1 (c) again, we figure that the transition between summer and winter occurs at different levels of sea-ice area. Toward winter, this occurs at around 8 million km², corresponding to the ocean area enclosed by the Arctic perimeter. Toward summer, on the other hand, the transition occurs at a value larger than

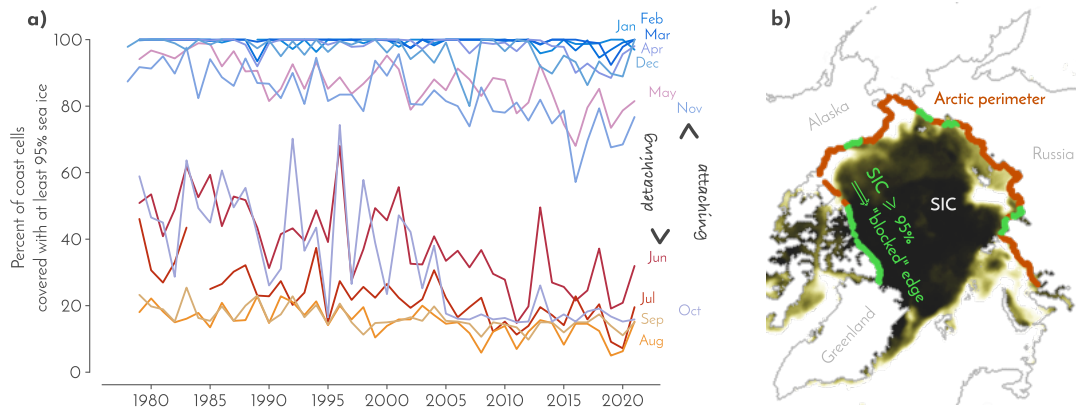


Figure 2.2: Blocking of the sea-ice edge along the Arctic perimeter. (a) shows time series for each month depicting the fraction of the Arctic perimeter that is blocked by the sea-ice edge. (b) shows the Arctic perimeter mask (dark orange, exaggerated thickness for display purpose) and segments in which the SIC (yellow to black shadings) is above 95 % (light green). The cells in these segments are eventually counted and divided by the total amount of cells covered by the Arctic perimeter mask to result in the time series plotted in (a).

10 million km². This may seem contradictory to the blocking hypothesis at first. However, I argue that this effect is a consequence of the following two mechanisms:

First, while growing a certain area of sea ice demands relatively little energy withdrawal, melting the same area requires a much higher energy input since the ice has become thicker over winter (Massonnet et al., 2018). This difference in the pace of growth versus melt results in different monthly mean values around when the blocking or detaching occurs. After summer, the ice edge can move freely first, reaching the Arctic perimeter with a sea-ice area of around 8 million km². Since the areal changes per day are relatively large up to this point due to a high growth pace, the attaching and subsequent blocking are expected to take place around this value. On the other hand, during the melting season, the areal fraction that disappears every day is much smaller compared to the areal gain that happens during the cold season. The resulting monthly mean is, therefore, relatively high.

Second, during winter, ice has also grown in regions further south of the Arctic perimeter. While the ice edge is, in general, assumed to retreat toward the Arctic perimeter over the course of the melting season, some of these southern regions lose their winter sea ice only later in the season. This is particularly true for the Baffin Bay and the Canadian Archipelago. Consequently, the total Arctic SIA is still relatively high when the detaching occurs.

Paying attention again to the time series in Figure 2.2 (a), it also appears that the May and November time series start to branch off the



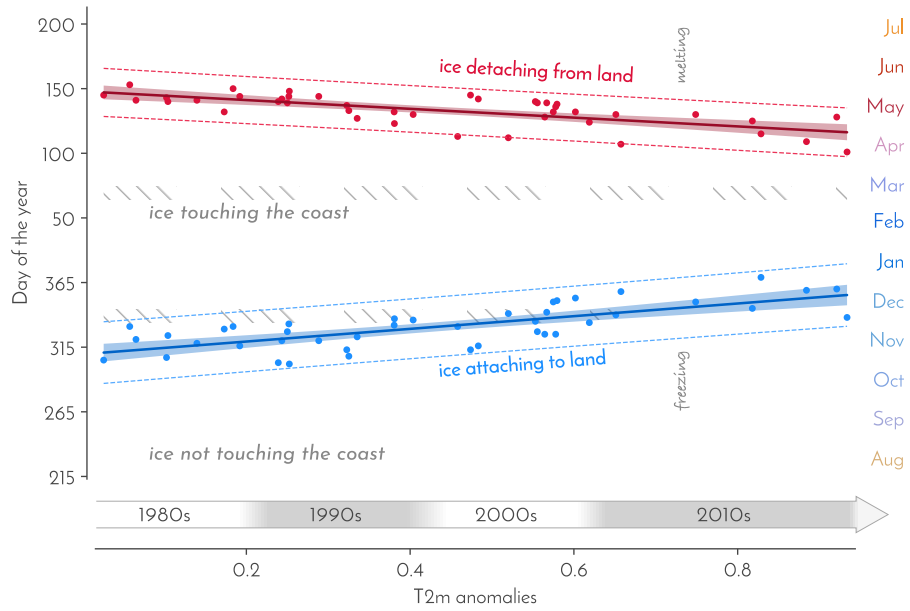


Figure 2.3: Day of the year at which the sea-ice edge attaches to and detaches from the Arctic perimeter, plotted against global mean temperature anomalies (reference period: 1961–1990). The colored shadings around the regression line represent the 95 % confidence interval of the fit, and the dashed lines the 95 % prediction interval. The gray hatchings mark the season of the year during which the Arctic perimeter fully hinders the ice edge from moving further south. Days of the year are roughly mapped to the respective months, indicated on the right. Note that the y-axis starts with August.

cluster of “high coverage” states. This indicates that the sea-ice edge is slowly retreating so far that the blocking and freeing-up shifts further into wintertime. To examine this further, I repeated the above-described analysis for daily data, which enabled me to determine the coverage state of the Arctic perimeter for each single day of the year. This way, I wanted to detect potentially existing shifts in the timing and investigate if these shifts occur gradually or are bound to a specific event.

I considered the ice edge to be blocked by the coast when at least 85 % of the Arctic perimeter is covered by sea ice according to the above definition ($SIC \geq 95\%$ in the respective grid cell). By comparing the above retrieved coverage states to this threshold and taking the first day after summer and the last day after winter when the profile is above the threshold, I determined the day of the year at which the blocking and detaching occur, respectively.

Figure 2.3 shows the results of this analysis. Since a shift in the timing would be due to the northward shift of the ice edge, and that northward shift would be caused by rising global temperatures, I plotted the days of the year at which the events occur against temperature anom-

lies. I found that the timing of the ice *attaching* to the coastline has been shifting with a rate of around 4 days per tenth degree of global warming, starting in October at the beginning of the record and ending in early December at the end of the record. Similarly, the timing of the ice *detaching* from the coastline has been shifting with a rate of around -3 days per tenth degree of global warming, starting in June at the beginning of the record and advancing into May from 2010 onward.

The sensitivity is robust and linear in each of the two cases, and I do not find any reason to assume that this will change in the future based on the mechanisms I have outlined above. From the events' progression into other seasons, it follows that the sensitivities of sea-ice area to temperature changes will change accordingly. Hence, I can say with high confidence that the rapid sensitivity change observed at high emission levels in long-run model simulations such as the one performed by Li et al. (2013) is a direct consequence of the geographic blocking effect. Rapid ice loss is expected to occur once the sea-ice edge no longer transgresses the Arctic perimeter.

2.3. THE SENSITIVITIES OF INDIVIDUAL REGIONS

For my final investigation of this chapter, I looked into the sensitivities of individual regions of the Arctic. When looking at satellite records, it seems that some regions lose their sea ice at higher rates than others. There have been a multitude of studies investigating individual regions and the physical mechanisms that drive the sea ice dynamics and that are characteristic of these regions. However, only few studies have investigated the regional signals in the scope of the overall pan-Arctic sea-ice loss. Onarheim et al. (2018) looked into the temporal evolution of the different regions of the Arctic and how they compare in the picture of the overall sea-ice loss. However, despite providing a good description of the temporal changes, their study, which is mainly based on time series analysis, neglects the physical mechanisms driving these changes.

Here, I investigate how sea ice in the individual regions of the Arctic responds to global warming and how these regions contribute to the large-scale picture. For this purpose, I performed linear regression analysis for each of the regions defined in Figure 1.2 and analyzed them in the context of the pan-Arctic changes.

I found that the linear relationship between sea-ice area and global temperature holds in general also on higher-resolved regional scales. However, one should keep in mind that regions that are limited in extent might be in a saturation state at certain times. That is, if the region is entirely ice-free or fully ice-covered for certain periods, one wants to exclude these time stamps from the regression analysis because they would bias the result otherwise. Both undersaturation (for example, when a region is constantly ice-free at high temperatures) and over-



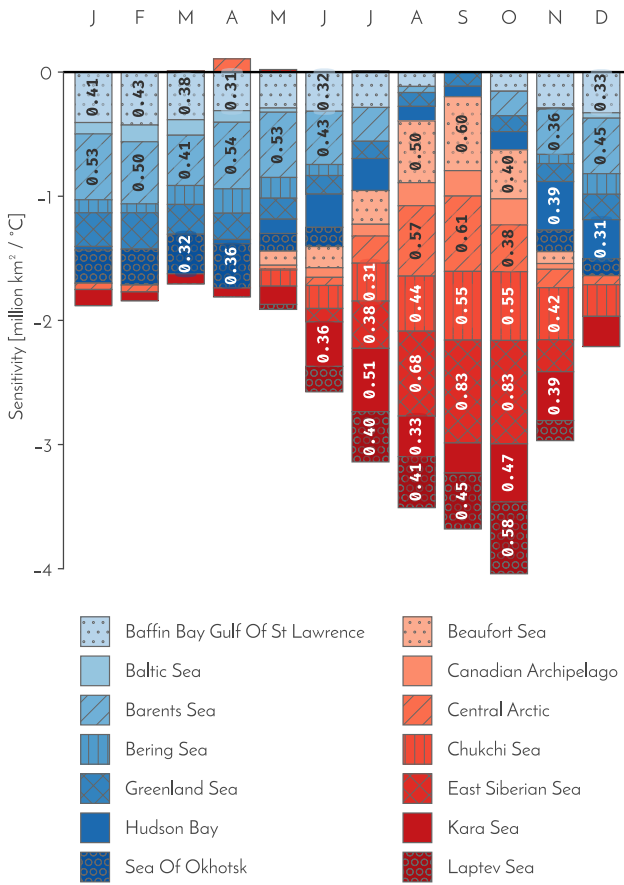


Figure 2.4: Observed sensitivities of individual regions of the Arctic (in million km² / °C). Regions are clustered by winter-active (blue colors) and summer-active (red colors) regions and ordered alphabetically within each group. Regions can be distinguished by color shadings and hatches. For regions with a sensitivity greater than 0.4 million km² / °C the respective value is annotated.

saturation (permanently fully ice-covered at low temperatures) would lead to an underestimation of the true sensitivity. Filtering the data accordingly beforehand, I calculated sensitivities for each region and most seasons, which are displayed in Figure 2.4.

The figure shows how the individual sensitivities sum up to the pan-Arctic sensitivity, reliably explaining the contribution of the individual regions to the overall signal. Regions south of the Arctic perimeter are typically characterized by higher sensitivities in winter (blue shadings in Figure 2.4) as opposed to regions further north that exhibit the strongest sensitivities in summer (red shadings).

I find the strongest winter sensitivities of -0.53 million km² / °C in the Barents Sea, followed by the Baffin Bay / Gulf of St. Lawrence and the Sea of Okhotsk. The Barents Sea is more driven by the strong Atlantic inflow than by the local air temperatures (Onarheim and Årthun, 2017; Dörr et al., 2021). However, the sensitivity to global temperatures is still statistically significant and pronounced, confirming that global

temperature is a good indicator of the overall energy in the system. Over the winter, sensitivities remain relatively constant—not only in the pan-hemispheric signal but also in the individual regions.

Toward summer, the pan-hemispheric sensitivity gradually increases due to a northward shift of the ice edge and regions like Baffin Bay and the Canadian Archipelago losing their ice cover relatively late in the melting season (as argued above). Finally, in summer, I find the highest sensitivities in the East Siberian Sea with -0.83 million $\text{km}^2/\text{°C}$, followed by the Central Arctic, the Chukchi Sea, the Laptev Sea, and the Kara Sea. The overall sensitivity keeps increasing until reaching its maximum value in October with about -4 million $\text{km}^2/\text{°C}$. Around that time, the ice edge eventually retreated north of the Arctic perimeter; meanwhile, regions further south also lost their ice cover.

The ice can now move freely within the boundaries of the Arctic perimeter. During the freezing period, the ice starts to expand until finally reaching the coastline, described by the Arctic perimeter, which blocks the ice at most points from moving further south. This is the point at which the pan-Arctic sensitivity starts to rapidly decrease again. The same is true for the summer-active regions, which are located north of the Arctic perimeter and, therefore, are subject to the blocking. Only winter-active regions exhibit increased sensitivities as they are located further south, where the ice edge can still move unhindered.

Note that, for the sake of discussing sensitivities in the framework of global warming, I use a different domain (global) for the temperature compared to what is depicted in Figure 2.1 (Arctic temperature). Since the change of the seasonal cycles differs between the Arctic and the global temperature, we obtain the maximum sensitivity at different times of the year. However, this choice of domain does not affect the timing of the breakpoints between summer and winter, underlining the blocking hypothesis's robustness.

Considering the combination of sensitivities and ice area that has already been lost over the past, I can now infer which regions will likely lose their remaining sea ice in specific seasons first. Based on my results, I expect that the East Siberian Sea, the Chukchi Sea, and the Laptev Sea are among the regions that will lose their remaining summer sea ice first. The Barents Sea will likely be the first region to experience an ice-free winter season and, therefore, be ice-free all year.



3

AN ASSESSMENT OF ARCTIC SURFACE OCEAN PARTIAL PRESSURE OF PCO₂

In this chapter, we move to the second subject, namely the Arctic's regional surface ocean pCO₂. Estimating pCO₂ of the Arctic Ocean is extremely challenging due to the sparse availability of observations and the complex interplay of various processes that influence the pCO₂ dynamics. Over the last few years, there have been growing advances in the development of techniques enabling extensive regional data coverage despite the limited availability of observations (e.g. Rödenbeck et al., 2013; Landschützer et al., 2013, 2016). A number of studies have assessed the global pCO₂ field of such estimates (e.g. Zeng et al., 2014; Rödenbeck et al., 2015; Laruelle et al., 2017), with good overall agreement between different products. However, hardly any studies have focused on the Arctic domain.

Yasunaka et al. (2023) were the first to present synthesized estimates of Arctic Ocean pCO₂ from a range of data products, including models and observation-based data products. Their study provides estimates of the historical pCO₂ alongside CO₂ fluxes as well as the annual mean CO₂ uptake and its trend over the past decades. However, large uncertainties remain based on the wide range of estimates between the different data products.

Evidently, we have not yet gained a comprehensive understanding of the relevant dynamics and processes in these high-latitude regions, resulting in this large disagreement between individual products. Getting a better knowledge of past and future regional and seasonal dynamics and processes of the Arctic Ocean's carbon cycle is hence crucial in order to complement our picture of the overall carbon dynamics in the Arctic Ocean and to increase confidence in these data products.

In order to help fill this gap, I investigated two data products that have been successfully used for global ocean studies, providing pCO₂ fields up to 90 °N. Both data products consist of pCO₂ estimates, relying on different methods to fill the gaps in the observational record (see the Infobox 3.1 for more details).

I started with a general exploration of the mean state of the Arctic Ocean's pCO₂ field and its evolution over time. This is followed by an EOF analysis to decompose the spatio-temporal variability into its dominant patterns, helping identify the dominant drivers governing the pCO₂ dynamics in the high and the low Arctic. Finally, I investigated changes in the timing of the seasonality and in the amplitude of the



Infobox 3.1: pCO₂ data sets used in this study

MPIM-SOM-FFN:

The *Max Planck Institute for Meteorology Self-Organizing Map Feed-Forward Network (MPIM-SOM-FFN)* reconstructs the sea surface pCO₂ field at a monthly 1°×1° resolution over the open ocean and, spanning the period from 1982 to 2021. The method uses a two-step neural network approach with the following inputs as proxy fields:

Variable	Source
Sea surface temperature	Huang et al. (2021)
Sea surface salinity	Good et al. (2013)
Mixed-layer depth	De Boyer Montégut et al. (2004)
Chlorophyll a	GlobColour (ACRI-ST, France)
Atmospheric pCO ₂	Global Monitoring Laboratory (NOAA, USA)
Ocean pCO ₂ climatology	Takahashi et al. (2009)

Refs: Landschützer et al. (2013, 2016) and Jersild et al. (2017)

Jena-MLS:

The *Jena-Carboscope mixed layer scheme (Jena-MLS)* is primarily based on spatio-temporal interpolation of the pCO₂ observation data from the Surface Ocean CO₂ Atlas (SOCAT) database but also compatible with the dynamics of ocean mixed-layer carbon content, that is, taking into account the buffer effect. The pCO₂ field in this product is available at a daily 2.5°×2° resolution from 1957 to 2021.

Refs: Rödenbeck et al. (2013, 2022)

seasonal cycle. The results of this analysis are presented in more detail in appendix B, and I will summarize the most critical outcomes in this chapter.

3.1. THE MEAN STATE OF PCO₂ AT DIFFERENT SCALES

Both data sets are proven to yield reliable results with respect to changes in the global ocean. However, large differences between the two data sets become apparent if we focus on higher latitudes in the North (Figure 3.1), indicating that pCO₂ changes in the Arctic are less well understood.

The annual mean pCO₂ increases between 1982 and 2021, in agreement between the two products. However, differences occur in the interannual variability and in the amplitude of the seasonal cycle (not shown). I also find that the period from 1982 to around 2005 is characterized by some anomalous features, for which I did not find expla-

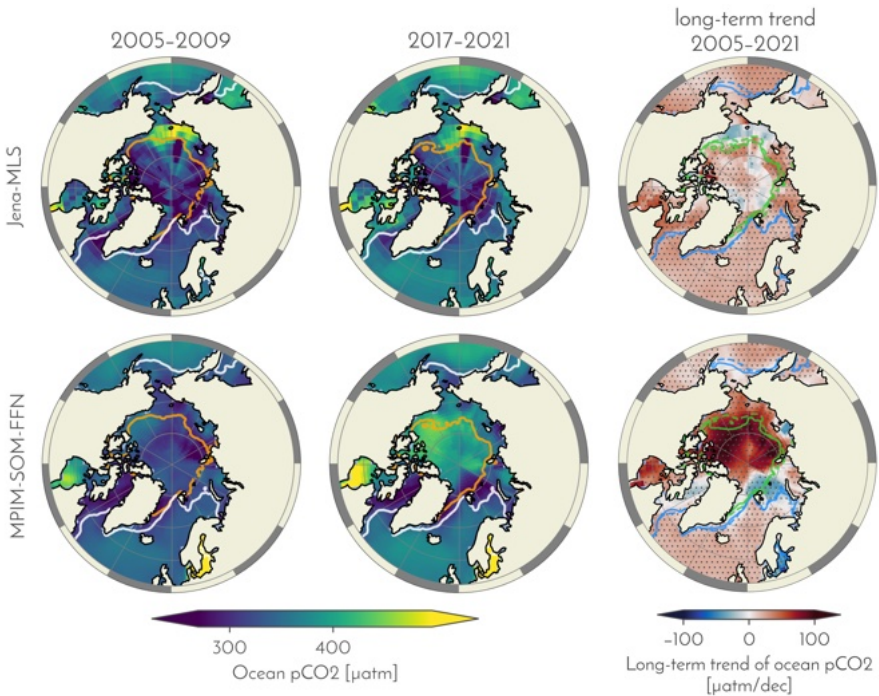


Figure 3.1: Mean states of Arctic ocean surface pCO₂ and its evolution over time. Each row shows the data of a different data set—Jena-MLS in the top row and the MPIM-SOM-FFN in the bottom row. The right-most panel shows the long-term trend of the annual mean state between 2005 and 2021. Orange (white) contour lines mark the respective average September (March) sea-ice edge (NASA Team). In the right-most panels, the solid (dashed) contour lines mark the respective states in 2005 (2021).

nations in the literature. Given the fact that most of the measurements were collected after 2005, I focus on the period after 2005 for the rest of the analysis.

Both data sets display a relatively consistent increase of the mean state pCO₂ field over this period. However, while the sub-Arctic is represented by similar long-term trends in both data sets, trends in the high Arctic are much stronger pronounced in the MPIM-SOM-FFN as opposed to the Jena-MLS. In these high-latitude and, to a large part, ice-covered regions, the trends shown by the MPIM-SOM-FFN are partly more than four times stronger than in the Jena-MLS, which exhibits no visible differences between trends in the sub-Arctic and trends in the high Arctic. Besides these large differences in the high Arctic, both data sets agree that the ocean surface pCO₂ generally increases in all regions, with notable exceptions in the vicinity of the summer sea-ice margin.



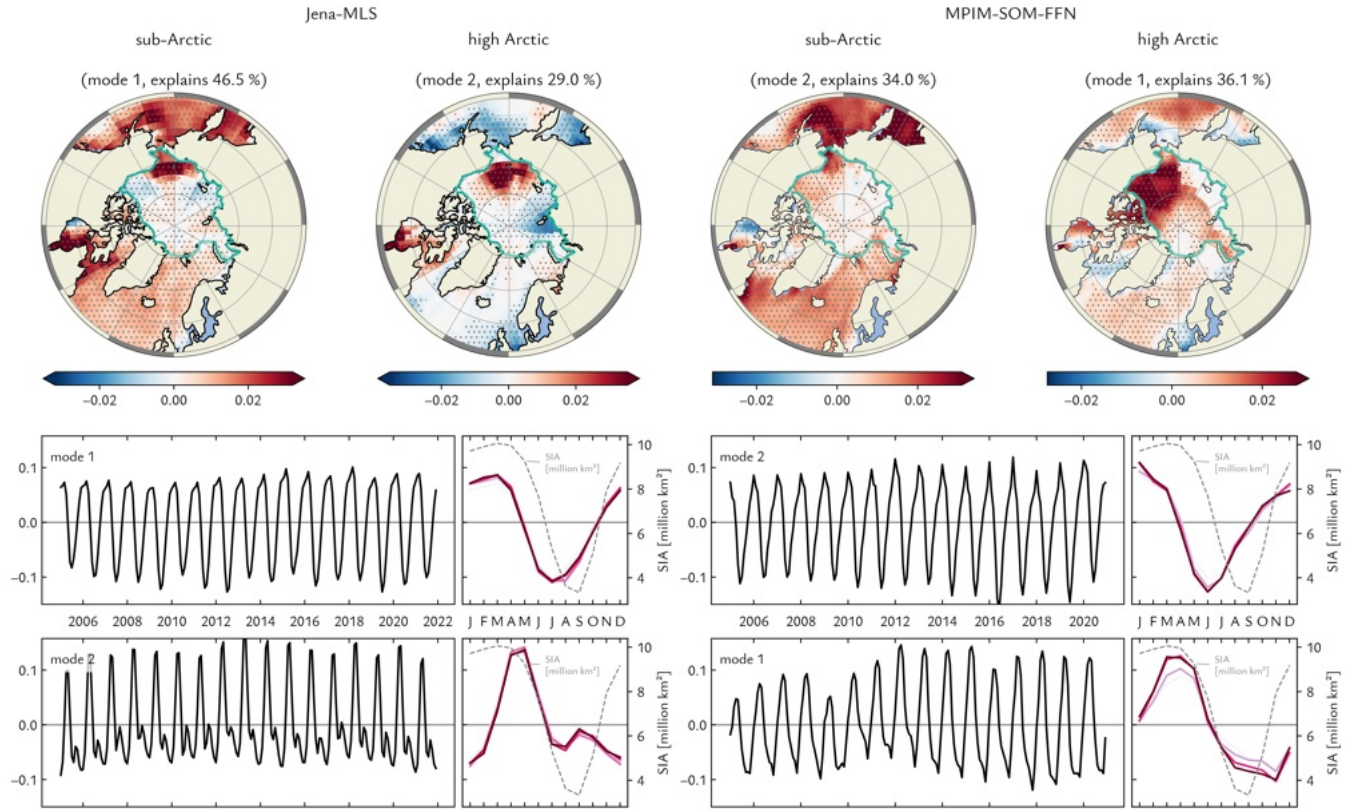


Figure 3.2: EOFs and PCs of the first two modes. The maps in the top row show the eigenvectors (EOF patterns) of the first two modes. The light-teal path marks the area defined as the *high Arctic* (also compare Figure 1.2). The time series below show the corresponding temporal evolution of these spatial variability patterns (principal components) and their respective seasonality. The shadings from magenta to black mark different periods between 2005 and 2021. Overlaid is the seasonal cycle of Arctic sea-ice area in units of million km².

3.2. DOMINATING PATTERNS IN THE HIGH AND THE SUB-ARCTIC

In the following section, I will delve into the spatio-temporal variability patterns in the two data sets by investigating the results from an EOF analysis (compare Figure 3.2). EOF analysis is a statistical tool that identifies and ranks dominant patterns of spatial or temporal variability within a data set by decomposing the data into orthogonal modes. Each mode consists of an eigenvector (a map with spatial variability patterns) and an eigenvalue (a time series describing the temporal evolution of the spatial variability patterns).

For both data sets, the first two modes explain more than 70 % of the total variance, so I will limit the discussion to these two modes in the following. For the MPIM-SOM-FFN, the explained variance of the first two modes is pretty similar to each other (36 % and 34 %), and the patterns in the eigenvector maps resemble the patterns of the complemen-

tary modes of the Jena-MLS; that is, the first mode of the Jena-MLS corresponds well to the second mode of the MPIM-SOM-FFN, and vice versa (compare the maps in Figure 3.2). Hence, I will call the first mode of the Jena-MLS and the second mode of the MPIM-SOM-FFN the *sub-Arctic related mode* and the second mode of the Jena-MLS and the first mode of the MPIM-SOM-FFN the *high-Arctic related mode*. This choice is made according to where the respective modes show the most pronounced spatial variability (compare Figure 3.2).

EOF analysis is sensitive to domain selection. For the present case, I restrict the domain to the area north of 50 °N prior to the EOF analysis. At each pixel, I removed the long-term linear trend from the monthly time series to focus on the variability of the data and filled missing values with the long-term mean. This way, these pixels can be considered by the EOF analysis without contributing to the variability. I also masked out the Baltic Sea as this area has exceptionally high pCO₂ values, especially in the MPIM-SOM-FFN, and would otherwise lead to undesired domination of the variability pattern.

The sub-Arctic-related eigenvector map in both data sets shows overall positive values for this domain (compare Figure 3.2). I find particularly high values in the Pacific inflow region and Hudson Bay. The Atlantic side, although also continuously positive, is characterized by generally lower values. The high Arctic (the area enclosed by the teal line in the eigenvector maps) is represented by relatively weak values, with partly even slightly negative values in the Jena-MLS. One exception here is the Chukchi Sea, which exhibits strong positive values in both data sets.

The temporal evolution of these spatial variability patterns is displayed by the principal component (PC) of the respective mode. The sub-Arctic-related PC exhibits a relatively symmetric seasonality profile and is strongly anti-correlated with the seasonal cycle of solar irradiance and surface temperature. Both data products agree reasonably well in this matter. The anti-correlation between the PC's seasonal profile and the solar irradiance hints at a weak temperature-driven component in the sub-Arctic related mode. I tested this assumption by performing a temperature decomposition after Takahashi et al. (1993), which confirmed that the temperature-driven component is relatively weak, accounting for less than 20 % of the total pCO₂ trend (not shown).

In contrast to SST, biological activity leads to a drawdown of CO₂ in summer when stimulated by high light abundance (e.g. Bergeron and Tremblay, 2014; Arrigo and van Dijken, 2015). When light gets scarce in winter, this mechanism is turned down. Hence, I conclude that, from the multitude of factors that potentially influence the pCO₂ dynamics in these regions, temperature is nearly negligible, and changes in the pCO₂ are mainly driven by biological activity and the physical exchange of CO₂ across the air-sea interface. Over the past, the decline of the sea-ice cover has led to longer growing seasons and hence to an



increase in net primary production (Arrigo et al., 2008; Arrigo and van Dijken, 2011, 2015), underlining the assumption that biological activity dominates here.

The high-Arctic-related mode is characterized by strong positive values in the Chukchi Sea, again with good agreement between both data sets. In the case of the MPIM-SOM-FFN, this positive field widely extends across the Beaufort Sea to the Canadian Archipelago. The Jena-MLS, in turn, shows a pretty heterogeneous field in the high Arctic with pronounced negative values in the Laptev Sea. In this region, the MPIM-SOM-FFN contains areas of missing data due to spatial gaps in one of the proxy fields (the mixed-layer depth) during the winter months. These gaps, however, are mainly attributable to areas with sea-ice cover and are treated accordingly before performing the EOF analysis.

The high-Arctic-related PC exhibits a sinusoidal seasonality with a zero crossing at mid-year. This profile coincides with the seasonal cycle of the northern-hemispheric sea-ice cover and hence hints at dynamics closely related to the seasonality of the sea ice. Since these two profiles are strongly correlated, I argue that, for the high-Arctic domain, processes resulting in a net decrease in pCO₂ dominate during the sea-ice melt season, whereas processes leading to a net increase in pCO₂ dominate during the sea-ice growth season.

Separating the spatio-temporal variability via EOF analysis revealed that the ocean pCO₂ dynamics in the Arctic are dominated by distinct patterns that can be attributed processes either mainly related to solar irradiance (in the sub-Arctic) or primarily associated with sea-ice dynamics (in the high Arctic). Particularly in the high Arctic, the two data sets show large differences in the spatial variability patterns, indicating that the pCO₂ dynamics in this region are less well understood. However, the temporal evolutions of these variability patterns, displayed by the respective principal component, resemble one another, building confidence in the regions with pronounced variability in the eigenvector maps.

While the Jena-MLS shows hardly any changes in the seasonality profile, the high-Arctic-related seasonality profile of the MPIM-SOM-FFN indicates potential for a shift in the seasonality of pCO₂ in this region. Therefore, in the next section, I will look closer into the seasonality with respect to changes in timing and amplitude.

3.3. CHANGES IN TIMING AND AMPLITUDE OF SEASONALITY

In a model study from 2022, Orr et al. found reasonable indications for future seasonal shifts. Investigating the long-term evolution of Arctic average pCO₂, they found that seasonal variations of pCO₂ may increase, and the historical summer low will likely turn into a summer high under mid-to-high-level emission scenarios. They did not report any changes in the historical period, though. However, since spatial av-

eraging always smooths out regional features and anomalies, it seems reasonable to believe that changes in seasonality might already occur earlier than these model projections suggest. The temporal evolution of the PC from my EOF analysis indicates that such shifts might be already present in the historical record and have been possibly missed due to the large-scale spatial averaging.

Therefore, I investigated the timing of seasonal maxima and minima alongside the changes in the intra-annual amplitude of the seasonal cycle. I find hardly any change in the timing of the seasonal extrema for either of the two data sets, with slightly pronounced changes in the MPIM-SOM-FFN. However, the amplitude of the seasonal cycle shows a considerable increase in the MPIM-SOM-FFN data set, particularly in the high Arctic north of Canada, the Beaufort Sea, and the Chukchi Sea. The Jena-MLS data set shows only very little change in these regions.

I note that the two data products largely disagree here, making the results inconclusive. Still, given the pronounced changes in sea-ice cover over the past decades and a strong Arctic warming, it seems reasonable to assume that changes in the seasonality of $p\text{CO}_2$ are already present in the historical record and are worth further investigation. If this is the case, getting clarity on the seasonal changes in the affected regions would be an essential next step to better assess the impact of these changes on local ecosystems and to estimate future evolution in these areas.



4

SUMMARY AND CONCLUSIONS

4.1. MY FINDINGS ON SEASONAL AND REGIONAL CHANGES OF SEA-ICE AREA AND SEA-SURFACE PCO₂

As climate change progresses, regional changes in the Arctic are becoming increasingly important to various stakeholders. Transformations of the Arctic Ocean caused by the continuing retreat of sea ice due to global warming affect, in particular, the coast–ice transition zone, making it a subject of special interest to the shipping industry and indigenous people. However, also areas in the open ocean are influenced by the ongoing changes, particularly oceanic systems that the ice cover has shielded from the atmosphere over a long period. Changes in the oceanic carbon cycle in these areas are of particular interest as they determine the exchange of CO₂ between ocean and atmosphere and, therefore, the rate of ocean acidification in the Arctic, affecting whole ecosystems and, hence, the entire food chain.

Considering the evolution of these variables in the different domains, understanding their seasonal changes is at least equally important as the long-term changes of their mean state. Particularly, organisms that depend on the carbon chemistry in the ocean are highly sensitive to seasonal changes in their environment. However, seasonal changes in the sea-ice cover are also of increasing importance, not only because they have a more or less direct impact on the ecosystems mentioned above but also because the dynamics in the sea-ice cover have a vast influence on the environment, fauna, society, and industry.

Getting a more thorough understanding of seasonal and regional changes in the Arctic is therefore crucial to better estimate the impacts of climate change on these systems and to develop strategies for adapting to these changes. In times of ultra-high-resolution satellite imagery and continuous development toward high-resolution climate models, it is important to also shift the overall research perspective to a more regional level.

With this thesis, I aim to contribute to this shift by investigating two crucial indicators affected by a warming climate: Arctic sea-ice coverage and surface ocean pCO₂. In the following, I present the key findings on each of the research objects I formulated in the introduction of this thesis before ending this chapter with some conclusions.



ON THE SENSITIVITY OF ARCTIC SIA TO GLOBAL WARMING

In my first study (see chapter 2 and appendix A), I systematically analyzed the seasonal cycle of Arctic sea-ice area (SIA) sensitivities with respect to global warming. I started by investigating the changes in the pan-Arctic sensitivities over the seasonal cycle, examining the timing of the changes and the underlying processes. From this point, a series of questions emerged, for which I highlight the key results in the following:

- Monthly SIA sensitivities display a stronger month-to-month variability in summer than in winter. This separation of the seasonal cycle into a summer and a winter season is marked by two breakpoints (May/June and October/November), arising from the geographic blocking of the sea-ice edge.
- I systematically quantified the blocking effect proposed by Eisenman (2010) and determined the day of the year on which the sea-ice edge touches the coastline and the day it detaches from it again.
- Two conclusions arise from this finding: First, these events related to the blocking of the sea ice cause the sensitivity changes I found in the seasonal cycle at the beginning. Second, the timing of these events also changes linearly with global warming; the event of the ice attaching to the coastline delays by about 4 days per tenth degree of global warming, the timing of the ice detaching from the coastline advances by about 3 days per tenth degree of global warming.
- Consequently, the change in sensitivities eventually progresses into adjacent months, shortening the season during which the sea-ice edge is blocked along the Arctic perimeter by around 7 days per tenth degree of global warming.
- This also indicates that extrapolating SIA sensitivities for individual months should be performed with care as sensitivities, particularly in the winter season, might change in the future as soon as the sea-ice edge does not transgress the Arctic perimeter any more.
- Examining regional characteristics, I find which regions respond most sensitively to global warming and in which season. I find the strongest summer sensitivities in the East Siberian Sea (with $-0.83 \text{ million km}^2 / ^\circ\text{C}$), the Central Arctic, and the Beaufort Sea. Winter sensitivities are strongest in the Barents Sea (with $-0.53 \text{ million km}^2 / ^\circ\text{C}$), the Baffin Bay / Gulf of St. Lawrence, and the Sea of Okhotsk.

- Considering these findings together with the amount of SIA that has been lost over the past decades, one can estimate which regions will likely lose their entire sea-ice cover first and in what seasons. Accordingly, I expect that the ultimate loss of remaining summer sea ice will first occur in the East Siberian Sea, the Chukchi Sea, and the Laptev Sea. In contrast, the permanent loss of winter sea ice will likely occur first in the Barents Sea.

THE REGIONAL AND SEASONAL EVOLUTION OF ARCTIC SURFACE OCEAN PCO₂

For my second study (see chapter 3 and appendix B), I focused on ocean surface pCO₂ as a research subject. Using two different regional pCO₂ data products that make use of different techniques to fill in the observational gaps, I started my analysis with an overview of the mean state of pCO₂ and how it evolved over time. I then separated the spatio-temporal variability by performing an EOF analysis to identify the dominant patterns and governing processes in the high and the sub-Arctic. Finally, I looked at changes in the timing of the seasonality and in the amplitude of the seasonal cycle. The key findings can be summarized as follows:

- Both data products show a general increase in surface pCO₂ concentrations between 2005 and 2021. Trends in the sub-Arctic are consistently in the range between 15 µatm/dec to 30 µatm/dec in both products. However, trends in the high Arctic differ substantially between the two products: While the Jena-MLS shows no considerable difference compared to values in the sub-Arctic, the MPIM-SOM-FFN exhibits trends between 50 µatm/dec to 100 µatm/dec in the high Arctic Ocean.
- The EOF analysis reveals distinct seasonal patterns in the temporal evolution of pCO₂ in the sub-Arctic and the high Arctic. The sub-Arctic seasonal cycle of pCO₂ matches the inverse seasonal cycle of sea-surface temperature and solar irradiance, hinting at biological activity as the primary driver of seasonal pCO₂ variability in this region. In the high-Arctic, the seasonal cycle coincides with the seasonal cycle of SIA, indicating that processes linked to the variability of the sea-ice cover dominate here.
- According to the eigenvector maps of the EOF analysis, these seasonal patterns are most pronounced on the Pacific side of the sub-Arctic and in the Chukchi Sea and southern Hudson Bay in the high Arctic. The MPIM-SOM-FFN shows additional regions of high variability in the Beaufort Sea and adjacent areas north of Canada. However, the high variability in these areas is not captured in the Jena-MLS.



- Following the results from the EOF analysis and the outcomes from the model study by Orr et al. (2022), I explore potential shifts in the seasonality and changes in the seasonal amplitude. Overall, the Jena-MLS shows very little change as opposed to the MPIM-SOM-FFN, which exhibits a considerable increase in the amplitude and also clearer shifts in the timing of seasonal extrema. This is particularly true for the high Arctic north of Canada, the Beaufort Sea, and the Chukchi Sea. The results here are not conclusive, and the disagreement between the two products is large. However, given the importance of these changes for the ecosystems in these regions and considering the results from Orr et al. (2022), these findings are interesting results and should be further investigated.
- The combination of the first two modes from EOF analysis gives us a simple concept to describe the dynamics of surface ocean pCO₂ in the Arctic. In both data products, the first two modes explain more than 70 % of the variability. This may be helpful for benchmarking other data products and for developing further product versions.
- The MPIM-SOM-FFN looks more plausible in many aspects compared to the Jena-MLS. However, resolution and proxies used to fill in the observational gaps are important factors that need to be considered when interpreting the results. Jena-MLS uses a coarser resolution than MPIM-SOM-FFN and might, therefore, not capture certain smaller-scale processes.

4.2. IMPLICATIONS OF THIS DISSERTATION

In this dissertation, I investigated regional aspects of two different climate variables in the Arctic, namely sea-ice area and ocean surface pCO₂. While regional observations of sea-ice area are reasonably well developed and relatively reliable, observations of sea surface pCO₂ are still very sparse in both time and space. The implications of this dissertation have, therefore, various aspects:

The results of my first study contribute to a better understanding of the seasonal dependence of Arctic sea-ice area sensitivities to global warming. By identifying and quantifying the transition between summer and winter sensitivities and attributing it to geographic blocking, this study clarifies that the “kink” observed in some model studies (for example, in Li et al., 2013) is a consequence of geographic properties of the Arctic domain. This finding is important for future projections of Arctic sea-ice area, as it shows that the extrapolation of seasonal sea-ice area sensitivities is not robust and can lead to incorrect estimates of when the respective season will exhibit an ice-free state. With

the regional and geographically aware approach outlined here, we can also quantify the contribution of each individual region to the total northern-hemispheric sea-ice area sensitivity and even estimate when a specific region will lose its entire sea-ice cover.

The results of my second study provide a new perspective on the drivers of surface ocean pCO₂ in the Arctic and the regional and seasonal variability patterns in the different domains of the Arctic. Even though uncertainties remain, especially in the regions with poor observational coverage, the results give new insights into regional dynamics of long-term and seasonal pCO₂ changes. They show furthermore that EOF analysis can be used to assess the robustness of regional ocean surface pCO₂ products in the Arctic domain and to enhance the future development of these products. Since observing ocean parameters on a large scale is highly challenging in the Arctic, these products are a promising approach to estimating the dynamics of the oceanic carbon cycle in the Arctic. Improving our process understanding in these high-latitude regions is crucial and urgent since the Arctic experiences extreme and rapid changes due to the ongoing human-induced climate change. It is important to highlight the large uncertainties, particularly in the high Arctic, challenging quantitative regional analysis. Nevertheless, EOF analysis is a promising approach in order to identify whether or not a product is able to reproduce the dominant patterns in the different regions of the Arctic in a reasonable manner. Developing these products further is highly important as they will likely remain our only estimate of regional pCO₂ fields in the Arctic for the foreseeable future.

4.3. CONCLUDING REMARKS

With this thesis, I hope to contribute to a shift towards more regional and seasonal analysis of climate variables in the Arctic. Describing the changes on a pan-Arctic scale is an essential step for getting the big picture but often neglects the processes and dynamics that play a role on higher-resolved scales. The Arctic is a highly dynamic region with intricate geographic properties, and we will only manage to understand the system holistically if we consider the aspects on higher-resolved seasonal and regional scales, thereby keeping the large-scale evolution in mind. Since there is currently a lot of endeavor to increase the resolution of both observational tools (satellites) and simulations (models), it is time to move away from the Arctic-average thinking and towards a more regional perspective.



APPENDIX

The following appendix comprises two manuscripts I have written throughout my PhD, both intended for submission.



A

REGIONAL AND SEASONAL ARCTIC SEA-ICE LOSS RESPONDS LINEARLY TO GLOBAL WARMING

The work in this appendix is intended for submission to *The Cryosphere* as:

Ritschel, M. and D. Notz (2024). "Regional and seasonal Arctic sea-ice loss responds linearly to global warming".

AUTHOR CONTRIBUTIONS

MR and DN both conceptualized the study. MR performed the analysis and wrote the manuscript. DN contributed to the study design via discussions and reviewed and edited the manuscript. This work might be subject to further changes before it is submitted.



Abstract

The sensitivity of Arctic sea-ice coverage to global warming exhibits pronounced seasonality; Whereas during the winter, from November to May, sensitivities remain weak and stable at approximately -2 million $\text{km}^2/\text{ }^\circ\text{C}$, the summer months exhibit a pronounced change of the sensitivities, culminating at a maximum of -3.9 million $\text{km}^2/\text{ }^\circ\text{C}$ in October. This seasonal pattern results from coastal land masses effectively blocking the sea-ice edge's advance, leaving a disproportional smaller area variable during winter. Here, we determine the timing of this blocking effect—both the process of attachment and detachment—for each year of the satellite observation period. We find that, with rising temperatures, the timing shifts, and the attachment of the ice advances by approximately -33 days per degree warming, and detachment delays by about 43 days per degree warming. The shift in the timing highlights that the approach of extrapolating current sensitivities to predict future trends may not provide reliable insights for every season. Instead, these changes in the timing will lead to an intensification of winter sensitivities, with the potential to surpass current summer sensitivities. As these transitions will not occur simultaneously across the Arctic, we performed a region-specific sensitivity analysis, which allows us to pinpoint which Arctic areas will experience changes in winter sensitivities first, thereby providing critical insights into the evolving dynamics of Arctic sea-ice response to global warming. Given the combination of sensitivities and past sea-ice loss, we find, for example, that the East Siberian Sea, the Chukchi Sea, and the Laptev Sea will lose their remaining summer sea ice first. Such findings allow for better prognoses of how the different regions will evolve in the future under ongoing global warming and may support stakeholders and decision-makers in developing mitigation strategies.



A.1. INTRODUCTION

The retreat of Arctic sea ice with rising global temperatures is a phenomenon that models and observations largely agree upon. Yet, how the sea-ice cover in the Arctic has evolved specifically on a regional and seasonal scale and how these patterns are linked to global warming is among the most pressing and relevant questions that have not yet been answered satisfactorily in current sea-ice research.

The accompanying increase of open-water areas has a vast range of effects on the ecosystems, the surrounding, as well as physical and biogeochemical processes; Enhanced evaporation due to more water areas being exposed to the atmosphere may lead to changes and shifts in local weather patterns and seasons (e.g. Bailey et al., 2021), the opening of the sea ice cover results in increasing wave heights (Overeem et al., 2011; Casas-Prat and Wang, 2020) and accelerates coastal erosion along the shore, which is becoming less and less protected by fast ice (Barnhart et al., 2014; Nielsen et al., 2020), and more open-water areas eventually allow for enhanced exchange processes between ocean and atmosphere, such as heat, energy, and gas transfer (Steiner et al., 2013; Loose et al., 2014). Consequently, changes in the sea-ice cover have tremendous impacts on the local marine and terrestrial ecosystems (Lannuzel et al., 2020; Ingvaldsen et al., 2021; März et al., 2022; Steiner et al., 2021), local and global climate, the life of local communities (Meier et al., 2014; Huntington et al., 2022), as well as the shipping industry (Smith and Stephenson, 2013; Bennett et al., 2020; Wei et al., 2020; Wagner et al., 2020). Since the Arctic is warming stronger than the global average—up to four times more over the last four decades (Rantanen et al., 2022)—these changes are expected to continue drastically in the future. Hence, an improved understanding of the regional and seasonal changes in the sea-ice cover will be of increasing importance for the climate change adaptation policy of various stakeholders.

Many previous studies have looked into the temporal evolution of Arctic sea-ice coverage, providing detailed insights into the changes in sea-ice cover from pre-industrial times until today. However, climate change is not a function of time, and thus linear trends are not a robust descriptor of future changes, as these depend heavily on the scenario in question. To get a better understanding of how the observed changes in sea-ice area relate to global warming, various studies examined the relationship between sea-ice coverage and driving variables that can be put in context with global warming;

Olonscheck et al. (2019) showed that the variability of Arctic sea-ice coverage is primarily governed by changes in atmospheric temperature. Atmospheric temperatures, in turn, are proportionally tied to cumulative carbon emissions (Matthews et al., 2009) via the heat content of the atmosphere. Notz and Stroeve (2016) finally followed that linkage and unveiled a clear linear relationship between anthropogenic

CO_2 emissions and the evolution of Arctic sea-ice area—a relationship that can be observed throughout all the seasons (Stroeve and Notz, 2018; Niederdrenk and Notz, 2018). This robust linkage has eventually been found both in observations as well as in state-of-the-art climate models such as from the CMIP6 model ensemble. However, simulations seem to systematically underestimate the overall sensitivity (Winton, 2011; SIMIP Community, 2020), which is why a more thorough understanding of the inner-system processes is required.

What's more, the temporal and spatial evolution of Arctic sea ice differs distinctly across the seasons and regions of the Arctic (Onarheim et al., 2018) as satellite observations have been showing for more than four decades. Even if most climate models are, to a certain degree, able to reproduce the general evolution of the pan-Arctic sea ice, they deviate significantly from what we see in the observations once we look at higher resolved regional and seasonal scales. It remains unclear where these differences come from and how they correlate with the ability of the models to reproduce, for example, global warming.

Here, we complement the insights of Onarheim et al. (2018) by investigating the seasonal cycle of sea-ice sensitivity to atmospheric temperature both for the total sea-ice extent of the Northern Hemisphere as well as for various regions of the Arctic. We note that the regional evolution of Arctic sea ice is governed by a multitude of processes such as wind drag, ocean currents, etc. However, since thermodynamic growth has the biggest contribution and because the link to temperature and anthropogenic CO_2 emissions has shown to be highly robust, we will focus on these quantities as predictor variables.

We examine furthermore to which degree the clear separation of the seasonal cycle of northern-hemispheric sensitivities into winter and summer sensitivities is linked to the geographic features of the Arctic. Eisenman (2010) proposed that the geography of the Arctic could be responsible for the asymmetry in the seasonal cycle of sea-ice extent. In a thought experiment, he introduced a simple model of the Arctic Ocean being represented by a circle with two openings: one toward the Pacific, and one toward the Atlantic. The ice is imagined as an ideal disc, expanding and contracting around the pole. In summer, the entire ice cover resides within this circle, and its edge can move freely. However, when the ice expands during the freezing period, at a certain point, the ice edge will touch the perimeter of the circle and only be able to migrate through the two openings. As a result, the total area that can still vary in winter is much smaller compared to summer, when the whole disk around the pole can vary.

Various model studies have reported a sudden increase in winter sensitivities at an advanced level of global warming (e.g. Armour et al., 2011; Li et al., 2013). Some of these studies seek their explanation for this “kink” in the geographic effect described by Eisenman (2010) whereas others claim that they can certainly exclude it. For example,



Li et al. (2013) exclude geographic reasons for their observed change in March sensitivity as they say that the value at which they observe the sudden decrease is beyond the point when the sea ice has retreated from the surrounding land masses. They say, furthermore, (albeit not showing it) that they observe the most dominant decline in the central Arctic Ocean, where the ice edge mostly does not touch the land.

We think, however, that we can support the hypothesis of geographic blocking based on the observational data we analyze here, and that this will lead to changes in winter-time sensitivities as soon as the ice edge does not go beyond the land boundaries of the inner Arctic.

A.2. DATA AND METHODS

Sensitivities of sea-ice coverage with respect to atmospheric near-surface temperature are the core of our analysis. We chose sea-ice area instead of sea-ice extent as an estimate for the true sea-ice coverage. Sea-ice extent is defined as the area of grid cells with a sea-ice concentration of at least 15 % and is, therefore, dependent on the grid resolution. The differences in the grid cell sizes can result in large biases if this metric is used. Sea-ice area, on the other hand, is more sensitive to systematic errors in the algorithm of the respective product but closer to the true sea-ice coverage (Parkinson and Cavalieri, 2008; Notz, 2014).

A.2.1 *Arctic sea ice and temperature data*

Deriving Sea-Ice Area

We derive sea-ice area from sea-ice concentrations and the respective grid-cell areas from three different satellite data products to get an uncertainty estimate of the observations. We use the retrievals from the NASA Team algorithm (Cavalieri et al., 1984, 1997), the NASA Bootstrap algorithm (Comiso, 1986, 1995), and the OSI-SAF product from EUMETSAT (Lavergne et al., 2019; OSI SAF, 2017). The algorithms differ in various aspects, such as in the way they account for melt ponds in the brightness temperature data since these are hard to distinguish from open water bodies. As a rule of thumb, the NASA Bootstrap algorithm is known to maximize sea-ice area wherever possible, whereas the NASA Team tends to underestimate the true sea-ice coverage. OSI-SAF often lies somewhere in between the other two products. The resulting sensitivities can, therefore, differ depending on the product being used for calculating the sea-ice area. Satellite data are available from the end of 1978 until today. Hence, for our analyses, we constrain all data to the period from 1979 until 2022.

Sea-ice coverage is commonly given as concentration values, i.e. the fraction of a grid cell covered by sea ice. We derive sea-ice area by multiplying the sea-ice concentration of each grid cell with the total area

of the respective cell. For the NASA products, NSIDC provides a data product with the respective grid-cell areas (*NSIDC-0771*¹) whereas the OSI-SAF data lie on an EASE-2 grid with a uniform 25 km × 25 km resolution (Brodzik et al., 2012).

Choosing the predictor variables

For the temperature-related sensitivity analyses, we use the near-surface temperature data from the ERA5 reanalysis project (Muñoz Sabater, 2019; Hersbach et al., 2020), and the anomalies estimates from GIS-TEMP dataset (GISTEMP Team, 2023) and from HadCRUT (version 4, Morice et al., 2012). The ERA5 data have a meridional resolution of 31 km and are retrieved from the *Copernicus Climate Data Store*. The GIS-TEMP anomalies are on a 2° × 2° regular latitude-longitude grid. The HadCRUT data set combine land (CRUTEM4) and ocean SST anomalies (HadSST3) provided on a 5° × 5° regular grid.

We use temperature as the main predictor variable for our discussion since it is the main direct driver influencing the growth and decay of sea ice. We will start the analysis by investigating how Arctic sea ice responds to changes in the *local* atmospheric temperature, that is, we perform sensitivity analyses of the northern-hemispheric sea-ice area with changes in mean Arctic atmospheric temperature. For the later discussion, however, we use global annual atmospheric temperature anomalies as a predictor to put the changes into a clearer context of global warming.

All our analyses were also performed for anthropogenic CO₂ emissions, being the main driver of global warming and an easy-to-measure quantity due to the quick mixing of CO₂ around the globe. The emission values are obtained from the Global Carbon Budget (Friedlingstein et al., 2022) by summing up the *fossil emissions excluding carbonation* and the *land-use change emissions* from the *historical budget* in the Excel file, which can be fetched from the ICOS website². To obtain units in GtCO₂/yr, we multiply the values with a factor of 3.66, which corresponds to the molar ratio of carbon and CO₂. The results of the CO₂-related analysis are summarized in the tables A.3 and A.5.

Processing of the data

To get an uncertainty estimate of the observed sensitivities, we combine the sea-ice areas from the three satellite products with the different temperature data, respectively. Analog combinations of the three satellite datasets with anthropogenic CO₂ emissions are considered when we analyze sensitivities with respect to changes in the anthropogenic CO₂ emissions. Also, note that for the initial observation of

¹ <https://nsidc.org/data/nsidc-0771/versions/1>

² <https://www.icos-cp.eu/science-and-impact/global-carbon-budget/2020>



sea-ice sensitivity to local temperatures, we use the monthly time series of atmospheric temperature as a predictor in contrast to the later analysis for which we use anomalies of the global annual atmospheric temperature. For CO₂-related sensitivity analyses, we assume that CO₂ mixes quickly enough to be uniformly distributed over the globe. That is, we take the cumulative sum of the year-to-year changes of the anthropogenic emissions and use the annual mean CO₂ concentration for our sensitivity analyses. Seasonal sensitivities with respect to anthropogenic CO₂ emissions are, therefore, the response of the sea-ice area of the respective season to changes in the annual value of cumulative CO₂ emissions.

All pre-processing steps are performed on the gridded data until they are eventually transformed into 1D time series of the individual regions. The data are all kept on their native grids, thereby avoiding artifacts that can arise from interpolation during regridding. For the transformation from 2D fields to 1D time series we use the following weighting schemes: Sea-ice area is summed up across all selected cells, and temperatures are averaged with weights based on the cell sizes. The CO₂ data from the *Global Carbon Project* are already globally averaged. These time series are then used for the sensitivity analyses on different regional and seasonal domains.

To analyze sensitivities for different regions of the Arctic we defined polygons in a shape file, based on the areal definitions of the *MASIE* regions, which are, for example, listed at nsidc.org/data/masie/browse_regions and used in a multitude of other studies (see Figure A.1). The shape file is then processed via the *geopandas* (Jordahl et al., 2020) and the *regionmask* (Hauser et al., 2021) python libraries, and, for each grid type of the target data, a mask file is generated based on the polygons in the shape file. These masks are finally applied to each corresponding data set via the *Climate Data Operator* toolbox (Schulzweida, 2020), thereby ensuring that the masked regions are befittingly mapped on each grid type. Finally, these regional sub-sets are transformed into 1D time series as mentioned in the paragraph above. This procedure turned out to yield the most robust and performant results.

A.2.2 Sensitivity analyses

To get a better understanding of the mechanisms governing the regional evolution of Arctic sea ice, instead of comparing temporal trends, we analyze sensitivities of sea-ice area in the different domains with respect to changes in atmospheric temperature and anthropogenic CO₂ emissions. Our approach is based on the work of Notz and Stroeve, 2016 and Niederdrenk and Notz (2018) who found robust linear relationships between northern-hemispheric sea-ice area and atmospheric temperature as well as anthropogenic CO₂ emissions.

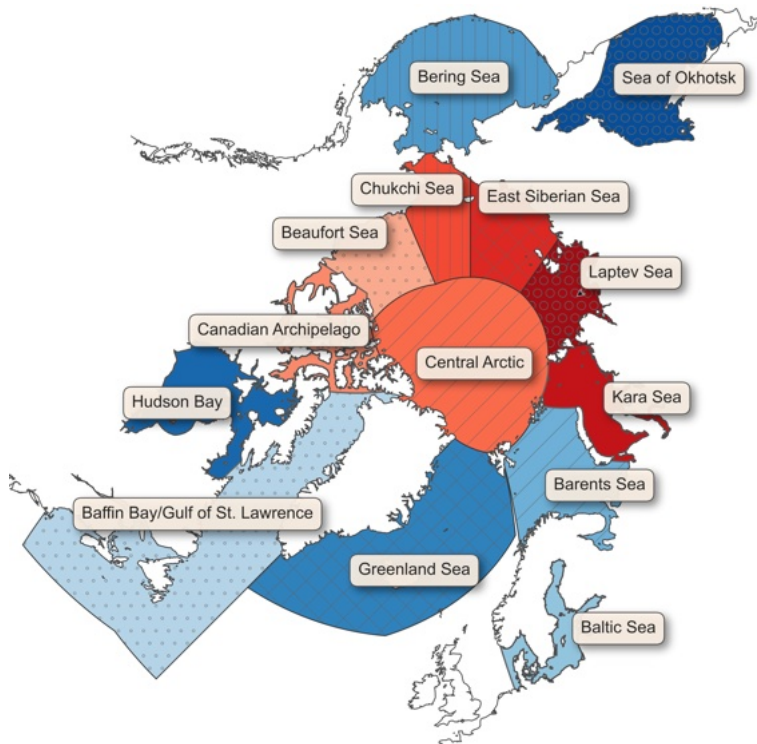


Figure A.1: Regions of the Arctic as being used in this study. The coordinates are based on the definitions given by the National Snow & Ice Data Center (NSIDC). Red and blue regions are later in the paper defined as summer-active and winter-active regions.

Data pre-selection for linear regression

When we performed regression analysis on the time series of the various Arctic sub-regions as defined in the previous section, we experienced that the theory of the linear relationship breaks down sometimes. This is in particular the case for regions that have been either fully ice-covered or fully ice-free for a certain range of the predictor variable (global atmospheric temperature).

The three example sketches in Figure A.2 (a) illustrate this problem; In both of the first two cases (panel I and II), the ascertained sensitivity is underestimated (we will refer to both states as “saturated” in the following). The result is only correct if all data considered for the regression analysis are sensitive to the predictor variable (panel III). For having the regression algorithm detect the *true* sensitivity, it is therefore crucial to exclude these saturated parts of the time series from the analysis.

Let's consider, for example, the time series of April sea-ice area in the Kara Sea and atmospheric temperature in Figure A.2 (b). While the profiles let us assume the existence of a correlation between the two variables, the profile of the sea-ice time series is indeed so flat that it is nearly impossible to determine the proper range that one should



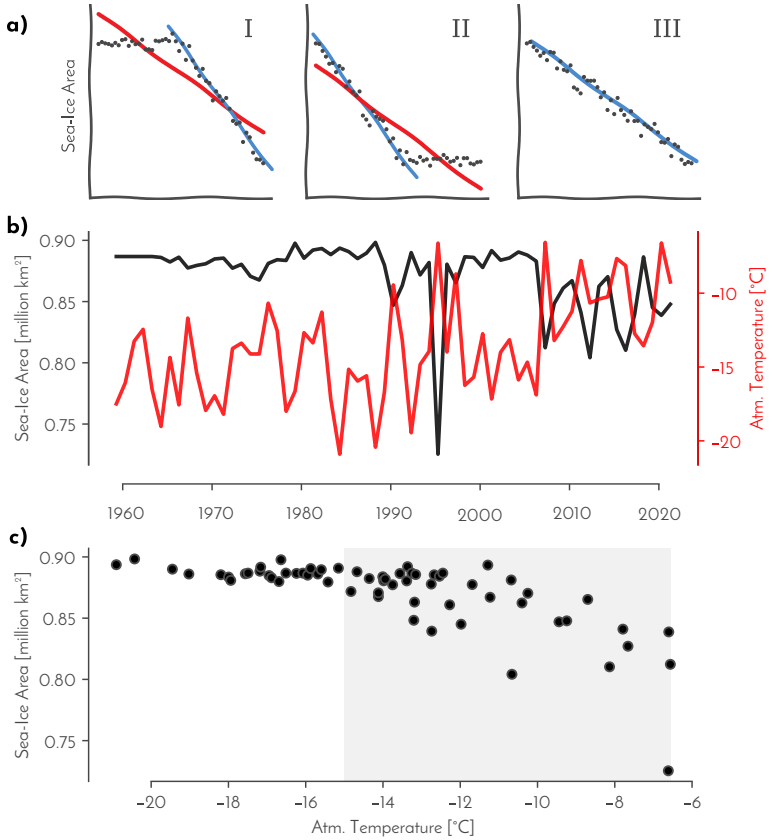


Figure A.2: (a) The three sketches depict cases of underestimating the slope due to (I) initially fully ice-covered and (II) entirely ice-free conditions. Only in panel (III) does the regression over the full range get the slope right. (b) Example time series of April sea-ice area in the Kara Sea and atmospheric temperature. In the original sea-ice area time series, nearly no trend is visible, although there is a correlation between the two variables. (c) Re-ordering the data by the predictor variable (here: Atm. Temperature), allows us to properly determine the correct *window of reasonable sensitivity* (shaded area).

use for the sensitivity analysis. The temporal trend determined by fitting a linear regression to the whole time series would yield a very weak result. However, by sorting the data by the predictor variable (here: temperature), it becomes obvious that for low temperatures up to around -15°C , the region is fully ice-covered and only reacts to temperatures above that threshold (Figure A.2 c). Thus, we want to ignore the values below the threshold in our sensitivity analysis.

We determine the start and the end of this *window of reasonable sensitivity* by comparing the smoothed profile of the re-ordered sea-ice area series against an upper and a lower threshold before performing the actual regression on the data. The start of the window is defined by the point at which the signal falls first below the upper threshold, the end is defined accordingly by the first crossing of the lower threshold. For

our analyses, we set the lower threshold to 5 % of the data maximum and the upper threshold to the minimum + 95 % of the data range. If all data lie below the lower threshold (ice-free state, e.g. in some regions during summer) or entirely above the upper threshold (fully covered state, e.g. in some regions during winter), no regression is performed.

Computing sensitivities via standard linear regression

Once the data are constrained by this *window of reasonable sensitivity*, we perform a standard linear regression on each subset of the data (grouping by regions and seasons). For the regression, we want to ensure that we have a minimum of data points available since constraining the window of reasonable sensitivity reduces the amount of data points that are eventually considered in the linear regression. For our analyses, we set a threshold of $\frac{1}{3}$ for data that we want to have available for the linear regression. That is, from a total of 43 values per season (43 years in the observed period), at least 14 values should be left to yield a meaningful regression result. If the amount of data left after constraining the window falls below that threshold, no linear regression is performed and NaN is returned. The linear regression is done with the *Ordinary Least Square regression solver* of the `scipy` python library (Virtanen et al., 2020). The solver returns the regression coefficients (slope and intercept) along with the standard error of regression and the F statistic. For significance testing, we rely on the p value of the F statistic and define an $f_p < 0.05$ (corresponding to a 95 % confidence level) implying statistical significance.

A.2.3 *Geographic muting*

To follow up on the theory of the simplified circle model described by Eisenman (2010), who demonstrated how the geography of the Arctic influences the sensitivities, we construct a mask along the inner Arctic coastline, which we refer to as the *Arctic perimeter* in the following. The mask is shown in Figure A.6 (b) and depicts the grid cells along the coast at which the sea ice is assumed to be blocked from further expansion in winter. We count then for each time step the number of grid cells that are covered with at least 95 % of sea ice. This number divided by the total number of grid cells of our mask gives us a time series of the fraction of the Arctic perimeter which is covered by ice. The timings of the blocking (attaching/detaching of the ice) are eventually determined by comparing this profile with a threshold of 85 % and finding the first day after summer and the last day after winter when the profile is above the threshold. We suggest this value as a reasonable estimate for the percentage of the Arctic perimeter that should be ice-covered so that the ice edge is considerably blocked. Once this threshold is permanently exceeded during the freezing season, we say



that the ice is attached to the coast and hence blocked from further southward movement. Once the profile falls permanently below the threshold during the melting seasons, the ice has loosened from the coast and can move freely again. For some time steps, we realized that there are occasionally ice patches along the coast, even though there is still quite a lot of open water in front of the shore. These patches would lead to a bias in the counting and are therefore removed by applying a graphical filter routine, which erases patches of ice that are smaller than a given threshold and not connected to the main ice body.

A.3. THE SEASONAL CYCLE OF NORTHERN-HEMISPHERIC SEA-ICE SENSITIVITY TO LOCAL TEMPERATURE CHANGES

A short leading note: When we describe observations of sea-ice area in the following, we usually refer to the mean of the three data products (OSI-SAF, NASA Team, and NASA Bootstrap) if not declared otherwise. For sensitivities, we usually compute the linear regression first for every single of the possible product combinations (sea-ice area and temperatures) and then take the average of the resulting values. Also, in the following, we will use the term *high* or *large sensitivities* for large absolute values even if the actual values of the regression slopes are negative (declining sea-ice area with increasing temperatures). The analog holds for low absolute values.

An inspection of the seasonal cycles of northern-hemispheric sea-ice area and Arctic mean atmospheric temperature as they are depicted in Figure A.3 (a) and (b) reveals an asymmetric behavior; Arctic sea-ice area has declined substantially over the past four decades with more pronounced changes in the summer months than in winter. Its intra-annual amplitude hence *increased* over time (a). On the other hand, the seasonal patterns of Arctic air temperatures show greater changes in the winter months due to enhanced Arctic Amplification in this season (Rantanen et al., 2022), resulting in a *reduction* of the intra-annual amplitude (b).

When we plot the values of these two variables against each other, thereby grouping them by months, we can determine the sensitivity of sea-ice area to changes in atmospheric temperature for the different seasons (Figure A.3 c). In the profile of the seasonal cycle of these sensitivities, three main features stand out: From around November to May, the values are found to be all in a similar range and deviate only little around the March minimum where about -0.13 million km 2 of sea-ice are lost per degree of Arctic warming, corresponding to a

bit more than $\frac{1}{3}$ of the size of Norway³. Toward the summer months, however, sensitivities gradually increase, reaching a maximum of -1.3 million $\text{km}^2/\text{°C}$ in August (more than three times the area of Norway).

The transitions between May and June and between October and November mark two breakpoints in the seasonal cycle, separating it into a winter half and a summer half. Next, we are going to investigate the regional patterns of sea-ice sensitivity to see whether the spatio-temporal information can give us some hints on where and why these changes occur.

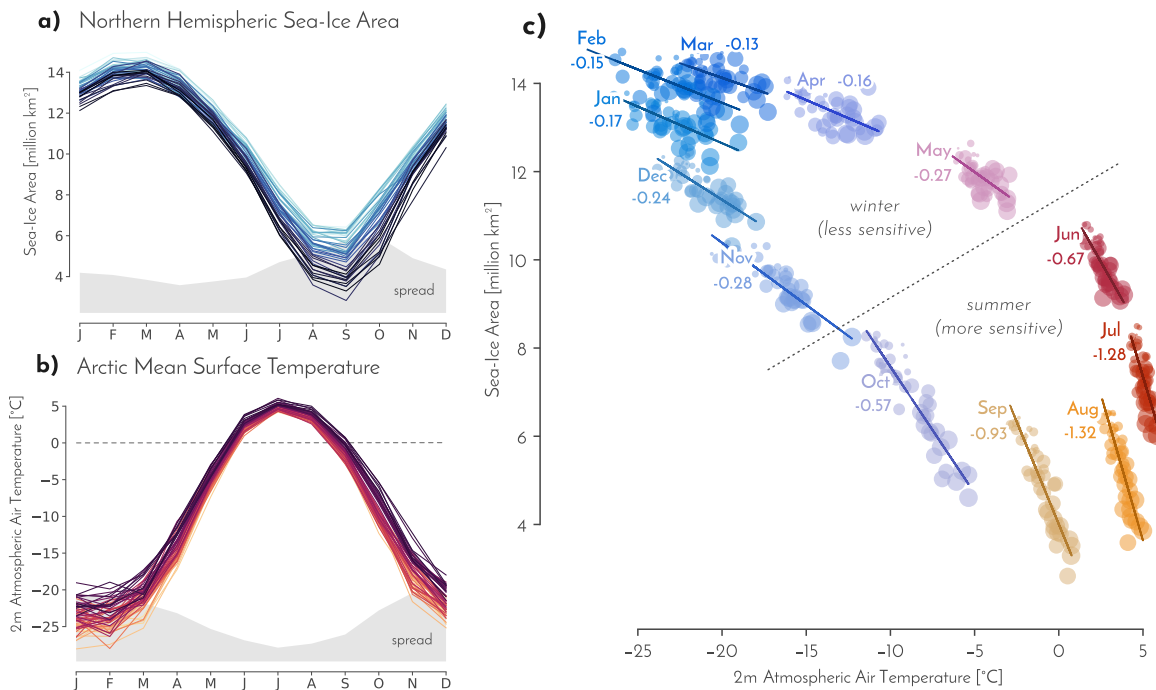


Figure A.3: **Left:** Seasonal cycles of (a) NH SIA and (b) Arctic mean TAS over time. Darker shadings represent more recent time steps. The grey-shaded area represents the spread of the respective month across the entire time series from 1979 to 2022. **Right, (c):** Monthly sensitivities of NH SIA (averaged across the three data products) with respect to spatially averaged Arctic TAS. Values denote the respective seasonal sensitivity in million $\text{km}^2/\text{°C}$. Markers of one month share the same color, with their size increasing over time. The breakpoints between May/June and October/November separate the seasonal cycle into a winter and a summer season.

³ According to https://en.wikipedia.org/wiki/List_of_countries_and_dependencies_by_area, the total area of Norway is about 385 200 km^2



A.4. UNDERSTANDING THE REGIONAL PROCESSES AND THE SEPARATION OF THE SEASONAL CYCLE OF NH SENSITIVITIES

When we look at the spatio-temporal evolution of Arctic sea-ice coverage, a vastly heterogeneous picture emerges. It appears, however, that the advance and the retreat of the ice follow consistent regional patterns in most of the years.

To assess regional responses to global warming and their contributions to pan-Arctic sensitivity, we computed historical sea-ice area sensitivities for 14 regions. We preprocessed the data according to appendix A.2.2 to account for full ice coverage or open-water states during specific seasons in some regions. The resulting sensitivities are displayed in Figure A.4 along with the relative amount of sea-ice area that has been lost over the observed period from 1979 to 2022 compared to the mean of the first decade.

The sensitivities of individual regions

Depending on the timing of the maximum sensitivity, we cluster the regions into two groups: Regions that exhibit the strongest sensitivity (darkest shading per region in Figure A.4, indicated by a small red star) in the months from November to May we refer to as winter-active regions (blue frames), whereas regions with the strongest sensitivities in the summer months (June to October) are identified as summer-active regions (orange frame). These two seasonal clusters generally agree with the classification introduced by Onarheim et al. (2018), who group their study domains in *summer mode* and *winter mode* regions according to whether they show their most pronounced (temporal) trends during the summer or winter months, respectively. Note that in their study they analyze temporal trends, which indicate the absolute loss in each region over time, whereas in Figure A.4, the color shading indicates the relative loss over time. Hence, strong trends in Onarheim et al. (2018) do not necessarily comply with dark colors (big relative loss) or big circles (strong sensitivity) depicted in Figure A.4.

We observe strongest summer sensitivities in the *East Siberian Sea* (with -0.83 million $\text{km}^2/\text{°C}$ in September), the *Central Arctic*, and in the *Beaufort Sea*, followed by the *Chukchi Sea*, the *Laptev Sea*, and the *Kara Sea*. Winter sensitivities are strongest in the *Barents Sea* (-0.53 million $\text{km}^2/\text{°C}$), followed by the *Baffin Bay / Gulf of St. Lawrence* and the *Sea of Okhotsk*. Absolute values as well as statistical significance can be found in Table A.2. Regions further south typically show stronger sensitivities in winter as opposed to regions further north, which are mostly fully covered by sea ice during that period of the year and, therefore, show only weak or no sensitivity at all. In contrast, these north-

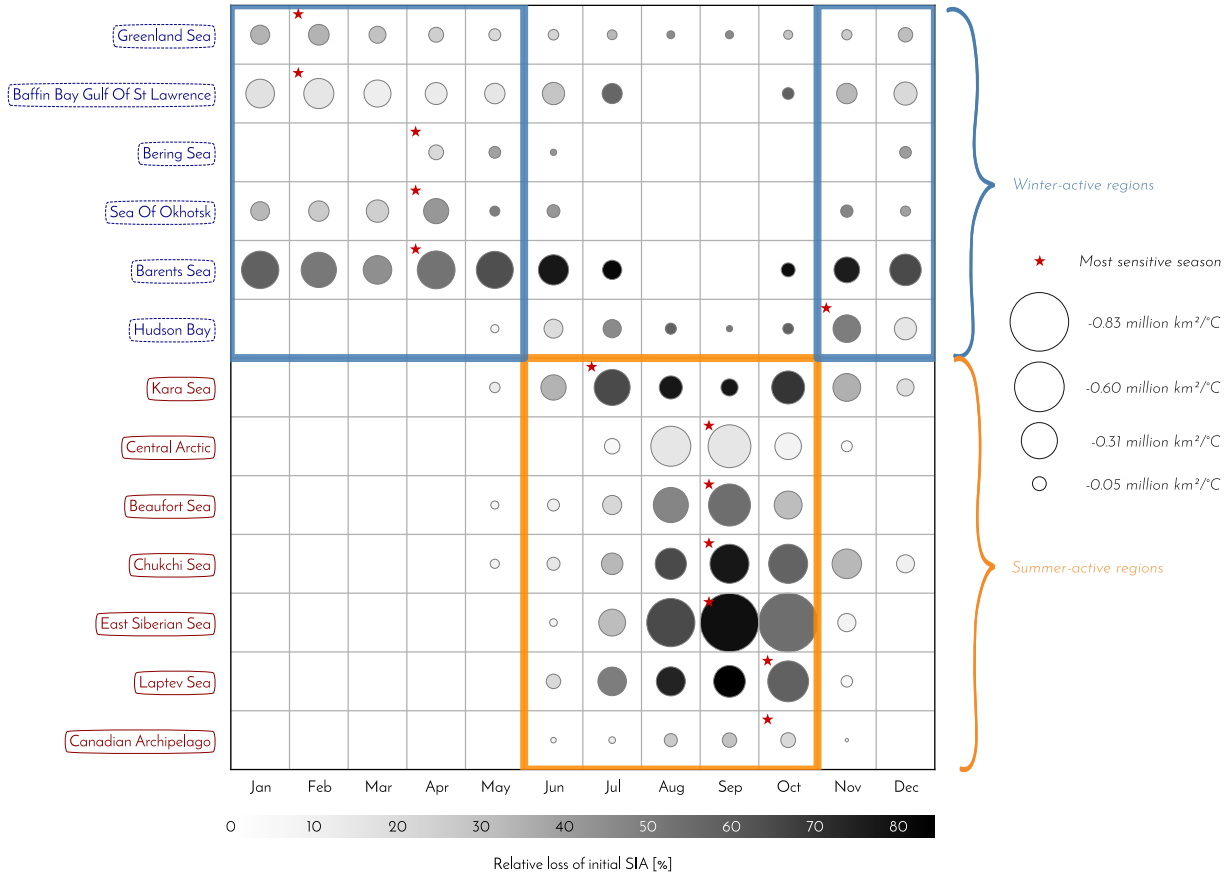


Figure A.4: Sensitivities (circle size) and observed sea-ice loss (color shadings) for all regions and seasons. Regions are ordered by the occurrence of their respective maximum sensitivity (indicated by the small red star in the upper left corner of the respective entry in the matrix). Fill color represents the loss of sea-ice area relative to the beginning of the record. That is, we take the difference between the 1979–1989 mean and the 2011–2022 mean. Circle area represents the sensitivity, normalized by the maximum value of all entries. Cases in which no linear regression could be performed are left empty, meaning that empty entries in summer represent ice-free conditions, whereas empty entries in winter months represent full ice coverage. We also only display values that are statistically significant ($f_p < 0.05$). Regions are clustered into winter-active areas (blue frame) and summer-active areas (orange frame).

ern regions exhibit sensitivities mostly in summer when the ice starts to retreat into these regions, whereas regions in the South are mostly ice-free during the summer.

Some exceptions stand out, however: The Hudson Bay is located further south but is almost entirely surrounded by land. This hinders the ice from expanding further south during the freezing period but also keeps it for longer during spring as cold air coming across the land keeps the temperatures fairly low. Still, compared to the relatively



weak summer sensitivities there, the *loss* of sea ice over time has been quite significant (intense color shading in Figure A.4). Sea-ice dynamics in the Greenland Sea (along Greenland's east coast) are mostly mechanically driven via drift export through Fram Strait, resulting in a quite flat profile in its seasonal sensitivity cycle alongside a fairly uniform retreat of seasonal ice cover due to global warming. Finally, the Canadian Archipelago holds a lot of land fragments, making the sea ice there more susceptible to air being cooled down by the land masses. Embodying the most northern land masses together with Greenland, this is the area where we have long-lasting ice cover and where sensitivities are (until today) very weak.

Note that large sensitivities do not necessarily imply the biggest relative losses as indicated in Figure A.4. A region such as the Central Arctic may have a large total area and, due to a strong sensitivity in September, may have lost a big amount of sea ice. Relative to its total size and the ice that has been present during the first decade of the observed period, this loss can still be small compared to other regions. This also implies that entries in the matrix in Figure A.4 exhibiting a strong sensitivity (big circle) while having lost only a small fraction of their area (faint shading) may experience long-lasting losses in the future. Cases with big circles, on the other hand, can be expected to lose their remaining ice cover soon in the future, even more so if they have already lost a significant share of their area. Given the combination of big circles (strong sensitivity) and dark shadings (large relative loss), we expect that the East Siberian Sea, the Chukchi Sea, and the Laptev Sea are among the regions that will lose their remaining summer sea ice first.

Following the evolution of the seasonal cycle (reading Figure A.4 from left to right), we find that the sensitivities in the winter months remain fairly constant—not just in the total, pan-hemispheric signal (compare Figure A.3) but also considering the individual regions. From June, the regions further north start showing changes in the sea-ice cover, thereby gradually increasing toward the summer maximum, before they decrease again. However, the timing and the magnitude of the individual sensitivities differ across the regions—in contrast to the relative loss of sea-ice area, which has mainly happened along the Russian coast, starting in the Barents Sea and then following along the coast to the Chukchi Sea. From October to November then, most of the summer-active regions go back to zero sensitivity, and winter-active regions show increasing sensitivity again.

In Figure A.5, we depict this asymmetry of the seasonal cycle by showing the northern-hemispheric sensitivity to global temperature changes including the contributions of the individual regions. Over the winter months (November to May), it is mostly the Barents Sea that shows the strongest sensitivities. Being strongly influenced by the Atlantic inflow (Onarheim and Årthun, 2017; Dörr et al., 2021), its sen-

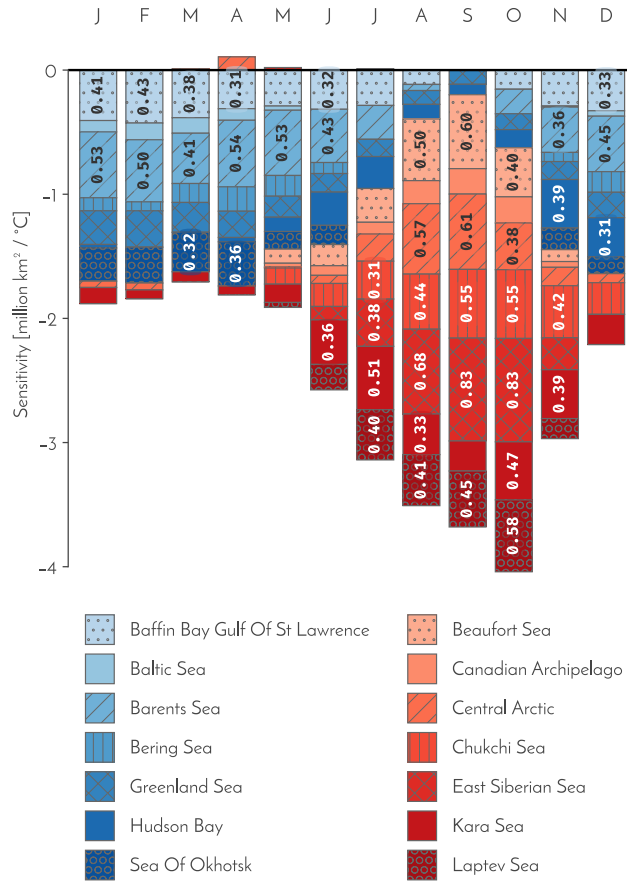


Figure A.5: Observed sensitivities for the entire Northern Hemisphere (in million $\text{km}^2/\text{°C}$). Regions are clustered by winter-active (blue colors) and summer-active (red colors) regions and ordered alphabetically within each group. Regions can be distinguished by color shadings and hatchings. Colors and hatchings are compliant with the representation in Figure A.1. For regions with a sensitivity greater than 0.4, the respective value is annotated.

sensitivity to local air temperatures is rather weak. However, in relation to the global temperature as an indicator of the system's energy, the signal is significantly strong. Then, during the transition from May to June, the Kara Sea contributes most to the strong sensitivity increase with a change by 0.23 million $\text{km}^2/\text{°C}$, followed by the Laptev Sea, the Beaufort Sea, and the Chukchi Sea. The summer months are mostly dominated by the East Siberian Sea—in particular in the peak season from August to October—, followed by the Central Arctic, the Beaufort Sea, and the Chukchi Sea. The transition between October and November then is mainly governed by the changes in the East Siberian Sea (with a decrease of 0.49 million $\text{km}^2/\text{°C}$) and the Laptev Sea.



Breakpoints in the NH seasonal cycle caused by geographic blocking

When we look closer at the timing of the transitions between winter and summer sensitivities, we find that the clustering of the regions according to the timing of their strongest sensitivity goes along with clustering them according to their geolocation; Winter-active regions are located mainly outside the coastline that encloses the inner oceanic part of the Arctic, summer-active regions are located inside that enclosed area. Eisenman (2010) introduced a theory according to which the geography of the Arctic may be responsible for the asymmetry in the seasonal cycle of Arctic sea-ice extent. Looking at the spatial extent of the seasonal sea-ice coverage over time, we find that the two breakpoints that we identified in Figure A.3 coincide with the transition of the sea-ice edge from the inner to the outer Arctic Ocean, indicating that a possible explanation for these breakpoints may be found in the theory proposed by Eisenman (2010).

We quantified the blocking effect in the hope of finding a confirmation of this idea; At first, we defined the boundary along the coastline, which encloses the inner part of the Arctic and hinders the ice edge from moving southward once encountered by the ice (Figure A.6, b). We refer to this boundary as the *Arctic perimeter* in the following. By masking the sea-ice concentration data with this Arctic perimeter, we counted grid cells with more than 95 % sea-ice concentration along this coastline and divided the number by the total number of grid cells in the mask (see appendix A.2.3). This results in a time series for each month (Figure A.6, a) displaying the fraction of the coastline that is covered with ice. At high values, the ice has expanded so far that it is attached to the largest part of the coastline. In this state, it is blocked in most directions by the surrounding land and hence hindered in how freely it can move. At low values, on the other side, the ice has mostly detached from the coast (after spring) or is not reaching it yet (before winter) and can, therefore, migrate freely within the inner part of the Arctic.

The time series are separated into two clusters (high and low coverage), with the “gap” defined by the transition from May to June and from October to November underlining the geographic muting effect being the cause for the abruptness of the transition. As expected, the breakpoint between October and November takes place at a sea-ice area that is around 8 million km², which corresponds to the ocean area enclosed by the Arctic perimeter (compare Table A.8). The breakpoint at May/June, however, is observed at higher absolute values (greater than 10 million km²; compare Figure A.3). This may seem like it contradicts the argument of the geographic muting hypothesis. However, we believe that the cause lies likely in the combination of two different effects:

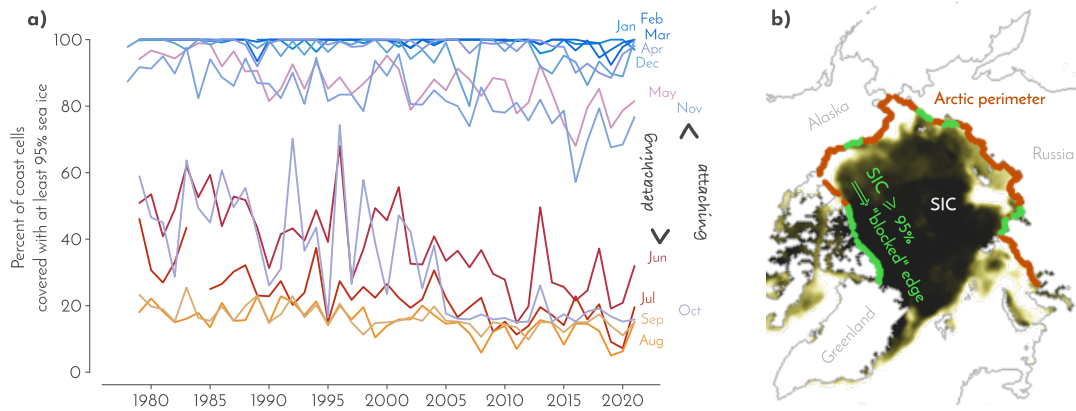


Figure A.6: Blocking of the sea-ice edge along the Arctic perimeter. (a) shows time series for each month representing the percentage of cells along the coastline that are covered by at least 95 % sea ice relative to the coastline defined as the *Arctic perimeter*. (b) shows the Arctic perimeter mask (dark orange, exaggerated thickness for display purpose) and segments in which the SIC (yellow to black shadings) is above 95 % (light green). The cells in these segments are eventually counted and divided by the total amount of cells covered by the Arctic perimeter mask to result in the time series plotted in (a).

First, the different paces of growth and melt—growing a certain area takes only little energy effort whereas melting the same area after it has thickened during winter requires a large energy input (e.g. Massonnet et al., 2018)—result in different monthly means around the timing of the blocking; In October when the ice is only partly touching the coast already, the ice can still freely expand, growing a large area at each time interval.

When the sea-ice area reaches the mentioned threshold of approximately 8 million km², typically occurring in November, the expanding sea ice reaches the Arctic perimeter, where its further southward motion becomes constrained. This limitation manifests in the form of ice extending through the straits leading to the Atlantic and Pacific oceans, as well as through the Canadian Archipelago, Hudson Bay, and Baffin Bay. This phenomenon implies that when this constriction takes place later in the respective month, the mean sea-ice area for that season tends to be lower. Conversely, during the melting season, once the ice detaches, it exhibits minimal changes within a comparable time frame.

The second cause lies in regions outside the Arctic perimeter that still have ice at that time of the year. For example, the Hudson Bay (with an ocean area of 1.2 million km²) as well as large parts of the Canadian Archipelago (with an ocean area of 0.8 million km²) both show an extensive sea-ice coverage as they lose their ice only late in the season.



In consequence, this results in the following effects: After summer, when the sea ice is concentrated in the central part of the Arctic Ocean and starts to expand due to atmospheric cooling, the sea-ice area that has grown until the Arctic perimeter is touched is pretty much equal to the area encompassed by the Arctic perimeter (around 8 million km²). Depending on the exact timing of the blocking this results in monthly values slightly below or above this value. After winter, in turn, when the ice retreats, parts of the Canadian Archipelago, the Hudson Bay, and the Baffin Bay still exhibit ice coverage, therefore yielding a higher value in the total sea-ice area when the ice starts detaching from the Arctic perimeter (Gupta et al., 2022; Hochheim and Barber, 2014).

To investigate the exact timing of the blocking and how this might change over time, we repeated the above analysis with daily data and determined the day of the year at which the blocking and detaching occurs.

Timing and evolution of the geographic blocking

Figure A.7 shows the days of the year at which the blocking and the detaching occur. The temperature anomalies are calculated with respect to the 1961–1990 average, entailing that the values at the beginning of the time series in 1979 lie around zero and go up to around 1 °C of global warming with respect to the reference period. The timing of the ice *attaching* to the Arctic perimeter takes place during October at the beginning of the time series and progresses over time with rising global temperatures through November to the beginning of December. Accordingly, the October profile in Figure A.6 shows relatively high values at first (about 50 %) before it drops down suddenly to below 20 % in 2005, namely when the attaching progresses into November.

The timing of the ice *detaching* from the land takes place in June at the beginning of the time series, but then slowly advances into May from around 2010 onward, resulting in a reduction in the according profile in Figure A.6 (although not as strong as in the October/November profile). The timing of the ice *attaching* to the coast delays to later in the year with a sensitivity of around 43 days per degree warming, equivalent to a rate of roughly 7.5 days per decade. For the ice *detaching* from the coast, the sensitivity is slightly weaker with an advance to earlier in the year by around –33 days per degree warming, equivalent to a rate of about –4.4 days per decade. This also indicates that the season during which the ice is not touching the Arctic perimeter and, therefore, can move unhindered is prolonged over time (non-hatched area between the two profiles in Figure A.7).

Due to the timing of the geographic blocking progressing into other months, the sensitivities of the affected months will change over time, too. This becomes obvious from Eisenman's thought model according to which, once the ice edge does not touch the Arctic perimeter any-

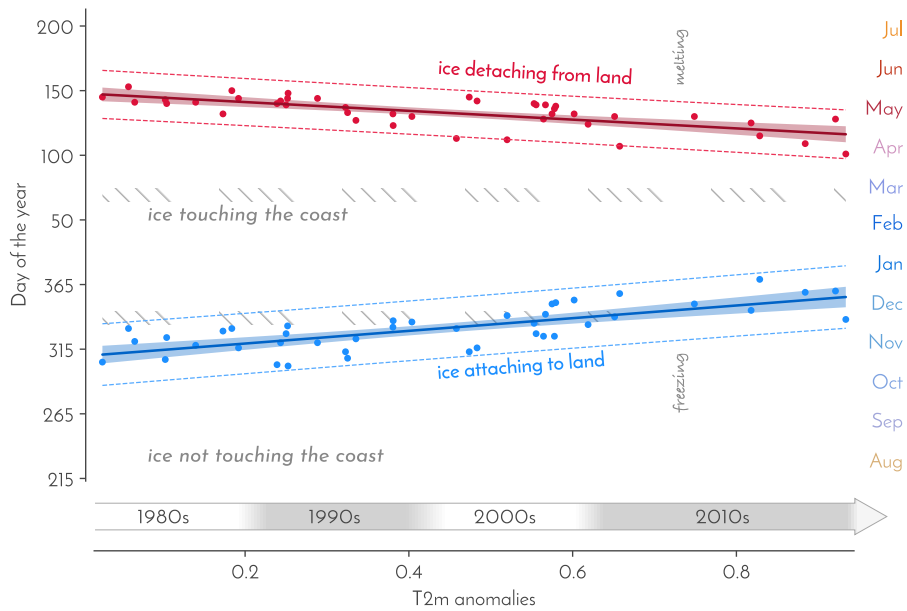


Figure A.7: The day of the year at which the ice is attaching to (blue line) or detaching from (red line) the Arctic perimeter, respectively, plotted against global mean temperature anomalies (reference period: 1961–1990). The attaching delays to later in the year with a sensitivity of 43 days per degree warming, the detaching advances with a rate of 33 days per degree warming, corresponding to about 7.5 days per decade and –4.4 days per decade, respectively. The colored shadings around the regression line mark the 95 % confidence interval of the fit and the dashed lines the 95 % prediction interval. The grey hatching marks the season of the year, during which the Arctic perimeter is fully touched by ice, that is, the ice is blocked from moving further south during that time of the year. Days of the year are roughly mapped to the respective month, ignoring leap years. Note that the y axis starts with August.

more, the resulting area that can freely vary becomes larger, and therefore, the sensitivity of the sea-ice cover to external forcing increases. The difference in the rates is likely due to the different paces of growth and melt;

Let's assign a certain latitudinal position of the sea-ice edge to a certain temperature during the seasonal cycle. If we take global warming into consideration and assume uniformly rising seasonal temperatures, then the point in time at which the blocking/detaching takes place will be reached later during the freezing period and earlier during the melting period. At the same time, also as a consequence of global warming, the sea-ice edge will be located further north. Due to the differences in growth and melt rates, the sea-ice edge overcomes a greater distance between $t_{\text{attaching}-1}$ and $t_{\text{attaching}}$ than during the melting, when the sea-



ice edge detaches from the coast between $t_{\text{detaching}-1}$ and $t_{\text{detaching}}$. Consequently, the resulting area that grows between t_{a-1} and t_a is larger than the area that melts during t_{d-1} and t_d .

A.5. CONCLUSIONS

We used observation data from three different satellite products (*NASA Team*, *NASA Bootstrap*, and *OSISAF*) alongside atmospheric near-surface temperature re-analysis data from *ERA5* to examine how Arctic sea-ice area responds to global warming both on seasonal and regional scales. Following up on a study by Notz and Stroeve (2016), we found linear relationships between Arctic sea-ice area and near-surface temperature anomalies also on these higher-resolved scales.

It often seems obvious to extrapolate these results to estimate the point (in time, temperature, or anthropogenic CO₂ emissions) at which the Arctic faces ice-free conditions (commonly defined as the sea-ice area falling below 1 million km²) as is done in a multitude of studies. However, the seasonal cycle of northern-hemispheric sensitivities exhibits two major breakpoints that hint at external mechanisms other than just thermodynamics that let us assume that extrapolation of these trends cannot be robustly performed for all seasons;

We found that these abrupt changes in the seasonal cycle are not an intrinsic property of seasonal thermodynamics or complex feedback mechanisms but are linked to the timing of geographic muting—a theory that was introduced by Eisenman (2010). Once the expanding ice does not extend any further than the Arctic perimeter (defined by the land masses surrounding the inner Arctic Ocean) in a given month, the areal fraction that responds to global warming increases significantly. In the historical record, this is found at the transition points between May and June and between October and November.

With our analysis, we could demonstrate that the segregation of winter and summer sensitivities is closely linked to the timing of the blocking of the sea-ice edge by the Arctic perimeter, and also, that the strength of the seasonal sensitivities will change accordingly in the future, namely once the respective month does not experience geographic muting of the ice edge anymore.

We find that the timing of the ice edge *attaching* to the Arctic perimeter delays with about 43 days per degree of global warming, while the timing of the ice edge *detaching* from the Arctic perimeter advances with a rate of around 33 days per degree of global warming. The difference in the rates can likely be attributed to the fact that growing a certain area of ice happens in a time span relatively short compared to melting the same area again. This change in winter sensitivities specifically affects regions located north of the Arctic perimeter.

To investigate the regional impact and spatial patterns of seasonal sensitivities, we defined a set of 14 different regions in the Arctic. The

linearity between sea-ice area and mean global temperature also holds on these higher-resolved scales. Care should be taken, however, when linear regressions are performed on regional sea-ice area as most regions experience a state of saturation (fully ice-covered or fully ice-free) during certain time steps and would, therefore, lead to an underestimation of the slope if the data are not pre-filtered accordingly.

The various regions contribute differently to the total sensitivity of northern-hemispheric sea-ice area. Strongest winter contributions can be observed in the Barents Sea, which has already lost the majority of its sea-ice area over the last four decades and is therefore expected to experience first all-year ice-free conditions. Strongest summer contributions can be attributed to the eastern Russian seas (East Siberian Sea and Laptev Sea) and also the Chukchi Sea and the Beaufort Sea.

As soon as the winter ice edge does not traverse the openings of the Arctic perimeter anymore, the total ice area that can dynamically vary will be much larger than today. Therefore, the sensitivities in the affected seasons are expected to increase significantly compared to the current winter sensitivities. Regions within the Arctic perimeter that have shown, until now, no changes in sea-ice coverage in certain seasons of the year will then also exhibit sensitivities as global warming continues.

We believe furthermore that it is likely that these changes will even exceed nowadays summer sensitivities as year-to-year changes in winter sea-ice area will likely be larger due to the faster areal change during freezing.

DATA AVAILABILITY

We used the following data sets for our study, all being publicly available: For our sea-ice area estimates we used *OSI-SAF* (OSI SAF, 2017) and the *NASA Bootstrap* and the *NASA Team* algorithms (Meier et al., 2021). The *OSI-SAF* data can be accessed through the *EUMETSAT Data Services* (<https://navigator.eumetsat.int/product/EO:EUM:DAT:MULT:OSI-450>), the *NASA* data can be downloaded from NSIDC (<https://nsidc.org/data/g02202/versions/4>). For the temperature estimates we used *ERA5* (Muñoz Sabater, 2019), available at ECMWF (www.ecmwf.int/en/forecasts/dataset/ecmwf-reanalysis-v5), *GISTEMP* (GISTEMP Team, 2023; Lenssen et al., 2019, available at <https://data.giss.nasa.gov/gistemp/>), and *HadCRUT4* (Morice et al., 2012, available at www.metoffice.gov.uk/hadobs/hadcrut4/).



ADDITIONAL TABLES

The following tables provide the exact values from our sensitivity analysis, obtained via linear regression. We display the slope of the regression alongside the standard error of regression in one table plus, in an additional table, the r^2 for the respective results. Table A.6 shows the amount of data points that were left after filtering the data according to appendix B.2. Table A.8 provides an estimate of the ocean area of each of the 14 regions that we defined in Figure A.1.

Table A.1: Sensitivity values (slope of linear regression) and the standard error of regression [$1 \times 10^4 \text{ km}^2/\text{°C}$] for every region and season with respect to changes in Arctic temperature.

Domain	Northern Hemisphere	Arctic	Baffin Bay / Gulf of St. Lawrence	Baltic Sea	Barents Sea	Beaufort Sea	Bering Sea	Canadian Archipelago
January	-25.93 ± 4.23		-3.18 ± 1.91	-0.86 ± 0.41	-8.23 ± 1.50		-1.80 ± 1.27	
February	-21.89 ± 4.07		-1.68 ± 1.82	-1.37 ± 0.49	-7.23 ± 1.38		-2.06 ± 1.20	
March	-24.54 ± 4.99		-2.57 ± 2.11	-2.01 ± 0.57	-7.52 ± 1.56		-2.60 ± 1.49	
April	-28.98 ± 3.70		-3.69 ± 1.40	-1.68 ± 0.31	-9.28 ± 1.58		-2.20 ± 1.53	
May	-51.38 ± 5.65		-7.38 ± 1.62	-0.91 ± 0.21	-16.44 ± 2.63		-2.11 ± 1.63	-0.71 ± 0.29
June	-84.79 ± 8.44		-10.54 ± 1.77	-0.02 ± 0.16	-16.42 ± 2.32		-5.65 ± 1.72	-2.49 ± 0.89
July	-136.16 ± 15.55		-13.16 ± 2.08	0.41 ± 0.27	-9.02 ± 2.08		-13.82 ± 3.20	-4.70 ± 0.96
August	-143.31 ± 12.28		-9.61 ± 2.15		-2.13 ± 2.18		-19.69 ± 3.33	-8.31 ± 1.49
September	-114.87 ± 9.92						-17.54 ± 2.50	-6.97 ± 1.33
October	-77.76 ± 6.09		-3.26 ± 1.04		-4.17 ± 0.95		-7.06 ± 1.31	-3.86 ± 0.72
November	-38.49 ± 3.79		-3.84 ± 0.91	-0.04 ± 0.06	-6.64 ± 0.95		-1.31 ± 0.51	-0.99 ± 0.29
December	-33.65 ± 4.66		-4.90 ± 1.22	-0.49 ± 0.21	-8.17 ± 1.40		-2.46 ± 1.06	-0.60 ± 0.21

Domain	Central Arctic	Chukchi Sea	East Siberian Sea	Greenland Sea	Hudson Bay	Kara Sea	Laptev Sea	Sea Of Okhotsk
January	-0.86 ± 0.68			-4.51 ± 0.96	-0.88 ± 1.66		-2.34 ± 1.05	-3.27 ± 1.54
February	-0.55 ± 0.51			-3.12 ± 0.84			-4.29 ± 1.54	-4.03 ± 1.50
March	0.31 ± 0.65			-3.07 ± 0.90			-1.97 ± 0.66	-5.80 ± 1.87
April	1.58 ± 0.59			-2.84 ± 0.73	-0.73 ± 0.48		-3.05 ± 0.92	-6.12 ± 1.59
May	-0.98 ± 0.83	-1.63 ± 0.96		-1.58 ± 2.25	-3.95 ± 1.00		-5.01 ± 0.98	-3.97 ± 1.37
June	-2.84 ± 1.66	-4.74 ± 1.50		-4.53 ± 1.41	-3.77 ± 1.20		-8.70 ± 2.41	-14.58 ± 1.99
July	-10.67 ± 2.63	-11.74 ± 2.57		-16.67 ± 3.69	-5.12 ± 1.73		-12.38 ± 2.52	-22.15 ± 3.79
August	-23.88 ± 3.61	-17.41 ± 2.52		-29.70 ± 3.73	-3.93 ± 1.25		-4.40 ± 1.38	-12.42 ± 2.50
September	-19.66 ± 3.27	-16.02 ± 2.32		-25.71 ± 3.14	-2.77 ± 1.09		-1.42 ± 0.86	-14.83 ± 2.00
October	-7.58 ± 1.40	-10.10 ± 1.40		-15.88 ± 1.84	-1.98 ± 0.62		-2.30 ± 0.79	-11.21 ± 1.34
November	-2.52 ± 0.78	-5.66 ± 1.15		-4.95 ± 1.24	-2.35 ± 0.49		-4.90 ± 1.20	-6.93 ± 1.04
December	-1.50 ± 0.80	-4.11 ± 1.48			-2.78 ± 1.04		-4.29 ± 1.52	-4.38 ± 1.38

Values that are not statistically significant ($f_p \geq 0.05$) are set in grey color. Empty fields correspond to cases in which no regression could be performed.



Table A.2: Sensitivity values (slope of linear regression) and the standard error of regression [$1 \times 10^4 \text{ km}^2/\text{ }^\circ\text{C}$] for every region and season with respect to changes in global temperature.

Domain	Northern Hemisphere	Arctic	Baffin Bay / Gulf of St. Lawrence	Baltic Sea	Barents Sea	Beaufort Sea	Bering Sea	Canadian Archipelago
January	-189.36 ± 18.87	-99.70 ± 14.99	-40.64 ± 9.93	-9.14 ± 2.12	-53.05 ± 8.42		-10.50 ± 7.58	
February	-199.74 ± 25.07	-92.32 ± 18.94	-42.64 ± 10.59	-13.47 ± 2.98	-50.00 ± 9.28		-7.23 ± 8.38	
March	-174.54 ± 24.45	-75.67 ± 17.47	-38.36 ± 10.15	-12.49 ± 2.99	-40.50 ± 8.61		-15.25 ± 8.12	
April	-185.92 ± 19.06	-88.83 ± 16.12	-31.08 ± 7.58	-9.34 ± 1.92	-53.60 ± 9.63		-19.64 ± 8.78	
May	-190.59 ± 15.99	-125.82 ± 13.97	-28.95 ± 5.16	-3.40 ± 0.68	-52.53 ± 9.68	-11.36 ± 3.59	-16.69 ± 5.10	-2.95 ± 1.25
June	-239.96 ± 20.20	-195.03 ± 17.47	-31.56 ± 4.32	0.01 ± 0.44	-42.90 ± 6.59	-17.00 ± 4.52	-8.87 ± 2.01	-7.76 ± 1.74
July	-309.95 ± 25.65	-280.96 ± 23.64	-28.46 ± 4.15	1.13 ± 0.54	-27.34 ± 5.22	-27.19 ± 6.80		-9.45 ± 2.02
August	-348.13 ± 28.90	-339.55 ± 28.60	-11.58 ± 8.00		-5.21 ± 8.54	-49.71 ± 7.69		-18.55 ± 3.79
September	-367.14 ± 34.56	-365.24 ± 34.50				-59.55 ± 7.73		-20.47 ± 4.58
October	-396.82 ± 34.58	-390.09 ± 34.62	-15.46 ± 6.08		-19.70 ± 5.37	-39.52 ± 6.48		-21.05 ± 3.64
November	-257.10 ± 21.29	-210.55 ± 20.97	-28.90 ± 5.28	-0.89 ± 0.40	-36.45 ± 6.91	-9.67 ± 4.30	-7.38 ± 2.56	-4.63 ± 1.24
December	-213.92 ± 17.07	-127.50 ± 16.20	-32.79 ± 5.74	-4.34 ± 0.96	-44.68 ± 7.35		-16.61 ± 5.41	

Domain	Central Arctic	Chukchi Sea	East Siberian Sea	Greenland Sea	Hudson Bay	Kara Sea	Laptev Sea	Sea Of Okhotsk
January	-5.13 ± 4.24			-27.13 ± 5.75	-2.83 ± 5.89	-12.96 ± 7.35		-26.72 ± 8.76
February	-5.54 ± 4.19			-29.28 ± 4.77		-7.13 ± 8.40		-28.89 ± 10.09
March	1.04 ± 5.24			-24.03 ± 4.15		-8.15 ± 4.41		-31.79 ± 10.26
April	10.66 ± 10.11			-21.17 ± 3.86	-3.48 ± 2.74	-7.12 ± 3.73		-35.60 ± 9.50
May	-0.82 ± 2.89	-12.96 ± 3.65	2.07 ± 5.03	-16.88 ± 3.05	-11.57 ± 2.57	-14.79 ± 3.24	-4.20 ± 2.55	-14.19 ± 4.69
June	-6.54 ± 4.95	-18.51 ± 3.50	-10.83 ± 3.84	-14.92 ± 2.78	-26.82 ± 6.22	-35.83 ± 6.01	-20.54 ± 3.81	-15.50 ± 6.80
July	-21.89 ± 5.47	-30.51 ± 4.50	-38.07 ± 7.27	-13.83 ± 3.30	-25.75 ± 5.23	-51.05 ± 7.10	-40.46 ± 6.85	
August	-56.70 ± 8.87	-44.35 ± 5.65	-68.34 ± 9.59	-11.15 ± 2.87	-11.72 ± 3.57	-32.68 ± 5.67	-41.16 ± 6.37	
September	-60.67 ± 11.15	-55.33 ± 6.99	-82.83 ± 10.44	-11.41 ± 3.38	-8.42 ± 3.98	-24.23 ± 6.41	-45.09 ± 7.82	
October	-37.62 ± 7.57	-55.36 ± 6.82	-83.29 ± 9.50	-12.79 ± 3.02	-14.84 ± 4.02	-46.77 ± 8.86	-57.91 ± 7.97	
November	-14.82 ± 5.09	-41.88 ± 6.55	-25.78 ± 7.08	-14.47 ± 3.17	-39.09 ± 6.69	-39.34 ± 7.37	-16.18 ± 5.41	-17.40 ± 4.75
December	-7.31 ± 4.39	-25.51 ± 6.92		-20.49 ± 5.13	-31.46 ± 7.44	-24.29 ± 6.42		-13.59 ± 4.70

Values that are not statistically significant ($f_p \geq 0.05$) are set in grey color. Empty fields correspond to cases in which no regression could be performed.

Table A.3: Sensitivity values (slope of linear regression) and the standard error of regression [1×10^{-1} million km 2 /Gt CO $_2$] for every region and season with respect to changes in anthropogenic CO $_2$ emissions.

Domain	Northern Hemisphere	Arctic	Baffin Bay / Gulf of St. Lawrence	Baltic Sea	Barents Sea	Beaufort Sea	Bering Sea	Canadian Archipelago
January	-138.05 ± 9.58	-69.77 ± 8.70	-28.88 ± 7.22	-6.54 ± 1.51	-37.41 ± 4.91	-6.61 ± 5.22		
February	-145.48 ± 13.15	-68.28 ± 11.68	-28.69 ± 8.31	-9.10 ± 2.30	-39.03 ± 5.64	-7.07 ± 6.07		
March	-127.06 ± 15.12	-63.55 ± 11.12	-24.34 ± 8.24	-8.75 ± 2.25	-33.49 ± 5.12	-8.30 ± 6.04		
April	-126.30 ± 13.45	-56.67 ± 9.75	-19.40 ± 5.98	-6.80 ± 1.42	-39.22 ± 6.02	-8.52 ± 6.55		
May	-126.65 ± 11.14	-85.61 ± 8.79	-17.87 ± 4.04	-2.58 ± 0.49	-39.52 ± 5.90	-9.16 ± 3.87	-1.36 ± 0.84	
June	-164.00 ± 12.11	-131.54 ± 9.87	-22.14 ± 3.10	-0.25 ± 0.29	-31.75 ± 3.82	-11.99 ± 3.13	-6.63 ± 1.27	-4.94 ± 1.23
July	-208.48 ± 13.66	-187.22 ± 12.01	-20.11 ± 2.76	0.63 ± 0.37	-18.80 ± 3.33	-20.54 ± 4.47	-7.07 ± 1.34	
August	-235.05 ± 14.89	-228.33 ± 14.78	-13.87 ± 4.64			-35.67 ± 4.96	-13.52 ± 2.54	
September	-250.44 ± 18.30	-248.86 ± 18.33				-40.81 ± 5.13	-15.26 ± 3.08	
October	-259.15 ± 19.72	-253.92 ± 19.91	-10.80 ± 5.67			-27.72 ± 4.40	-12.39 ± 2.48	
November	-169.87 ± 13.20	-136.67 ± 12.14	-18.17 ± 3.87	-0.60 ± 0.20	-27.44 ± 3.95	-5.67 ± 2.07	-4.59 ± 1.60	-2.51 ± 0.71
December	-150.10 ± 10.31	-91.86 ± 8.91	-20.76 ± 4.36	-3.76 ± 0.66	-36.24 ± 3.81	-10.25 ± 3.85		

Domain	Central Arctic	Chukchi Sea	East Siberian Sea	Greenland Sea	Hudson Bay	Kara Sea	Laptev Sea	Sea Of Okhotsk
January	-1.91 ± 2.50			-20.62 ± 3.55	0.11 ± 5.27	-10.45 ± 4.84		-23.18 ± 5.87
February	-3.20 ± 2.43			-22.08 ± 2.97		-7.34 ± 7.31		-27.66 ± 7.11
March	-0.95 ± 3.54			-18.95 ± 2.53		-8.97 ± 4.58		-28.48 ± 7.37
April	7.36 ± 1.91			-14.94 ± 2.64	-0.57 ± 2.40	-4.25 ± 2.20		-28.42 ± 6.83
May	-1.04 ± 2.38	-10.12 ± 2.55		-11.93 ± 2.11	-7.30 ± 2.02	-7.89 ± 2.05	-3.32 ± 1.48	-10.47 ± 3.43
June	-6.52 ± 2.89	-13.28 ± 2.34	-3.76 ± 2.54	-10.07 ± 1.94	-20.03 ± 4.75	-23.86 ± 3.75	-11.34 ± 2.35	
July	-14.74 ± 3.44	-22.41 ± 2.67	-20.51 ± 4.73	-9.23 ± 2.18	-18.35 ± 4.00	-36.11 ± 4.04	-22.61 ± 4.08	
August	-36.28 ± 4.95	-32.57 ± 3.02	-42.57 ± 6.50	-7.54 ± 1.92	-9.64 ± 2.73	-24.51 ± 3.32	-24.36 ± 4.28	
September	-39.37 ± 6.37	-40.02 ± 3.88	-54.76 ± 6.75	-7.38 ± 2.29	-9.67 ± 2.58	-19.35 ± 4.41	-28.81 ± 5.07	
October	-23.16 ± 4.55	-37.61 ± 4.30	-51.48 ± 6.17	-8.86 ± 2.03	-13.97 ± 4.04	-33.55 ± 5.42	-35.87 ± 4.67	
November	-8.26 ± 3.15	-27.82 ± 4.23	-14.32 ± 5.28	-10.91 ± 2.02	-26.93 ± 5.42	-25.90 ± 4.38	-7.46 ± 2.62	
December	-4.49 ± 2.69	-15.92 ± 4.94		-16.87 ± 3.32	-19.19 ± 5.65	-16.56 ± 4.28	-10.51 ± 3.45	

Values that are not statistically significant ($f_p \geq 0.05$) are set in grey color. Empty fields correspond to cases in which no regression could be performed.



Table A.4: r^2 for temperature-related sensitivities for every region and season*. Values that are not statistically significant ($f_p \geq 0.05$) are set in grey color.

Empty fields correspond to cases in which no regression could be performed due to saturation effects.

Domain month	Northern Hemisphere	Arctic	Baffin Bay / Gulf of St. Lawrence	Baltic Sea	Barents Sea	Beaufort Sea	Bering Sea	Canadian Archipelago
January	0.71	0.52	0.29	0.31	0.50		0.05	
February	0.64	0.41	0.28	0.33	0.41		0.02	
March	0.60	0.38	0.26	0.29	0.35		0.08	
April	0.70	0.47	0.29	0.36	0.43		0.11	
May	0.78	0.66	0.43	0.35	0.42	0.23	0.20	0.16
June	0.77	0.75	0.56	0.00	0.51	0.26	0.45	0.32
July	0.78	0.78	0.53	0.10	0.45	0.28		0.34
August	0.78	0.78	0.09		0.03	0.50		0.37
September	0.73	0.73				0.59		0.33
October	0.76	0.76	0.19		0.29	0.48		0.45
November	0.78	0.71	0.42	0.19	0.40	0.19	0.22	0.26
December	0.79	0.61	0.45	0.28	0.48		0.19	

Domain month	Central Arctic	Chukchi Sea	East Siberian Sea	Greenland Sea	Hudson Bay	Kara Sea	Laptev Sea	Sea Of Okhotsk
January	0.04		0.35		0.01	0.13		0.19
February	0.05		0.48		0.03			0.17
March	0.01		0.45			0.15		0.19
April	0.06		0.42	0.05	0.12			0.26
May	0.01	0.37	0.01	0.43	0.34	0.36	0.08	0.18
June	0.05	0.40	0.17	0.41	0.31	0.46	0.41	0.26
July	0.29	0.53	0.40	0.29	0.36	0.56	0.46	
August	0.49	0.60	0.55	0.26	0.29	0.44	0.50	
September	0.42	0.60	0.61	0.22	0.23	0.27	0.46	
October	0.38	0.62	0.65	0.30	0.40	0.40		0.56
November	0.18	0.50	0.42	0.33	0.45	0.41	0.32	0.48
December	0.08	0.38	0.28	0.31	0.30			0.17

*) In case of a simple linear regression, the square of the Pearson correlation coefficient r is equal to the coefficient of determination R^2 .

Table A.5: r^2 for CO₂-related sensitivities every region and season*. Values that are not statistically significant ($f_p \geq 0.05$) are set in grey color. Empty fields correspond to cases in which no regression could be performed due to saturation effects.

Domain	Northern Hemisphere	Arctic	Baffin Bay / Gulf of St. Lawrence	Baltic Sea	Barents Sea	Beaufort Sea	Bering Sea	Canadian Archipelago
January	0.84	0.62	0.29	0.31	0.60			0.04
February	0.77	0.52	0.23	0.28	0.55			0.03
March	0.68	0.54	0.18	0.27	0.52			0.05
April	0.69	0.49	0.21	0.35	0.52			0.04
May	0.77	0.71	0.33	0.37	0.54	0.19	0.12	0.07
June	0.82	0.81	0.56	0.02	0.64	0.27	0.58	0.29
July	0.86	0.86	0.57	0.07	0.50			0.42
August	0.86	0.86	0.29					0.42
September	0.83	0.83						0.39
October	0.82	0.81	0.13					0.39
November	0.80	0.76	0.36	0.30	0.55	0.19	0.23	0.24
December	0.84	0.73	0.36	0.37	0.70	0.15		

Domain	Central Arctic	Chukchi Sea	East Siberian Sea	Greenland Sea	Hudson Bay	Kara Sea	Laptev Sea	Sea Of Okhotsk
January	0.03			0.46	0.00	0.19		0.28
February	0.07			0.58		0.06		0.28
March	0.00			0.58		0.20		0.28
April	0.39			0.44	0.00	0.14		0.31
May	0.01	0.43		0.45	0.26	0.30	0.14	0.19
June	0.13	0.45	0.05	0.40	0.31	0.51	0.37	
July	0.33	0.65	0.33	0.31	0.34	0.67	0.44	
August	0.57	0.75	0.52	0.27	0.33	0.58	0.45	
September	0.49	0.73	0.63	0.21	0.47	0.36	0.46	
October	0.40	0.66	0.64	0.33	0.40	0.49	0.60	
November	0.16	0.52	0.30	0.42	0.38	0.47	0.35	
December	0.09	0.34		0.40	0.23	0.35		0.18

*) In case of a simple linear regression, the square of the Pearson correlation coefficient r is equal to the coefficient of determination R^2 .



Table A.6: Amount of data points available for the temperature-related regression analysis.

Domain	Northern Hemisphere	Arctic	Baffin Bay / Gulf of St. Lawrence	Baltic Sea	Barents Sea	Beaufort Sea	Bering Sea	Canadian Archipelago	Central Arctic	Chukchi Sea	East Siberian Sea	Greenland Sea	Hudson Bay	Kara Sea	Laptev Sea	Sea Of Okhotsk
January	42	42	42	42	42	0	42	0	41	0	0	42	6	26	0	42
February	42	39	43	43	43	0	43	0	39	0	0	43	0	14	0	43
March	40	39	43	43	43	0	43	0	27	0	0	43	0	9	0	43
April	42	36	42	42	42	0	42	0	11	0	0	42	18	19	0	42
May	42	42	42	42	28	42	30	28	7	42	42	38	21	42	42	42
June	43	43	43	14	43	43	8	43	35	43	43	43	43	43	43	5
July	42	42	14	33	42	0	42	42	42	42	42	42	42	42	42	0
August st	43	43	8	0	8	43	0	43	43	43	43	43	29	43	43	0
September	43	43	0	0	3	43	0	43	43	43	43	43	6	39	40	0
October	43	43	30	3	35	43	0	43	43	43	43	43	16	43	43	0
November	43	43	25	42	28	27	28	43	43	43	43	43	9	43	43	5
December	42	42	42	0	0	38	27	0	42	42	36	0	0	42	42	42

Table A.7: Amount of data points available for the CO₂-related regression analysis.

Domain	Northern Hemisphere	Arctic	Baffin Bay / Gulf of St. Lawrence	Baltic Sea	Barents Sea	Beaufort Sea	Bering Sea	Canadian Archipelago	Central Arctic	Chukchi Sea	East Siberian Sea	Greenland Sea	Hudson Bay	Kara Sea	Laptev Sea	Sea Of Okhotsk
January	41	41	41	41	41	0	41	0	41	0	0	41	8	21	0	41
February	36	34	41	41	41	0	41	0	32	0	0	41	18	0	0	41
March	34	31	41	41	41	0	41	0	20	0	0	41	10	0	0	41
April	40	36	40	40	0	40	0	0	11	0	0	40	18	17	0	40
May	40	40	40	40	27	40	27	32	28	4	40	35	21	40	40	40
June	41	41	13	41	8	41	41	34	41	40	41	41	41	41	41	5
July	40	40	13	32	40	0	40	40	40	40	40	40	40	40	40	0
August	41	41	11	0	3	41	0	41	41	41	41	41	27	41	41	0
September	41	41	0	1	41	0	41	41	41	41	41	41	6	36	39	0
October	41	41	27	4	33	41	3	41	41	41	41	41	16	41	41	0
November	41	41	41	26	41	26	30	27	41	41	41	41	5	4	4	4
December	41	41	41	0	41	0	39	26	0	41	41	35	0	0	41	41

Table A.8: Sizes of the different regions as defined in Figure A.1 including the total ocean area of the Arctic and the Northern Hemisphere.

Region	Size [million km ²]
Baffin Bay/Gulf of St. Lawrence	3.9
Baltic Sea	0.5
Barents Sea	1.6
Beaufort Sea	1.0
Bering Sea	2.3
Canadian Archipelago	0.8
Central Arctic	3.5
Chukchi Sea	0.9
East Siberian Sea	1.1
Greenland Sea	3.7
Hudson Bay	1.2
Kara Sea	0.9
Laptev Sea	0.8
Sea of Okhotsk	1.6
Sum of the regions enclosed by the <i>Arctic perimeter</i>[†]	8.2

[†]) Defined as the coastline at which the expanding ice is hindered of further southward expansion.



B

UNLOCKING THE ARCTIC OCEAN'S CARBON CYCLE: EXPLORING REGIONAL AND SEASONAL CHANGES OF SURFACE OCEAN PCO₂ IN A WARMING ARCTIC

The work in this appendix is intended for submission as:

Ritschel, M., E. Frajka-Williams, and P. Landschützer (2024). "Unlocking the Arctic Ocean's carbon cycle: exploring regional and seasonal changes of surface ocean pCO₂ in a warming Arctic"

AUTHOR CONTRIBUTIONS

MR conceived and designed the study, performed the analysis, and wrote the manuscript. EF-W and PL contributed to the study design, discussed the results, and reviewed the manuscript. This work might be subject to further changes before it is submitted.



Abstract

The Arctic Ocean's carbon cycle is undergoing vast transformations, with major implications for ecosystems and the global climate. Yet, observations of surface ocean pCO₂ in these high latitudes are still highly sparse, resulting in unreliable estimates of seasonal and regional air-sea CO₂ flux changes. Regional studies are consequently restricted to model data or point-wise observations. This is currently changing as novel techniques allow for sophisticated gap-filling in the observational record, providing continuous fields of surface ocean pCO₂. However, uncertainties in these products are still large, and their performance in the Arctic domain is widely unknown. We use two such data sets, which rely on distinct gap-filling methods, to investigate regional and temporal changes in their pCO₂ fields. Both products show an increase in the annual mean pCO₂ throughout most of the Arctic domain. However, the rate of the long-term change varies strongly between regions and is inconsistent between the products at a regional scale. While these regional patterns are distinct, a spatio-temporal decomposition via EOF analysis reveals that seasonal variations show consistent behavior between the two products. We find that the first two modes, which together explain more than 70 % of the total variability, capture the pCO₂ changes in the sub-Arctic and the high Arctic. The sub-Arctic follows a seasonal cycle that correlates negatively with the annual cycle of solar irradiance, hinting at biological activity stimulated by light availability being the main driver in this domain. Conversely, in the high Arctic, the seasonal pattern follows the cycle of sea-ice area, indicating that changes in the pCO₂ there are mostly caused by variations in the sea ice cover. Unraveling the complexities of the Arctic Ocean's carbon dynamics is a crucial step toward better understanding the dominant processes driving the Arctic carbon cycle. This will become even more important in the future when regions in the Arctic experience drastic changes as global warming progresses.



B.1. INTRODUCTION

The Arctic Ocean's carbonate system has been relatively isolated from interactions with the atmospheric carbon cycle due to the perennial presence of sea ice. Nonetheless, the separation between the Arctic Ocean and the overlying atmosphere is currently undergoing major changes as the sea ice cover retreats as a result of human-induced climate change (IPCC, 2023; Yasunaka et al., 2023). In addition, the Arctic is also the region on Earth that shows the strongest response to global warming, e.g. with temperatures rising at about four times the global average rate (Rantanen et al., 2022), posing a high risk of altering oceanic properties and stressing marine ecosystems. Understanding changes in the carbonate system of the Arctic Ocean and their relation to changes in the Arctic domain is therefore of great importance, also for making reliable estimates of future changes as sea ice cover continues to decline.

As satellite records from the past four decades show, the decline of sea ice is, however, not uniform across the Arctic. In addition, the Arctic domain is characterized by intricate geographical features and multi-layered interactions between the atmosphere, the ocean, and the cryosphere, making regional characteristics meaningful. Therefore, taking into account these regional differences and changes is of even greater importance for developing an enhanced comprehension of the subject. The still long-lasting season of ice coverage and the rough conditions in these remote areas combined with months of absolute darkness make it challenging to collect continuous ocean CO₂ measurements, resulting in a small number of ship measurements (e.g. Bakker et al., 2016). Consequently, our understanding of the Arctic marine carbon cycle is largely based on individual point observational studies, typically limited to a specific period and domain (Cai et al., 2010). Although the importance of regional studies is regularly emphasized, such studies are based almost exclusively on model data (e.g. Orr et al., 2022). However, modern climate models still lack sufficient representation of biochemical processes in the Arctic domain, which may compromise their reliability.

Recent advances in methodology to fill gaps in sparse measurements of the sea surface partial pressure of CO₂ (pCO₂), which is the main driver determining direction and magnitude of the air-sea CO₂ exchange, now allow for more regional investigations (Ritter et al., 2017; Becker et al., 2021). These data products usually use machine learning or combine observations with model data, underpinning valuable insights into the global ocean or large-scale domains. Still, there is a dearth of literature concerning the Arctic domain. Recently, Yasunaka et al. (2023) have provided the first synthesis of such data products alongside state-of-the-art ocean biogeochemical models with a focus on the Arctic. While there is a broad agreement between methods that

the Arctic serves as a sink for human-made CO₂, one of their concluding statements notes the significant uncertainty that hinders quantitative analysis in these high-latitude areas. These uncertainties arise, in part, from the limited observations that serve as the foundation for these data sets. The greater the quantity of data accessible, the narrower the gaps to fill or the more precise the corresponding method's estimates. As visible from the SOCAT database records (Bakker et al., 2016), which encompass the majority of pCO₂ measurements obtained since 1982, the bulk of them were conducted post-2005.

Here, we use two commonly used pCO₂ data products (Rödenbeck et al., 2022; Landschützer et al., 2016) that employ distinct techniques for filling large data gaps in the Arctic to study the variability of the surface ocean pCO₂ and its drivers. We have chosen two complementary products that span the entire region up to 90°N and use sophisticated methods that take into account the dynamics of other proxy variables to predict the missing values in the pCO₂ field. For the rest of the document, we proceed as follows: After introducing the two data products and research methods employed in this study to evaluate the two data sets, we commence by providing an overview of the mean state and temporal evolution of the pCO₂ fields. We emphasize both similarities and variations in the two data sets and then conduct an EOF analysis to break down the spatio-temporal information and assess regional patterns and characteristics of the seasonality. Finally, we attempt to establish the link between the identified features and potential drivers and end with some concluding remarks.

B.2. DATA AND METHODS

For our analysis, we investigated two pCO₂ products, namely the Max Planck Institute for Meteorology Self-Organizing Map Feed-Forward Network (MPIM-SOM-FFN) method (Landschützer et al., 2016) and the Jena-Carboscope mixed layer scheme (Jena-MLS) method (Rödenbeck et al., 2013). These pCO₂ products cover data across the entire Arctic up to 90°N. However, they differ in the techniques used to estimate the pCO₂ to fill the gaps in the observational record.

The Jena-MLS is primarily based on spatio-temporal interpolation of the pCO₂ observation data from the SOCAT database but also compatible with the dynamics of ocean mixed-layer carbon content, i.e. taking into account the buffer effect (Rödenbeck et al., 2013, 2022). The pCO₂ field in this product is available at a daily 2.5°×2° resolution from 1957 to 2021.

The MPIM-SOM-FFN uses a two-step neural network approach (i.e. self-organizing map and feed-forward neural network) that takes as inputs sea surface temperature, sea surface salinity, mixed-layer depth, chlorophyll *a*, atmospheric pCO₂ and an ocean pCO₂ climatology. This technique reconstructs the sea surface pCO₂ field at a monthly 1°×1°



resolution over the open ocean and, spanning the period from 1982 to 2021 (Landschützer et al., 2013, 2016; Jersild et al., 2017). Note that the MPIM-SOM-FFN has some larger areas of missing data points in the high winter season (Jersild et al., 2017), which stem from gaps in the mixed-layer depth proxy (De Boyer Montégut et al., 2004). These areas are mainly attributable to regions with sea-ice cover and thus have little effect on our analysis. However, for our EOF analysis (see below), where these missing areas *do* affect our analysis, we make the assumption of no changes under sea ice by filling these missing values with zero after having the data detrended and the long-term mean subtracted to minimize variability at these points. Sea ice is not used as an input parameter when estimating the pCO₂ fields in either of the two products, however, both products scale the final air-sea CO₂ flux by the fraction of sea-ice cover in each grid cell.

We also use sea-ice area and sea surface temperature to compare regional and seasonal pCO₂ patterns. Sea-ice area is calculated by multiplying sea ice concentration with the area of each cell. Land masses are masked before calculations are performed. As an estimate for the sea-ice concentration, we use the NASA Team and the NASA Bootstrap satellite retrievals from National Snow and Ice Data Center (NSIDC) (Comiso, 1995; Cavalieri et al., 1996). For sea surface temperatures, we rely on the estimates from the Optimum Interpolation Sea Surface Temperature (OISST) data set from NOAA (Huang et al., 2021). The seasonal profile is obtained through the first principal component from EOF analysis.

To assess the spatial changes of the mean state over time, we use the monthly data on the native product grids and average into pentads (5-year periods). The long-term trend is calculated as a linear regression on the annual means at each pixel. We use spatial averages over the global domain (all ocean surface area), the Northern Hemisphere, and the Arctic (here, defined as the oceans north of 60 °N) to create time series of data to analyze temporal changes over larger regions.

Combined spatial and temporal variability is assessed using EOF analysis. The calculation was carried out using the *xeofs* Python package Rieger and Levang, 2023, and the EOFs were rotated using *Varimax* rotation. Some data preparation was needed prior to calculating the EOFs: First, the spatial field was restricted to the domain north of 50 °N, and the Baltic Sea was masked out as this region shows especially large pCO₂ values in the MPIM-SOM-FFN, which would dominate the variability patterns. Then, at each pixel, the long-term linear trend was removed from the monthly time series of pCO₂, and missing values were filled with the long-term mean. This way, these pixels can be considered for the EOF analysis, but the mean-filled missing values would not contribute to the variability. The average seasonal cycles, which

we show alongside the time series of the principal components, were computed from the principal components of each of the first and second modes of variability.

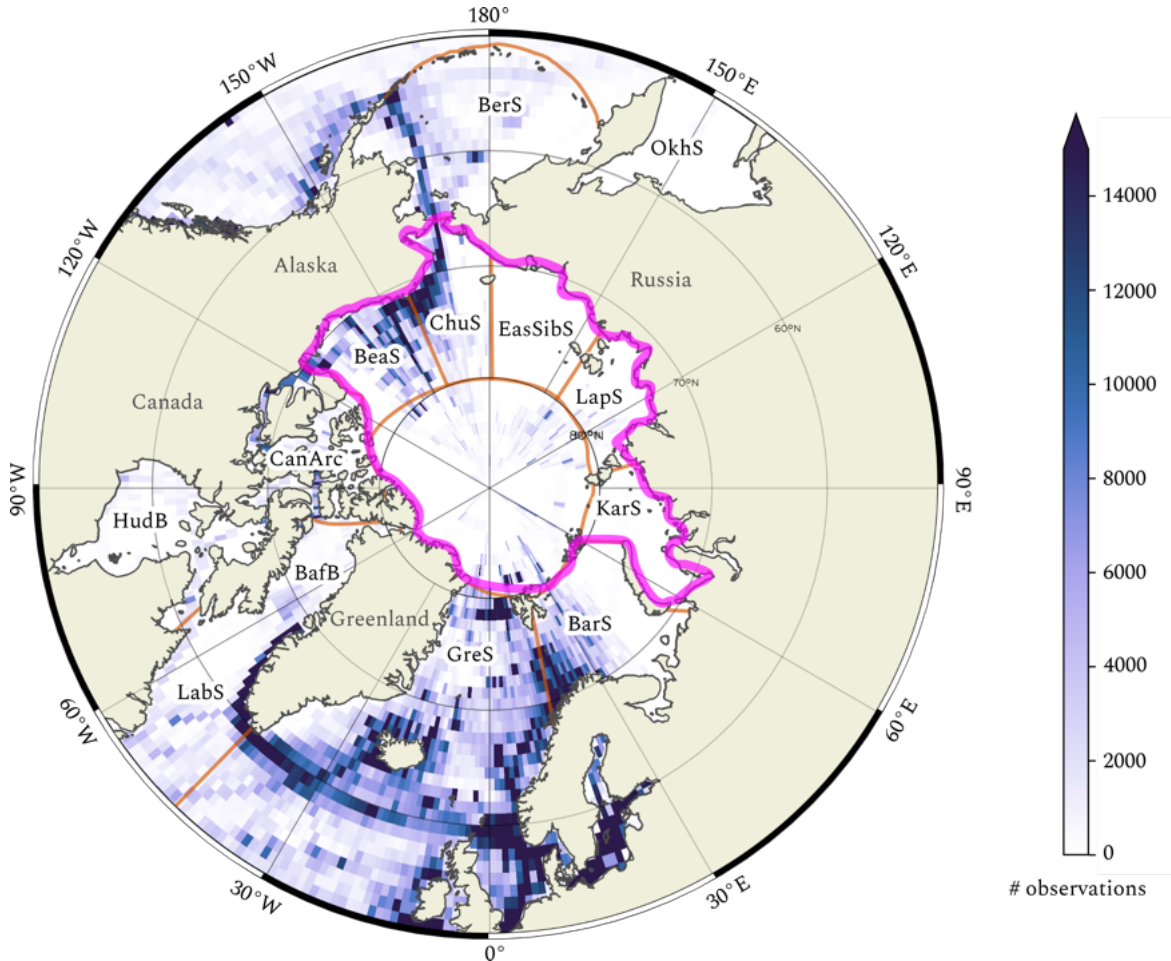


Figure B.1: Overview of the different Arctic regions alongside the total number of pCO₂ measurements in the SOCAT database between 1982 and 2021. Regions of the high Arctic: Beaufort Sea (BeaS), Chukchi Sea (ChuS), East Siberian Sea (EasSibS), Laptev Sea (LapS), and Kara Sea (KarS). Regions of the sub-Arctic: Bering Sea (BerS) and Sea of Okhotsk (OkhS) on the Pacific Side, and Barents Sea (BarS), Greenland Sea (GreS) and the Labrador Sea (LabS) on the Atlantic side, together with the Baffin Bay (BafB), the Hudson Bay (HudB), and the Canadian Archipelago (CanArc). The magenta line separates the high Arctic and sub-Arctic. Orange boundaries indicate basin segments.

To assess the timing of seasonal maxima and minima in different regions and the change in the seasonal amplitude, we use the monthly time series in each region, then determine the timing (month) of maximum and minimum, and finally average over 5-year periods. The amplitude is the difference between annual maximum and minimum values.



In this work, we discuss features in different regions of the Arctic. These regions are displayed in Figure B.1 alongside the number of pCO₂ measurements that are registered in the SOCAT database and that have been collected between 1982 and 2021 and serve as the base for the two pCO₂ products' methods.

B.3. RESULTS & DISCUSSION

B.3.1 *The mean sea surface pCO₂*

We begin with a description of the mean state of the pCO₂ fields in the two data products and its evolution over time (Figure B.2). In both data sets, the regions of the sub-Arctic display relatively moderate CO₂ partial pressures of around 340 µatm, indicating that the surface ocean partial pressure is undersaturated with respect to the overlaying atmosphere but consistently increasing over time as human emissions progressed. These sub-Arctic regions are mostly ice-free for the majority of the year. Substantial variability is present in the high Arctic, both in terms of spatial distribution and change over time; the deltas between the 2nd and the 98th percentile for each pentad range from 91 µatm to 160 µatm for the MPIM-SOM-FFN and from 165 µatm to 185 µatm for the Jena-MLS (compare Figure B.2). Sea ice is present at the air-sea interface in the same area, where observations are highly scarce. Thus, we also find that the two products show the strongest differences in ice-covered areas.

Notably, the Jena-MLS exhibits an area of high pCO₂ around the Pacific opening, interrupted by a strong minimum in the center of the East Siberian Sea (west of the opening). Between the late 1980s and 2005, high pCO₂ levels with values exceeding 550 µatm markedly expanded in spatial extent and absolute value. Additionally, the southern Hudson Bay registered pCO₂ levels higher than 500 µatm. The MPIM-SOM-FFN product exhibits a relatively uniform rise across the Arctic with some non-uniformity of the trend in the high Arctic. During the latter period (2017–2021), there was a marked increase in the Hudson Bay and the Beaufort Sea. In both data sets, we find the high pCO₂ areas within the high Arctic and the Hudson Bay.

Despite the significant spatial differences between pCO₂ from the two products (Figure B.2), both data sets show similar mean state and evolution on a global scale (Figure B.3), illustrating that (a) the Arctic is less well understood than its global ocean counterpart and (b) Arctic pCO₂ (and subsequent air-sea fluxes) play a minor role as these local differences do not translate into a global disagreement. Discrepancies appear in particular when we limit the area to the high Arctic. The global and northern hemisphere pCO₂ averages exhibit a positive trend in both data sets, roughly tracking the atmospheric pCO₂ signal but with a slightly lower rate. In the Arctic, both data sets show

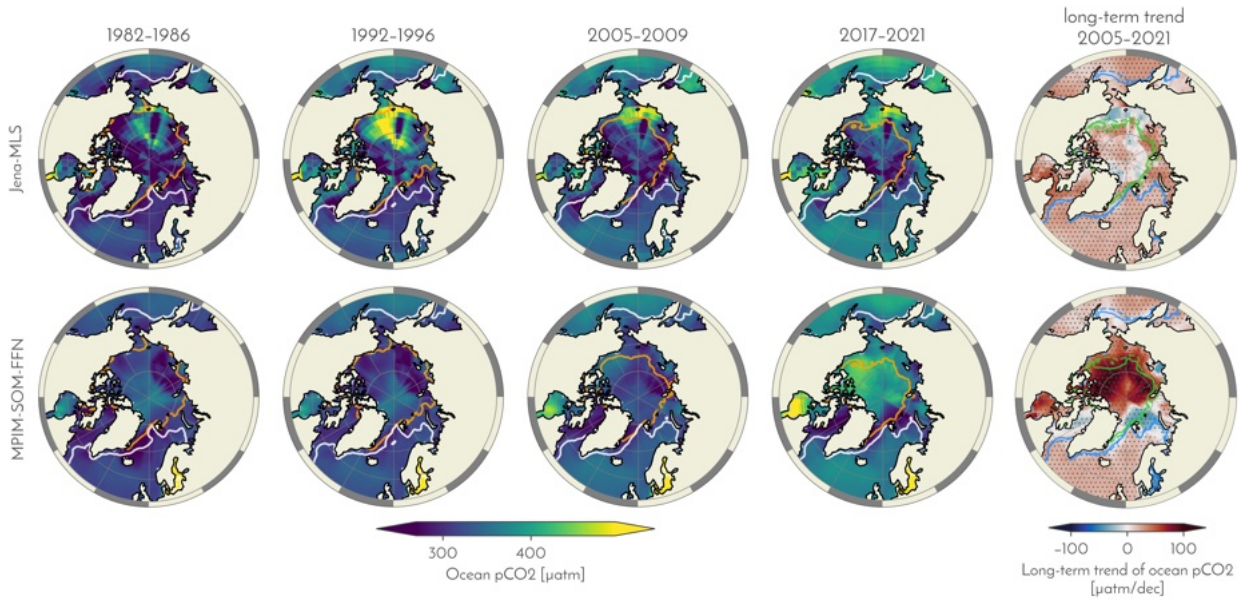


Figure B.2: Mean states of ocean pCO_2 for different pentads (5-year periods) and long-term trend (2005–2021; right-most column). Orange (white) contour lines mark the respective average September (March) sea-ice edge (NASA Team). In the right-most panels, the solid (dashed) contour lines mark the respective states in 2005 (2021).

a total increase of the annual mean pCO_2 between 1982 and 2021, but they differ in the interannual variations and in the amplitude of intra-annual changes. The pronounced high in the Jena-MLS from 1989–1999 is striking in the spatial average, exhibiting a change of around 40 μatm within 10 years. This increase is not apparent in the MPIM-SOM-FFN product, which shows almost no change in the annual mean over 1984–2004. Given the lack of observations and literature studies, it remains impossible to verify the correct magnitude of the sea surface pCO_2 in this period.

While in the Jena-MLS product, the amplitude of the seasonal cycle changes little over the whole period, in the MPIM-SOM-FFN product, the amplitude increases nearly 4-fold during the first data sparse years. From 2000 onward, the amplitude stays reasonably constant, illustrating that the seasonal cycle proves little reliable before 2000 in the MPIM-SOM-FFN method. We thus conclude that the distinct phenomena discussed above in the data products are likely caused by the scarce observational coverage before 2005 (compare Figure B.6). Therefore, in the following, we focus on the period between 2005 and 2021, where pCO_2 observations are more abundant in the Arctic (Figure B.6).

Considering the long-term trend from 2005 to 2021 (Figure B.2, right-most panels), we find an increase in ocean pCO_2 in almost all regions with notable exceptions, mainly in the vicinity of the summer sea-ice margin. Trends are generally higher and more spatially variable in the



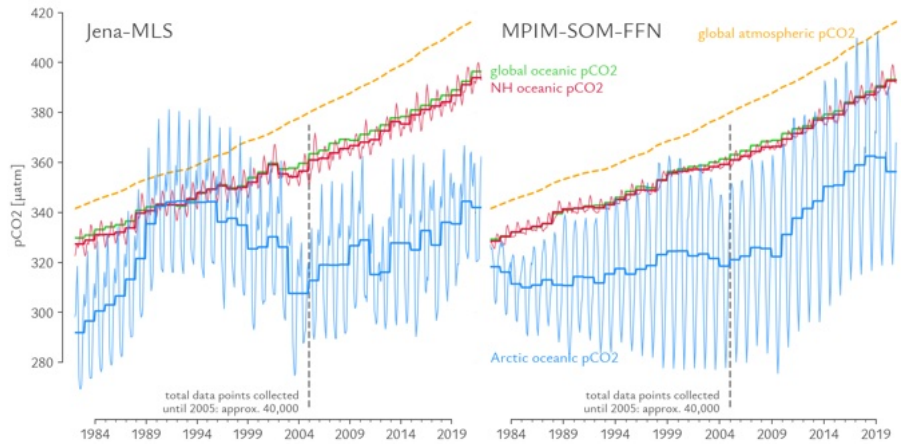


Figure B.3: Time series of atmospheric global (orange), and oceanic global (green), northern-hemispheric (red) and Arctic (blue) pCO₂ for Jena-MLS (left) and MPIM-SOM-FFN (right).

MPIM-SOM-FFN, reaching maximum values of more than +100 μatm per decade in the Kara Sea and around the Beaufort Gyre. The difference between the two products is largest in the central Arctic. This region is also the part of the Arctic that is, up to date, covered by sea ice for most days of the year.

Overall, both products agree on an increase in the annual mean pCO₂ but exhibit considerable spatial and temporal differences in the magnitude of the trend and the change in seasonal variability. In the next step, we separate the spatial from the temporal information, thereby examining trends and seasonal variability.

B.3.2 A spatio-temporal decomposition hints at dominating drivers

Figure B.4 displays the first two EOFs and the temporal evolution of these patterns represented by the respective principal component. In both data sets, the first two modes together explain more than 70 % of the overall variability, so we limit the following narrative to the first two modes.

Overall, we find better agreement between the first mode of the Jena-MLS data set and the second mode of the MPIM-SOM-FFN. This is somewhat surprising given the spatial and temporal difference observed in the mean and trend. The similarity of the complementary modes is apparent in both the spatial eigenvectors (EOF maps) and the temporal variability given by the respective principal component. The EOFs for each product show the strongest values in the sub-Arctic regions and share a dipole feature in the Hudson Bay with negative values in the western part and positive values in the East. Amplitudes are highest in the Pacific and lower in the Atlantic. The high in the Chukchi Sea is more pronounced in the Jena-MLS. However, note that the Jena-

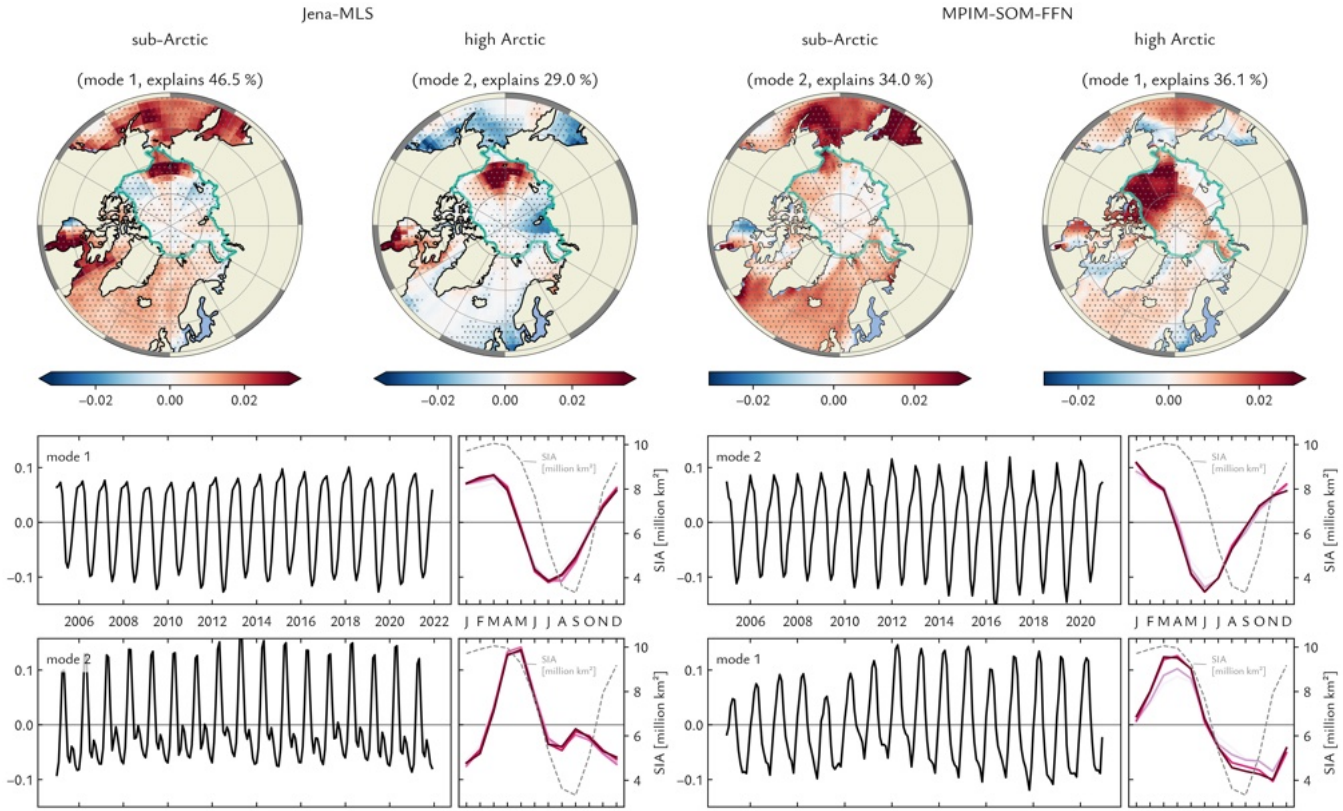


Figure B.4: Varimax-rotated EOFs and principal components (time series and seasonality) of the first two modes for each data set. The EOFs represent the spatial structure of the major patterns being responsible for the variability in the original time series. Dots mark the areas where the correlation between the principal component and the original data is statistically significant ($p < 0.05$). The light-teal path marks the area defined as the *high Arctic* (also compare Figure 1.2). Note that the order in the MPIM-SOM-FFN modes is swapped for easier comparison of the modes between the two data products. The principal components (PC; time series depicted in the lower panels) indicate how the amplitude of each EOF pattern (mode 1 and mode 2) varies with time. Next to the PC is the seasonality of the respective PC (solid lines; the color range from light to dark magenta represents past to present) alongside the seasonality of the Arctic sea-ice area (dashed gray line). The values on the right y-axis represent the sea-ice area in Mio. km².

MLS product has a relatively coarse spatial resolution, so individual cells might overestimate a specific value's spatial extent. Both principal components show a clear, regular seasonal cycle with its peak in winter and its minimum in summer.

The second-mode EOF of the Jena-MLS and the first-mode EOF of the MPIM-SOM-FFN are characterized by strong positive values in the high Arctic, specifically in the Chukchi Sea and, in the case of the MPIM-SOM-FFN, also in the Beaufort Sea and north of Canada, potentially extrapol-



lating the signal from the Chukchi Sea to the neighboring waters. The Jena-MLS exhibits an area of negative values in the Kara Sea, which the MPIM-SOM-FFN does not capture. Regions around the southern coastlines on the Pacific side and east and west of Greenland are characterized by slightly negative values. These spatial patterns go along with another seasonal pattern in the principal component, with the high in late spring and the minimum in August/September for the MPIM-SOM-FFN, or in December for the Jena-MLS—although the latter also exhibits a temporary low around August.

The spatial patterns displayed by the EOFs suggest that the first (second) mode of the Jena-MLS (MPIM-SOM-FFN) explains mainly the sub-Arctic variability, accompanied by a seasonality pattern in its corresponding PC that is fairly symmetric around summer. On the other hand, the spatial patterns of the second (first) mode of the Jena-MLS (MPIM-SOM-FFN) combined with the seasonality of the corresponding PC seem to represent predominantly changes in the high Arctic.

While processes driving the variations in the two products may differ for individual methods and could potentially be quantified by doing dedicated response function experiments, we here try to explain the observed variations and provide a qualitative comparison focusing on the spatial and temporal features shown by the two data sets.

In sub-Arctic regions that are characterized by perennial absence of ice, processes related to changes in temperature and/or light availability appear to dominate. Temperature-induced changes in pCO₂ are well understood and expected to show the characteristic of the temperature profile (Sarmiento and Gruber, 2006; Millero, 2013), which follows the seasonal cycle of solar irradiance, commonly described by a continuous profile south of 66°N. Concurrently, heightened light availability during summer stimulates photosynthetic biological activity, leading to a pCO₂-reducing drawdown effect. In winter, when sea ice starts to grow, biological activity is reduced to a minimum, and the pCO₂ drawdown effect is shut down.

Finally, the growth of a solid sea ice layer on top of the ocean surface impedes the physical air-sea gas exchange. It enhances the salinity and the content of DIC and TA of the under-ice seawater due to brine drainage (Worster and Rees Jones, 2015; Griewank and Notz, 2013; Rysgaard et al., 2007), leading to a net increase in surface ocean pCO₂ during the cold season. The input of freshwater due to the subsequent ice melt (e.g. Yamamoto-Kawai et al., 2005; Krishfield et al., 2014) leads to a net decrease of pCO₂ levels and enhanced stratification, hindering the surface water from vertical mixing with deeper layers (e.g. Toole et al., 2010; Maksym, 2019). These pCO₂ changes related to the growth and melt of sea ice are largely characterized by the so-called *Sea-Ice Carbon Pump* (Rysgaard et al., 2007; Grimm et al., 2016; Moreau et al., 2016).

The regions further north experience different conditions, mainly due to the longer-lasting sea-ice cover, which impedes the physical air-sea gas exchange for an extended period of the year. Enhanced release of brine and dissolved carbon due to thicker growing sea ice in these regions leads to elevated pCO₂ levels during the cold season. In contrast, temperature-driven changes in pCO₂ are minimal, especially in the presence of sea ice, when the temperature remains at the freezing point. Changes in pCO₂ related to biological activity occur slightly later in the year compared to sub-Arctic regions, as light availability is scarce in winter and increases only significantly once the ice is reasonably thin or has disappeared again.

Processes captured by the EOF analysis

The patterns revealed by the first two EOFs as shown above suggest that sub-Arctic and high-Arctic pCO₂ fields are dominated by different mechanisms.

The sub-Arctic profiles of the first-mode PC (Jena-MLS) and the second-mode PC (MPIM-SOM-FFN) show high anti-correlated resemblance to the seasonal cycle of solar irradiance, suggesting that temperature is of minor importance for the detected pCO₂ changes. A temperature decomposition following Takahashi et al. (1993) confirms the modest contribution of the thermal component, contributing less than 20 % of the overall pCO₂ trend in most regions, with the maximum values along the position of the winter sea-ice edge (not shown). Instead, non-thermal processes such as mixing or the consumption of CO₂ by enhanced biological activity during summer and the reverse process during winter are more likely to explain the behavior of the pCO₂ profile in these areas. Over the past decades, net primary production has been even enhanced by the reduction in sea ice cover and longer growing seasons (Arrigo et al., 2008; Arrigo and van Dijken, 2011, 2015).

In contrast, the high Arctic is characterized by a PC that matches the seasonality of sea-ice area, suggesting that the processes governing the change in pCO₂ in these areas are primarily influenced by the variability in the sea ice cover. Since the profiles are strongly correlated, we argue that, from the processes mentioned above, those that result in a net decrease in pCO₂ dominate during the sea ice melt season, and those resulting in a net increase in pCO₂ dominate during the sea ice growth season.

The lag between the first mode in Jena-MLS and the second mode in MPIM-SOM-FFN may be the result of the different amounts of variability explained by the respective mode. In the Jena-MLS, the first mode comprehensively accounts for the variability in the sub-Arctic regions (zero across large areas in the second mode EOF), explaining over 1.5 times more variability than the second mode. In contrast, in the MPIM-SOM-FFN, the sub-Arctic variability is captured through a com-



posite of both modes, explaining approximately the same percentage of variability. If we picture the sum of the two PC profiles of the MPIM-SOM-FFN, we obtain a profile that qualitatively resembles a right-shifted profile of the second mode (compare Figure B.4).

On the other hand, profiles associated with the high Arctic differ considerably between the two data sets. However, this region also shows considerable disagreement in the spatial patterns of the EOFs and the mean state fields (compare Figure B.2) and might be biased accordingly. In addition, the high-Arctic-related PC of the MPIM-SOM-FFN (first mode) shows a much more pronounced change in the amplitude over time compared with Jena-MLS, indicated by the different colors in the plot.

B.3.3 Changes in timing and amplitude of the seasonal cycle

Furthermore, the profile of the different modes, particularly in the MPIM-SOM-FFN, indicates potential for phase shifts in these profiles. A recent model study by Orr et al. (2022) proposed that the seasonality of the Arctic Ocean's pCO₂ may experience shifts in timing and amplitude by the end of the century. While this is a notable result, these projections might even underestimate the development as regional features may be smoothed out in the large-scale average the study focuses on. Hence, changes in seasonality may be already apparent in the present days if we look at the regional development of the historical pCO₂ signal. Data sparsity, particularly in the period before 2005, however, leaves us with little confidence that we can already detect such a shift in the past record.

Focusing on the data-richer period after 2005 and considering the timing of the seasonal minimum first (Figure B.5, top row), we notice that both data sets agree reasonably well in the regions outside the area of seasonal ice cover. However, inside the domain of seasonal ice cover, there are a few regions in which both data sets disagree: In the area around the Beaufort Sea and the Canada Basin, the Jena-MLS shows a seasonal minimum in both periods in late winter (early in the year) whereas the MPIM-SOM-FFN shows the seasonal minimum in late autumn or early winter. The same is true for the sectors 0°–30°E and 150°N–180°N north of 80°N. Note that these are also the regions where the first mode EOFs disagreed. The areas outside the high Arctic are similarly represented in both data sets, with only minor changes between the two time periods. Also, in the sector between 80°E and 130°E, the Jena-MLS tends to a timing earlier in summer, whereas the MPIM-SOM-FFN exhibits a timing in later summer. Looking at the different data sets individually, we notice that the timing in the Jena-MLS is nearly indistinguishable but varies in the MPIM-SOM-FFN: The latter

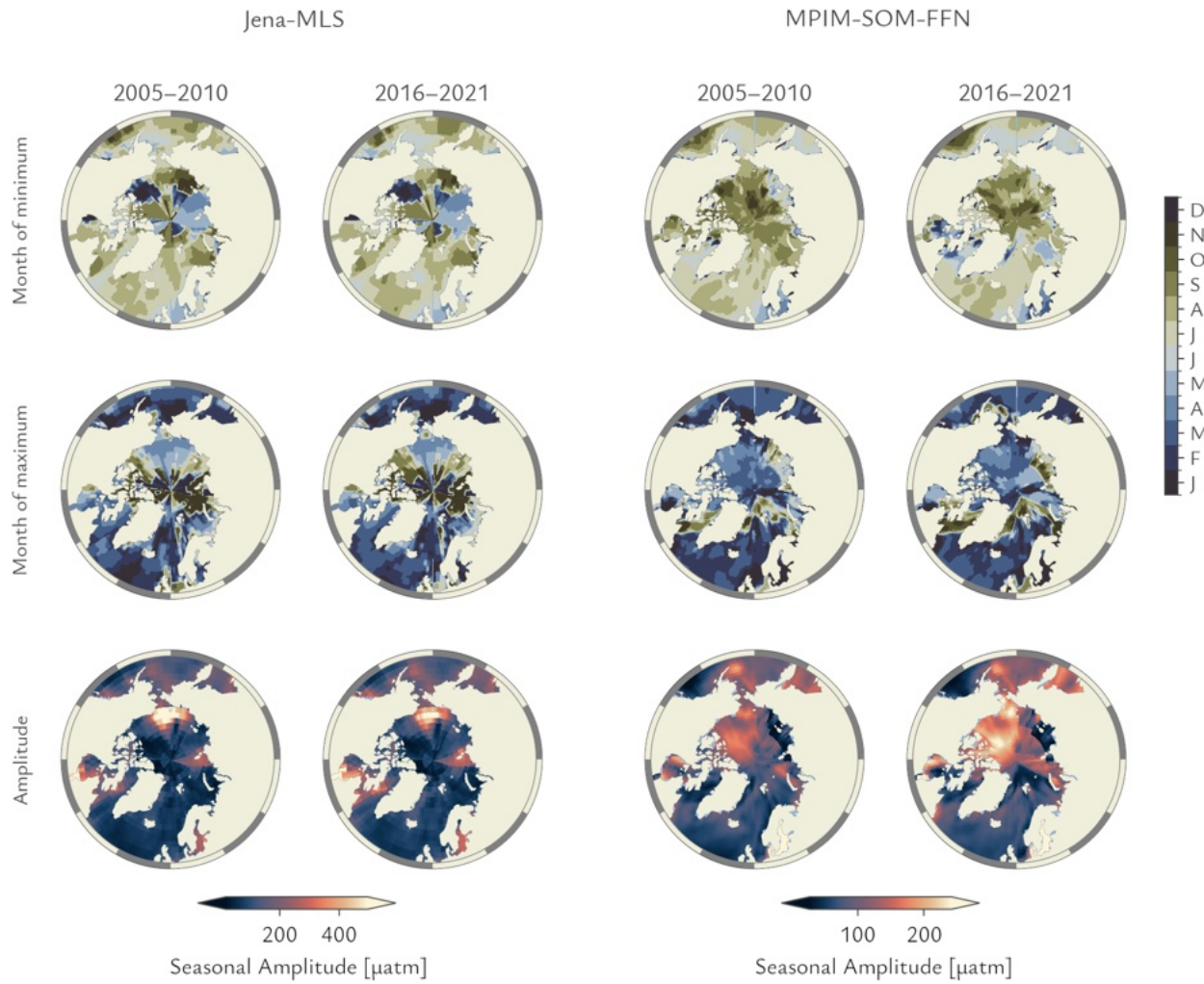


Figure B.5: Timing (month) of the ocean surface pCO₂ minimum (top row) and maximum (middle row) as well as the amplitude (bottom row) for different 5-year periods. Note the different color map extents of the amplitudes. The cyclic color bar representing the maps of timing equates dark shading with winter months and lighter shadings with summer months.

shows shifts in the minimum timing by a few months towards earlier in the year inside Hudson Bay as well as in the Barents Sea and the Norwegian Sea.

Also, concerning the timing of the seasonal maximum (Figure B.5, middle row), both data sets largely agree in the regions outside the zone of seasonal ice coverage and show only little change between the two time periods. However, they disagree in the high-Arctic regions, with the most extensive disagreements close to Canada and the northern part of Greenland, as well as in the Labrador Sea and around Svalbard. Regarding the shifts within the individual data sets, we also notice that the Jena-MLS exhibits only slight to no shifts. In contrast, the



MPIM-SOM-FFN reveals shifts in the timing of the maximum, in particular in front of the west coast of Alaska but also in the Baffin Bay and parts of the Kara Sea and the Barents Sea.

Looking finally at the amplitude of the seasonal cycle (Figure B.5, bottom row), we find common areas of high amplitudes, for example, the Chukchi Sea, the southern Hudson Bay, and a sector in the Kara Sea. The latter is interesting as this was a unique feature of the second mode EOF in the Jena-MLS data set, not shown by the MPIM-SOM-FFN. The area with the largest disagreement regarding amplitude characteristics is found north of Canada and Greenland. Here, the Jena-MLS shows the lowest values within the whole Arctic domain. In contrast, the MPIM-SOM-FFN reveals a region of high seasonal amplitude that intensifies over time. It is to note, however, that the range of the amplitudes displayed by the Jena-MLS is up to twice as large compared to the MPIM-SOM-FFN, with $\Delta p\text{CO}_2$ values of more than 500 μatm as opposed to around 300 μatm in the MPIM-SOM-FFN.

We are aware that, due to the large uncertainties, there are some caveats in how the data we used in this study represent regional information on seasonal characteristics. Also note that spatial gaps have been ignored and might lead to an underestimation of the maximum, which is assumed for most cases to take place in winter when these gaps occur. However, as the maxima are typically in late winter or early spring when the gaps are absent, we expect this to be a minor issue.

Considering the availability of observations in the different regions, the disagreements north of Canada and in the Russian seas are not too surprising as these regions have the sparsest observational data coverage. In contrast, a decent amount of observations is available for the Nordic Seas and the area around Alaska, comprising the Beaufort Sea, the eastern part of the Chukchi Sea, and the surrounding sea south of Alaska. Given the amount of available observations and the general differences between the two data sets, we do not attach much value to these findings in the timing and the seasonal amplitude. However, regarding the regions we trust more, it is interesting to see both an amplitude intensification and a seasonality shift already in the historical record. These changes can be of major importance for the ecosystems in these regions and should be further investigated.

B.4. CONCLUSIONS

In this study, we used two ocean surface pCO_2 products to investigate the spatial and temporal variability of pCO_2 in the Arctic and sub-Arctic oceans. The basin-scale agreement between the two data sets improved from 2005, when ship-based underway pCO_2 measurements became more routine. However, large discrepancies remain in the regional patterns of mean states and long-term trends due to the limited availability of direct pCO_2 observations.

Instead, we investigate the variability in both products, finding a general increasing tendency in surface pCO₂ concentrations between 2005 and 2021, as would be expected given the increase in atmospheric CO₂ concentrations over the same period. On a seasonal basis, the pattern of change showed strong similarities between the two pCO₂ products, in that there was a dominant seasonal cycle in the sub-Arctic with a peak in February and minimum in July, while the central Arctic pCO₂ concentration peaks in March with a minimum in August. The seasonal cycle of pCO₂ in the sub-Arctic obtained from EOF analysis matches the inverse seasonal cycle of sea surface temperature and solar irradiance. In the high Arctic, on the other hand, the timing coincides with the seasonal cycle in sea-ice area. As the timing of when the high Arctic is fully covered by sea ice changes under ongoing climate warming, we expect these variability patterns to change accordingly. In any case, the combination of the first two modes of the EOF analysis gives us a simple concept to describe the dynamics of surface ocean pCO₂ in the Arctic domain, which may be helpful for benchmarking other data products or for developing future product versions.

Given the difficulties of undertaking large-scale observations of ocean parameters in the Arctic via satellite, these products are a promising approach for more regional analysis of the oceanic carbon cycle in the Arctic despite the shortcomings discovered. One notable improvement can be achieved by continuing the measurement effort in the Arctic Ocean, as we show that since the start of regular Arctic Ocean observations around 2005, stronger conclusions can be drawn with respect to the changing Arctic carbon cycle. Since the Arctic experiences extreme changes under human-induced climate change, improving our process-understanding in this domain is of great importance and urgency. Our study reveals the strong connection between the seasonal carbon cycle and sea ice, and future sea-ice retreat may perturb the carbon cycle even further. We thus argue for increasing the effort of more continuous underway pCO₂ observations in the Arctic to better understand the seasonal through interannual changes of the Arctic Ocean carbon cycle and its sensitivity to future sea-ice retreat in a changing climate.



OPEN RESEARCH SECTION

We used the following data sets for our study, all being publicly available: The Jena-MLS data set was obtained from www.bgc-jena.mpg.de/CarboScope/oc/oc_v2023.html (last accessed: 2024-01-04). The MPIM-SOM-FFN data set was obtained from www.ncei.noaa.gov/access/ocean-carbon-acidification-data-system/oceans/SPCO2_1982_present_ETH_SOM_FFN.html (Jersild et al., 2017, last accessed: 2024-01-04). For the sea-ice area estimates we used the NASA Bootstrap and the NASA Team algorithms (Meier et al., 2021). The data can be downloaded from the NSIDC website (nsidc.org/data/go2202/versions/4).

ADDITIONAL FIGURES

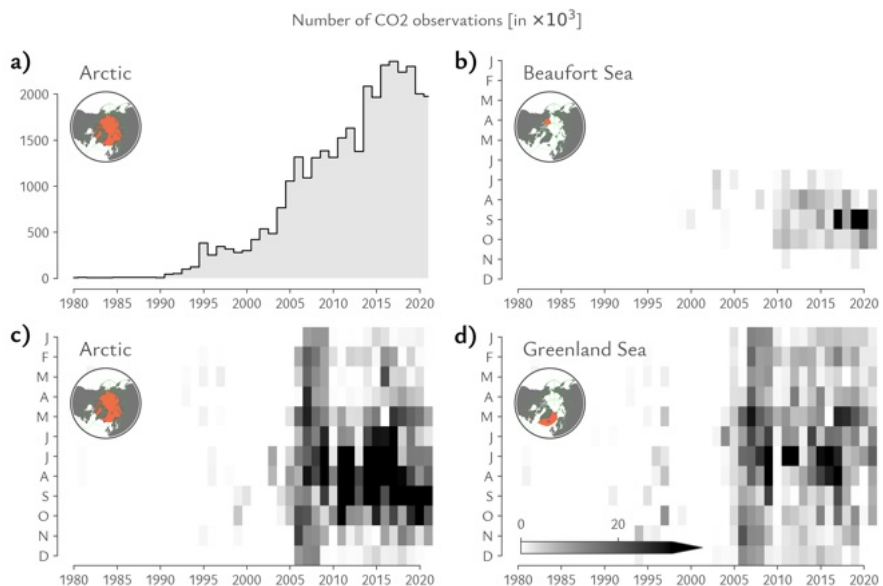


Figure B.6: SOCAT coverage for selected regions. (a) shows the observations taken in each year between 1980 and 2021 in the domain north of 66 °N. (b) – (d) show the number of observations for selected regions and for every month for the same period as covered in (a). The numbers are scaled by a factor of 1000.

BIBLIOGRAPHY

- Aagaard, K. and E. C. Carmack (1989): "The Role of Sea Ice and Other Fresh Water in the Arctic Circulation." *Journal of Geophysical Research* 94.C10. doi: 10/c9rgrh.
- Anderson, L. G. and S. Kaltin (2001): "Carbon Fluxes in the Arctic Ocean—Potential Impact by Climate Change." *Polar Research* 20.2. doi: 10/gfx74c.
- Armour, K. C., I. Eisenman, E. Blanchard-Wrigglesworth, K. E. McCusker, and C. M. Bitz (2011): "The Reversibility of Sea Ice Loss in a State-of-the-Art Climate Model." *Geophysical Research Letters* 38.16. doi: 10/cj5b4h.
- Arrigo, K. R. and G. L. van Dijken (2011): "Secular Trends in Arctic Ocean Net Primary Production." *Journal of Geophysical Research: Oceans* 116.C9. doi: 10/bj4nx6.
- Arrigo, K. R. and G. L. van Dijken (2015): "Continued Increases in Arctic Ocean Primary Production." *Progress in Oceanography* 136. doi: 10/f7mdc6.
- Arrigo, K. R., G. van Dijken, and S. Pabi (2008): "Impact of a Shrinking Arctic Ice Cover on Marine Primary Production." *Geophysical Research Letters* 35.19. doi: 10/bjv744.
- Bailey, H., A. Hubbard, E. S. Klein, K.-R. Mustonen, P. D. Akers, H. Marttila, and J. M. Welker (2021): "Arctic Sea-Ice Loss Fuels Extreme European Snowfall." *Nature Geoscience* 14.5. doi: 10/gjr8rd.
- Bakker, D. C. E. et al. (2016): "A Multi-Decade Record of High-Quality fCO₂ Data in Version 3 of the Surface Ocean CO₂ Atlas (SOCAT)." *Earth System Science Data* 8.2. doi: 10/f3sgd6.
- Barnhart, K. R., I. Overeem, and R. S. Anderson (2014): "The Effect of Changing Sea Ice on the Physical Vulnerability of Arctic Coasts." *The Cryosphere* 8.5. doi: 10/f6p45b.
- Bates, N. R. and J. T. Mathis (2009): "The Arctic Ocean Marine Carbon Cycle: Evaluation of Air-Sea CO₂ Exchanges, Ocean Acidification Impacts and Potential Feedbacks." *Biogeosciences* 6.11. doi: 10/fmhc3m.
- Bathiany, S., D. Notz, T. Mauritsen, G. Raedel, and V. Brovkin (2016): "On the Potential for Abrupt Arctic Winter Sea Ice Loss." *Journal of Climate* 29.7. doi: 10/f8f2dh.
- Becker, M., A. Olsen, P. Landschützer, A. Omar, G. Rehder, C. Rödenbeck, and I. Skjelvan (2021): "The Northern European Shelf as an Increasing Net Sink for CO₂." *Biogeosciences* 18.3. doi: 10.5194/bg-18-1127-2021.
- Bennett, M. M., S. R. Stephenson, K. Yang, M. T. Bravo, and B. De Jonghe (2020): "The Opening of the Transpolar Sea Route: Logistical, Geopolitical, Environmental, and Socioeconomic Impacts." *Marine Policy* 121. doi: 10/gmq4.
- Bergeron, M. and J.-É. Tremblay (2014): "Shifts in Biological Productivity Inferred from Nutrient Drawdown in the Southern Beaufort Sea (2003–2011) and Northern Baffin Bay (1997–2011), Canadian Arctic." *Geophysical Research Letters* 41.11. doi: 10/f59zhx.



- Brodzik, M. J., B. Billingsley, T. Haran, B. Raup, and M. H. Savoie (2012): "EASE-Grid 2.0: Incremental but Significant Improvements for Earth-Gridded Data Sets." *ISPRS International Journal of Geo-Information* 1.1. doi: 10/gchsww.
- Cai, W.-J., L. Chen, B. Chen, Z. Gao, S. H. Lee, J. Chen, D. Pierrot, K. Sullivan, Y. Wang, X. Hu, W.-J. Huang, Y. Zhang, S. Xu, A. Murata, J. M. Grebmeier, E. P. Jones, and H. Zhang (2010): "Decrease in the CO₂ Uptake Capacity in an Ice-Free Arctic Ocean Basin." *Science* 329.5991. doi: 10/fv9sxd.
- Casas-Prat, M. and X. L. Wang (2020): "Sea Ice Retreat Contributes to Projected Increases in Extreme Arctic Ocean Surface Waves." *Geophysical Research Letters* 47.15. doi: 10/gsv6t9.
- Cavalieri, D. J., P. Gloersen, and W. J. Campbell (1984): "Determination of Sea Ice Parameters with the NIMBUS 7 SMMR." *Journal of Geophysical Research: Atmospheres* 89.D4. doi: 10/bs9q9n.
- Cavalieri, D. J., C. L. Parkinson, P. Gloersen, and H. J. Zwally (1997): *Arctic and Antarctic Sea Ice Concentrations from Multichannel Passive-Microwave Satellite Data Sets: October 1978–September 1995 User's Guide*. Tech. rep. NASA-TM-104647.
- Cavalieri, D. J., C. Parkinson, P. Gloersen, and H. J. Zwally (1996): *Sea Ice Concentrations from Nimbus-7 SMMR and DMSP SSM/I-SSMIS Passive Microwave Data, Version 1*. doi: 10.5067/8GQ8LZQVLoVL.
- Comiso, J. C. (1986): "Characteristics of Arctic Winter Sea Ice from Satellite Multispectral Microwave Observations." *Journal of Geophysical Research* 91.C1. doi: 10/fc6wc6.
- Comiso, J. C. (1995): "SSM/I Sea Ice Concentrations Using the Bootstrap Algorithm."
- Davidson, S. C. et al. (2020): "Ecological Insights from Three Decades of Animal Movement Tracking across a Changing Arctic." doi: 10/gqx3bc.
- De Boyer Montégut, C., G. Madec, A. S. Fischer, A. Lazar, and D. Iudicone (2004): "Mixed Layer Depth over the Global Ocean: An Examination of Profile Data and a Profile-based Climatology." *Journal of Geophysical Research: Oceans* 109.C12. doi: 10/d7z4d9.
- Dörr, J., M. Árthun, T. Eldevik, and E. Madonna (2021): "Mechanisms of Regional Winter Sea-Ice Variability in a Warming Arctic." *Journal of Climate* 34.21. doi: 10/gnrmrf.
- Eisenman, I. (2010): "Geographic Muting of Changes in the Arctic Sea Ice Cover." *Geophysical Research Letters* 37.16. doi: 10/cn6wjx.
- Fetterer, F., K. Knowles, W. Meier, M. Savoie, and A. Windnagel (2017): *Sea Ice Index, Version 3*. doi: 10.7265/N5K072F8.
- Friedlingstein, P. et al. (2022): "Global Carbon Budget 2022." *Earth System Science Data* 14.11. doi: 10/gq7nxw.
- GEBCO Compilation Group (2022): *The GEBCO_2022 Grid - a Continuous Terrain Model of the Global Oceans and Land*. doi: 10.5285/EoFoBB8o-AB44-2739-Eo53-6C86ABC0289C.
- GISTEMP Team (2023): *GISS Surface Temperature Analysis (GISTEMP), Version 4*.

- Good, S. A., M. J. Martin, and N. A. Rayner (2013): "EN4: Quality Controlled Ocean Temperature and Salinity Profiles and Monthly Objective Analyses with Uncertainty Estimates: THE EN4 DATA SET." *Journal of Geophysical Research: Oceans* 118.12. doi: 10/gjqs34.
- Griewank, P. J. and D. Notz (2013): "Insights in Brine Dynamics and Sea-Ice Desalination from a 1D Model Study of Gravity Drainage."
- Grimm, R., D. Notz, R. Glud, S. Rysgaard, and K. Six (2016): "Assessment of the Sea-Ice Carbon Pump: Insights from a Three-Dimensional Ocean-Sea-Ice-Biogeochemical Model (MPIOM / HAMOCC)." *Elementa: Science of the Anthropocene* 4. doi: 10/gq3p5s.
- Gupta, K., A. Mukhopadhyay, D. G. Babb, D. G. Barber, and J. K. Ehn (2022): "Landfast Sea Ice in Hudson Bay and James Bay." *Elementa: Science of the Anthropocene* 10.1. doi: 10/gtdrqs.
- Hankel, C. and E. Tziperman (2021): "The Role of Atmospheric Feedbacks in Abrupt Winter Arctic Sea Ice Loss in Future Warming Scenarios." *Journal of Climate* 34.11. doi: 10/gpt6w5.
- Hauser, M., A. Spring, J. Busecke, and M. Van Driel (2021): *Regionmask: Version 0.8.0*. Zenodo. doi: 10.5281/ZENODO.5532848.
- Hersbach, H. et al. (2020): "The ERA5 Global Reanalysis." *Quarterly Journal of the Royal Meteorological Society* 146.730. doi: 10/ggg9wx7.
- Hochheim, K. P. and D. G. Barber (2014): "An Update on the Ice Climatology of the Hudson Bay System." *Arctic, Antarctic, and Alpine Research* 46.1. doi: 10/gtdqrq.
- Huang, B., C. Liu, V. Banzon, E. Freeman, G. Graham, B. Hankins, T. Smith, and H.-M. Zhang (2021): "Improvements of the Daily Optimum Interpolation Sea Surface Temperature (DOISST) Version 2.1." *Journal of Climate* 34.8. doi: 10/gnj287.
- Hunt, B. P. V., R. J. Nelson, B. Williams, F. A. McLaughlin, K. V. Young, K. A. Brown, S. Vagle, and E. C. Carmack (2014): "Zooplankton Community Structure and Dynamics in the Arctic Canada Basin during a Period of Intense Environmental Change (2004-2009)." *Journal of Geophysical Research: Oceans* 119.4. doi: 10/grn5rqt.
- Huntington, H. P., A. Zagorsky, B. P. Kaltenborn, H. C. Shin, J. Dawson, M. Lukin, P. E. Dahl, P. Guo, and D. N. Thomas (2022): "Societal Implications of a Changing Arctic Ocean." *Ambio* 51.2. doi: 10/gp6psv.
- IPCC (2023): *Climate Change 2021 – The Physical Science Basis: Working Group I Contribution to the Sixth Assessment Report of the Intergovernmental Panel on Climate Change*. 1st ed. Cambridge University Press. ISBN: 978-1-00-915789-6. doi: 10/gsjt6f.
- Ingvaldsen, R. B., K. M. Assmann, R. Primicerio, M. Fossheim, I. V. Polyakov, and A. V. Dolgov (2021): "Physical Manifestations and Ecological Implications of Arctic Atlantification." *Nature Reviews Earth & Environment* 2.12. doi: 10/gqqzqs.
- Jersild, A., P. Landschützer, N. Gruber, and D. C. E. Bakker (2017): *An Observation-Based Global Monthly Gridded Sea Surface pCO₂ and Air-Sea CO₂ Flux Product from 1982 Onward and Its Monthly Climatology (NCEI Accession 0160558)*. doi: 10.7289/V5Z899N6.



- Jordahl, K., J. V. D. Bossche, M. Fleischmann, J. Wasserman, J. McBride, J. Gerard, J. Tratner, M. Perry, A. G. Badaracco, C. Farmer, G. A. Hjelle, A. D. Snow, M. Cochran, S. Gillies, L. Culbertson, M. Bartos, N. Eubank, Max-albert, A. Bilogur, S. Rey, C. Ren, D. Arribas-Bel, L. Wasser, L. J. Wolf, M. Journois, J. Wilson, A. Greenhall, C. Holdgraf, Filipe, and F. Leblanc (2020): *Geopandas: V0.8.1*. Zenodo. doi: 10.5281/ZENODO.3946761.
- Krishfield, R. A., A. Proshutinsky, K. Tateyama, W. J. Williams, E. C. Carmack, F. A. McLaughlin, and M.-L. Timmermans (2014): "Deterioration of Perennial Sea Ice in the Beaufort Gyre from 2003 to 2012 and Its Impact on the Oceanic Freshwater Cycle." *Journal of Geophysical Research: Oceans* 119.2. doi: 10/grhf74.
- Landschützer, P., N. Gruber, D. C. E. Bakker, U. Schuster, S. Nakaoka, M. R. Payne, T. P. Sasse, and J. Zeng (2013): "A Neural Network-Based Estimate of the Seasonal to Inter-Annual Variability of the Atlantic Ocean Carbon Sink." *Biogeosciences* 10.11. doi: 10/f5jbxk.
- Landschützer, P., N. Gruber, and D. C. E. Bakker (2016): "Decadal Variations and Trends of the Global Ocean Carbon Sink: Decadal Air-Sea CO₂ Flux Variability." *Global Biogeochemical Cycles* 30.10. doi: 10/f9csrg.
- Lannuzel, D., L. Tedesco, M. van Leeuwe, K. Campbell, H. Flores, B. Delille, L. Miller, J. Stefels, P. Assmy, J. Bowman, K. Brown, G. Castellani, M. Chierici, O. Crabeck, E. Damm, B. Else, A. Fransson, F. Fripiat, N.-X. Geilfus, C. Jacques, E. Jones, H. Kaartokallio, M. Kotovitch, K. Meiners, S. Moreau, D. Nomura, I. Peeken, J.-M. Rintala, N. Steiner, J.-L. Tison, M. Vancoppenolle, F. Van der Linden, M. Vichi, and P. Wongpan (2020): "The Future of Arctic Sea-Ice Biogeochemistry and Ice-Associated Ecosystems." *Nature Climate Change* 10.11. doi: 10/ghmvhj.
- Laruelle, G. G., P. Landschützer, N. Gruber, J.-L. Tison, B. Delille, and P. Regnier (2017): "Global High-Resolution Monthly pCO₂ Climatology for the Coastal Ocean Derived from Neural Network Interpolation." *Biogeosciences* 14.19. doi: 10/gcf67c.
- Lasserre, F. (2019): "Arctic Shipping: A Contrasted Expansion of a Largely Destinational Market." *The GlobalArctic Handbook*. Ed. by M. Finger and L. Heininen. Cham: Springer International Publishing. ISBN: 978-3-319-91994-2 978-3-319-91995-9. doi: 10/mgj3.
- Lasserre, F. and O. Faury (2019): *Arctic Shipping: Climate Change, Commercial Traffic and Port Development*. London: Routledge. ISBN: 978-1-351-03746-4. doi: 10/mgj2.
- Lavergne, T., A. M. Sørensen, S. Kern, R. Tonboe, D. Notz, S. Aaboe, L. Bell, G. Dybkjær, S. Eastwood, C. Gabarro, G. Heygster, M. A. Killie, M. Brandt Kreiner, J. Lavelle, R. Saldo, S. Sandven, and L. T. Pedersen (2019): "Version 2 of the EUMETSAT OSI SAF and ESA CCI Sea-Ice Concentration Climate Data Records." *The Cryosphere* 13.1. doi: 10/gp32tt.
- Lenssen, N. J. L., G. A. Schmidt, J. E. Hansen, M. J. Menne, A. Persin, R. Ruedy, and D. Zyss (2019): "Improvements in the GISTEMP Uncertainty Model." *Journal of Geophysical Research: Atmospheres* 124.12. doi: 10/gj4hcg.
- Li, C., D. Notz, S. Tietsche, and J. Marotzke (2013): "The Transient versus the Equilibrium Response of Sea Ice to Global Warming." *Journal of Climate* 26.15. doi: 10/f45b9b.

- Loose, B., W. R. McGillis, D. Perovich, C. J. Zappa, and P. Schlosser (2014): "A Parameter Model of Gas Exchange for the Seasonal Sea Ice Zone." *Ocean Science* 10.1. doi: 10/f5tv3r.
- MacGilchrist, G., A. Naveira Garabato, T. Tsubouchi, S. Bacon, S. Torres-Valdés, and K. Azetsu-Scott (2014): "The Arctic Ocean Carbon Sink." *Deep Sea Research Part I: Oceanographic Research Papers* 86. doi: 10/f5xsbp.
- Maksym, T. (2019): "Arctic and Antarctic Sea Ice Change: Contrasts, Commonalities, and Causes." *Annual Review of Marine Science* 11.1. doi: 10/grnhws.
- Manizza, M., M. J. Follows, S. Dutkiewicz, D. Menemenlis, C. N. Hill, and R. M. Key (2013): "Changes in the Arctic Ocean CO₂ Sink (1996–2007): A Regional Model Analysis." *Global Biogeochemical Cycles* 27.4. doi: 10/p27.
- Manizza, M., D. Menemenlis, H. Zhang, and C. E. Miller (2019): "Modeling the Recent Changes in the Arctic Ocean CO₂ Sink (2006–2013)." *Global Biogeochemical Cycles* 33.3. doi: 10/gftvbj.
- Martin, T. and P. Wadhams (1999): "Sea-Ice Flux in the East Greenland Current." *Deep Sea Research Part II: Topical Studies in Oceanography* 46.6-7. doi: 10/b4kq7s.
- März, C., F. S. Freitas, J. C. Faust, J. A. Godbold, S. F. Henley, A. C. Tessin, G. D. Abbott, R. Airs, S. Arndt, D. K. A. Barnes, L. J. Grange, N. D. Gray, I. M. Head, K. R. Hendry, R. G. Hilton, A. J. Reed, S. Rühl, M. Solan, T. A. Souster, M. A. Stevenson, K. Tait, J. Ward, and S. Widdicombe (2022): "Biogeochemical Consequences of a Changing Arctic Shelf Seafloor Ecosystem." *Ambio* 51.2. doi: 10/gtdrqx.
- Massonnet, F., M. Vancoppenolle, H. Goosse, D. Docquier, T. Fichefet, and E. Blanchard-Wrigglesworth (2018): "Arctic Sea-Ice Change Tied to Its Mean State through Thermodynamic Processes." *Nature Climate Change* 8.7. doi: 10/gdnf9d.
- Matthews, H. D., N. P. Gillett, P. A. Stott, and K. Zickfeld (2009): "The Proportionality of Global Warming to Cumulative Carbon Emissions." *Nature* 459.7248. doi: 10/d7pjtb.
- Meier, W., F. Fetterer, A. Windnagel, and S. Stewart (2021): *NOAA/NSIDC Climate Data Record of Passive Microwave Sea Ice Concentration, Version 4*. doi: 10.7265/EFMZ-2T65.
- Meier, W. N., G. K. Hovelsrud, B. E. van Oort, J. R. Key, K. M. Kovacs, C. Michel, C. Haas, M. A. Granskog, S. Gerland, D. K. Perovich, A. Makshinas, and J. D. Reist (2014): "Arctic Sea Ice in Transformation: A Review of Recent Observed Changes and Impacts on Biology and Human Activity." *Reviews of Geophysics* 52.3. doi: 10/f6rxfm.
- Millero, F. J. (2013): *Chemical Oceanography*. 4th ed. Boca Raton: Taylor & Francis. ISBN: 978-1-4665-1249-8.
- Millero, F. J., T. B. Graham, F. Huang, H. Bustos-Serrano, and D. Pierrot (2006): "Dissociation Constants of Carbonic Acid in Seawater as a Function of Salinity and Temperature." *Marine Chemistry* 100.1-2. doi: 10/fqj93d.
- Moore, S. E. and H. P. Huntington (2008): "Arctic Marine Mammals and Climate Change: Impacts and Resilience." *Ecological Applications* 18.sp2. doi: 10/cbnzv6.



- Moreau, S., M. Vancoppenolle, L. Bopp, O. Aumont, G. Madec, B. Delille, J.-L. Tison, P.-Y. Barriat, and H. Goosse (2016): "Assessment of the Sea-Ice Carbon Pump: Insights from a Three-Dimensional Ocean-Sea-Ice Biogeochemical Model (NEMO-LIM-PISCES)." *Elementa: Science of the Anthropocene* 4. doi: 10/gtdrsx.
- Morice, C. P., J. J. Kennedy, N. A. Rayner, and P. D. Jones (2012): "Quantifying Uncertainties in Global and Regional Temperature Change Using an Ensemble of Observational Estimates: The HadCRUT4 Data Set." *Journal of Geophysical Research: Atmospheres* 117.D8. doi: 10/q4f.
- Muñoz Sabater, J (2019): *ERA5-Land Monthly Averaged Data from 2001 to Present*. Copernicus Climate Change Service (C3S) Climate Data Store (CDS). doi: 10.24381/CDS.68D2BB30.
- Niederdrenk, A. L. and D. Notz (2018): "Arctic Sea Ice in a 1.5°C Warmer World." *Geophysical Research Letters* 45.4. doi: 10/gc7qbq.
- Nielsen, D. M., M. Dobrynin, J. Baehr, S. Razumov, and M. Grigoriev (2020): "Coastal Erosion Variability at the Southern Laptev Sea Linked to Winter Sea Ice and the Arctic Oscillation." *Geophysical Research Letters* 47.5. doi: 10/gtdrsp.
- Nielsen, D. M., P. Pieper, A. Barkhordarian, P. Overduin, T. Ilyina, V. Brovkin, J. Baehr, and M. Dobrynin (2022): "Increase in Arctic Coastal Erosion and Its Sensitivity to Warming in the Twenty-First Century." *Nature Climate Change* 12.3. doi: 10/gpp6dr.
- Notz, D. (2014): "Sea-Ice Extent and Its Trend Provide Limited Metrics of Model Performance." *The Cryosphere* 8.1. doi: 10/f5twtt.
- Notz, D. and J. C. Stroeve (2016): "Observed Arctic Sea-Ice Loss Directly Follows Anthropogenic CO₂ Emission." *Science* 354.6313. doi: 10/f893zw.
- Notz, D. and M. G. Worster (2009): "Desalination Processes of Sea Ice Revisited." *Journal of Geophysical Research* 114. doi: 10/ffv2g2.
- OSI SAF (2017): *OSI-450Global Sea Ice Concentration Climate Data Record v2.0 - Multimission*. doi: 10.15770/EUM_SAF_OSI_ooo8.
- Olonscheck, D., T. Mauritzen, and D. Notz (2019): "Arctic Sea-Ice Variability Is Primarily Driven by Atmospheric Temperature Fluctuations." *Nature Geoscience* 12.6. doi: 10/gf4rd3.
- Onarheim, I. H. and M. Årthun (2017): "Toward an Ice-Free Barents Sea." *Geophysical Research Letters* 44.16. doi: 10/gbx556.
- Onarheim, I. H., T. Eldevik, L. H. Smedsrød, and J. C. Stroeve (2018): "Seasonal and Regional Manifestation of Arctic Sea Ice Loss." *Journal of Climate* 31.12. doi: 10/gfdtjx.
- Orr, J. C., V. J. Fabry, O. Aumont, L. Bopp, S. C. Doney, R. A. Feely, A. Gnanadesikan, N. Gruber, A. Ishida, F. Joos, R. M. Key, K. Lindsay, E. Maier-Reimer, R. Matear, P. Monfray, A. Mouchet, R. G. Najjar, G.-K. Plattner, K. B. Rodgers, C. L. Sabine, J. L. Sarmiento, R. Schlitzer, R. D. Slater, I. J. Totterdell, M.-F. Weirig, Y. Yamanaka, and A. Yool (2005): "Anthropogenic Ocean Acidification over the Twenty-First Century and Its Impact on Calcifying Organisms." *Nature* 437.7059. doi: 10/fss432.

- Orr, J. C., L. Kwiatkowski, and H.-O. Pörtner (2022): "Arctic Ocean Annual High in pCO₂ Could Shift from Winter to Summer." *Nature* 610.7930. doi: 10/gqxw7f.
- Overeem, I., R. S. Anderson, C. W. Wobus, G. D. Clow, F. E. Urban, and N. Matell (2011): "Sea Ice Loss Enhances Wave Action at the Arctic Coast." *Geophysical Research Letters* 38.17. doi: 10/dg98jp.
- Parkinson, C. L. and D. J. Cavalieri (2008): "Arctic Sea Ice Variability and Trends, 1979–2006." *Journal of Geophysical Research* 113.C7. doi: 10/bq9txq.
- Parmentier, F.-J. W., T. R. Christensen, L. L. Sørensen, S. Rysgaard, A. D. McGuire, P. A. Miller, and D. A. Walker (2013): "The Impact of Lower Sea-Ice Extent on Arctic Greenhouse-Gas Exchange." *Nature Climate Change* 3.3. doi: 10/f22pbv.
- Pithan, F. and T. Mauritsen (2014): "Arctic Amplification Dominated by Temperature Feedbacks in Contemporary Climate Models." *Nature Geoscience* 7.3. doi: 10/f5tqb2.
- Qi, D., Z. Ouyang, L. Chen, Y. Wu, R. Lei, B. Chen, R. A. Feely, L. G. Anderson, W. Zhong, H. Lin, A. Polukhin, Y. Zhang, Y. Zhang, H. Bi, X. Lin, Y. Luo, Y. Zhuang, J. He, J. Chen, and W.-J. Cai (2022): "Climate Change Drives Rapid Decadal Acidification in the Arctic Ocean from 1994 to 2020." *Science* 377.6614. doi: 10/gqwzvs.
- Rantanen, M., A. Y. Karpechko, A. Lipponen, K. Nordling, O. Hyvärinen, K. Ruosteenoja, T. Vihma, and A. Laaksonen (2022): "The Arctic Has Warmed Nearly Four Times Faster than the Globe since 1979." *Communications Earth & Environment* 3.1. doi: 10/h8qd.
- Rieger, N. and S. Levang (2023): *Xeofs: Comprehensive EOF Analysis in Python with Xarray: A Versatile, Multidimensional, and Scalable Tool for Advanced Climate Data Analysis*. Zenodo. doi: 10.5281/ZENODO.6323011.
- Ritter, R., P. Landschützer, N. Gruber, A. R. Fay, Y. Iida, S. Jones, S. Nakaoka, G.-H. Park, P. Peylin, C. Rödenbeck, K. B. Rodgers, J. D. Shutler, and J. Zeng (2017): "Observation-Based Trends of the Southern Ocean Carbon Sink." *Geophysical Research Letters* 44.24. doi: 10/gcw4q2.
- Rödenbeck, C., D. C. E. Bakker, N. Gruber, Y. Iida, A. R. Jacobson, S. Jones, P. Landschützer, N. Metzl, S. Nakaoka, A. Olsen, G.-H. Park, P. Peylin, K. B. Rodgers, T. P. Sasse, U. Schuster, J. D. Shutler, V. Valsala, R. Wanninkhof, and J. Zeng (2015): "Data-Based Estimates of the Ocean Carbon Sink Variability – First Results of the Surface Ocean pCO₂ Mapping Intercomparison (SOCOM)." *Biogeosciences* 12.23. doi: 10/gb9bnx.
- Rödenbeck, C., T. DeVries, J. Hauck, C. Le Quéré, and R. F. Keeling (2022): "Data-Based Estimates of Interannual Sea–Air CO₂ Flux Variations 1957–2020 and Their Relation to Environmental Drivers." *Biogeosciences* 19.10. doi: 10/gtdrqc.
- Rödenbeck, C., R. F. Keeling, D. C. E. Bakker, N. Metzl, A. Olsen, C. Sabine, and M. Heimann (2013): "Global Surface-Ocean pCO₂ and Sea-Air CO₂ Flux Variability from an Observation-Driven Ocean Mixed-Layer Scheme." *Ocean Science* 9.2. doi: 10/f43trr.

- Rolph, R. J., A. R. Mahoney, J. Walsh, and P. A. Loring (2018): "Impacts of a Lengthening Open Water Season on Alaskan Coastal Communities: Deriving Locally Relevant Indices from Large-Scale Datasets and Community Observations." *The Cryosphere* 12.5. doi: 10/gdn95m.
- Ross, J. (1835): *Narrative of a Second Voyage in Search of a North-West Passage, and of a Residence in the Arctic Regions during the Years 1829–1833*. Narrative of a Second Voyage in Search of a North-West Passage Bd. 1. A.W. Webster.
- Rysgaard, S., J. Bendtsen, L. T. Pedersen, H. Ramløv, and R. N. Glud (2009): "Increased CO₂ Uptake Due to Sea Ice Growth and Decay in the Nordic Seas." *Journal of Geophysical Research* 114.C9. doi: 10/fqmfps.
- Rysgaard, S., R. N. Glud, M. K. Sejr, J. Bendtsen, and P. B. Christensen (2007): "Inorganic Carbon Transport during Sea Ice Growth and Decay: A Carbon Pump in Polar Seas." *Journal of Geophysical Research* 112.C3. doi: 10/dkjmjd.
- SIMIP Community (2020): "Arctic Sea Ice in CMIP6." *Geophysical Research Letters* 47.10. doi: 10/gg9cxh.
- Sarmiento, J. L. and N. Gruber (2006): *Ocean Biogeochemical Dynamics*. Princeton: Princeton University Press. ISBN: 978-0-691-01707-5.
- Schulzweida, U. (2020): "CDO User Guide." doi: 10.5281/ZENODO.1435454.
- Sellheim, N. (2019): "Perceiving Dignity, Needs and Rights: Seal Hunting Communities and International Human Rights Standards." *The Global Arctic Handbook*. Ed. by M. Finger and L. Heininen. Cham: Springer International Publishing. ISBN: 978-3-319-91994-2. doi: 10.1007/978-3-319-91995-9_2.
- Serreze, M. C. and R. G. Barry (2011): "Processes and Impacts of Arctic Amplification: A Research Synthesis." *Global and Planetary Change* 77.1–2. doi: 10/fjb75v.
- Serreze, M. C. and R. G. Barry (2014): *The Arctic Climate System*. 2nd ed. Cambridge University Press. ISBN: 978-1-107-03717-5. doi: 10/mgj8.
- Shcherbina, A. Y., L. D. Talley, and D. L. Rudnick (2003): "Direct Observations of North Pacific Ventilation: Brine Rejection in the Okhotsk Sea." *Science* 302.5652. doi: 10/b6kcm.
- Smith, L. C. and S. R. Stephenson (2013): "New Trans-Arctic Shipping Routes Navigable by Midcentury." *Proceedings of the National Academy of Sciences* 110.13. doi: 10/f4vgbv.
- Søreide, J. E., E. Leu, J. Berge, M. Graeve, and S. Falk-Petersen (2010): "Timing of Blooms, Algal Food Quality and *Calanus glacialis* Reproduction and Growth in a Changing Arctic." *Global Change Biology* 16.11. doi: 10/c7c2zv.
- Steiner, N. S., W. G. Lee, and J. R. Christian (2013): "Enhanced Gas Fluxes in Small Sea Ice Leads and Cracks: Effects on CO₂ Exchange and Ocean Acidification." *Journal of Geophysical Research: Oceans* 118.3. doi: 10/ggvvbb.
- Steiner, N. S., J. Bowman, K. Campbell, M. Chierici, E. Eronen-Rasimus, M. Falardeau, H. Flores, A. Fransson, H. Herr, S. J. Insley, H. M. Kauko, D. Lanuzel, L. Loseto, A. Lynnes, A. Majewski, K. M. Meiners, L. A. Miller, L. N. Michel, S. Moreau, M. Nacke, D. Nomura, L. Tedesco, J. A. van Franeker, M. A. van Leeuwe, and P. Wongpan (2021): "Climate Change Impacts on Sea-Ice Ecosystems and Associated Ecosystem Services." *Elementa: Science of the Anthropocene* 9.1. doi: 10/gr5gd5.

- Stolla, M. K. (2023): "Understanding the Intermodel Spread of Simulated Arctic September Sea-Ice Sensitivity." MA thesis. Hamburg: Universität Hamburg.
- Stroeve, J. C. and D. Notz (2018): "Changing State of Arctic Sea Ice across All Seasons." *Environmental Research Letters* 13.10. doi: 10/gfrj9q.
- Takahashi, T., J. Olafsson, J. G. Goddard, D. W. Chipman, and S. C. Sutherland (1993): "Seasonal Variation of CO₂ and Nutrients in the High-Latitude Surface Oceans: A Comparative Study." *Global Biogeochemical Cycles* 7.4. doi: 10/fqbqkk.
- Takahashi, T., S. C. Sutherland, R. Wanninkhof, C. Sweeney, R. A. Feely, D. W. Chipman, B. Hales, G. Friederich, F. Chavez, C. Sabine, A. Watson, D. C. Bakker, U. Schuster, N. Metzl, H. Yoshikawa-Inoue, M. Ishii, T. Midorikawa, Y. Nojiri, A. Körtzinger, T. Steinhoff, M. Hoppema, J. Olafsson, T. S. Arnarson, B. Tilbrook, T. Johannessen, A. Olsen, R. Bellerby, C. Wong, B. Delille, N. Bates, and H. J. de Baar (2009): "Climatological Mean and Decadal Change in Surface Ocean pCO₂, and Net Sea–Air CO₂ Flux over the Global Oceans." *Deep Sea Research Part II: Topical Studies in Oceanography* 56.8-10. doi: 10/b77k3p.
- Thomas, D. N., ed. (2017): *Sea Ice*. Third edition. Chichester, UK; Hoboken, NJ: John Wiley & Sons. ISBN: 978-1-118-77838-8. doi: 10.1002/9781118778371.
- Toole, J. M., M.-L. Timmermans, D. K. Perovich, R. A. Krishfield, A. Proshutinsky, and J. A. Richter-Menge (2010): "Influences of the Ocean Surface Mixed Layer and Thermohaline Stratification on Arctic Sea Ice in the Central Canada Basin." *Journal of Geophysical Research: Oceans* 115.C10. doi: 10/d3mwfq.
- Tsukernik, M., C. Deser, M. Alexander, and R. Tomas (2010): "Atmospheric Forcing of Fram Strait Sea Ice Export: A Closer Look." *Climate Dynamics* 35.7-8. doi: 10/ctcvrm.
- Virtanen, P. et al. (2020): "SciPy 1.0: Fundamental Algorithms for Scientific Computing in Python." *Nature Methods* 17.3. doi: 10/ggj45f.
- Wagner, P. M., N. Hughes, P. Bourbonnais, J. C. Stroeve, L. Rabenstein, U. Bhatt, J. Little, H. Wiggins, and A. Fleming (2020): "Sea-Ice Information and Forecast Needs for Industry Maritime Stakeholders." *Polar Geography* 43.2-3. doi: 10/gtdrq2.
- Wei, T., Q. Yan, W. Qi, M. Ding, and C. Wang (2020): "Projections of Arctic Sea Ice Conditions and Shipping Routes in the Twenty-First Century Using CMIP6 Forcing Scenarios." *Environmental Research Letters*. doi: 10/ghbc5x.
- Winton, M. (2011): "Do Climate Models Underestimate the Sensitivity of Northern Hemisphere Sea Ice Cover?" *Journal of Climate* 24.15. doi: 10/cnbbtd.
- Worster, M. G. and D. W. Rees Jones (2015): "Sea-Ice Thermodynamics and Brine Drainage." *Philosophical Transactions of the Royal Society A: Mathematical, Physical and Engineering Sciences* 373.2045. doi: 10/gtdrst.
- Yamamoto-Kawai, M., N. Tanaka, and S. Pivovarov (2005): "Freshwater and Brine Behaviors in the Arctic Ocean Deduced from Historical Data of δ¹⁸O and Alkalinity (1929–2002 A.D.)" *Journal of Geophysical Research: Oceans* 110.C10. doi: 10/cjp6vw.

- Yasunaka, S., M. Manizza, J. Terhaar, A. Olsen, R. Yamaguchi, P. Landschützer, E. Watanabe, D. Carroll, H. Adiwira, J. D. Müller, and J. Hauck (2023): "An Assessment of CO₂ Uptake in the Arctic Ocean From 1985 to 2018." *Global Biogeochemical Cycles* 37.11. doi: 10.1029/2023GB007806.
- Yasunaka, S., E. Siswanto, A. Olsen, M. Hoppema, E. Watanabe, A. Fransson, M. Chierici, A. Murata, S. K. Lauvset, R. Wanninkhof, T. Takahashi, N. Kosugi, A. M. Omar, S. van Heuven, and J. T. Mathis (2018): "Arctic Ocean CO₂ Uptake: An Improved Multiyear Estimate of the Air–Sea CO₂ Flux Incorporating Chlorophyll a Concentrations." *Biogeosciences* 15.6. doi: 10/gdbdbt.
- Zeng, J., Y. Nojiri, P. Landschützer, M. Telszewski, and S. Nakaoka (2014): "A Global Surface Ocean fCO₂ Climatology Based on a Feed-Forward Neural Network." *Journal of Atmospheric and Oceanic Technology* 31.8. doi: 10/f6cjc4.

The little polar bear at the bottom of these pages is a children's book character invented by the Dutch illustrator Hans de Beer. His books have been published by NordSüd Verlag AG.

ERKLÄRUNG

Hiermit erkläre ich an Eides statt, dass ich die vorliegende Dissertationsschrift selbst verfasst und keine anderen als die angegebenen Quellen und Hilfsmittel benutzt habe. Des Weiteren versichere ich, dass die eingereichte schriftliche Fassung mit der elektronisch übermittelten identisch ist.

—

I hereby declare upon oath that I have written the present dissertation independently and have not used further resources and aids than those stated. Furthermore, I assure that the submitted written version is identical to the electronically submitted version.

Hamburg, January 2024

Markus Ritschel

Hinweis / Reference

Die gesamten Veröffentlichungen in der Publikationsreihe des MPI-M
„Berichte zur Erdsystemforschung / Reports on Earth System Science“,
ISSN 1614-1199

sind über die Internetseiten des Max-Planck-Instituts für Meteorologie erhältlich:
<https://mpimet.mpg.de/forschung/publikationen>

*All the publications in the series of the MPI -M
„Berichte zur Erdsystemforschung / Reports on Earth System Science“,
ISSN 1614-1199*

*are available on the website of the Max Planck Institute for Meteorology:
<https://mpimet.mpg.de/en/research/publications>*

